Okinawa Institute of Science and Technology
Graduate University

Thesis submitted for the degree

Doctor of Philosophy

Minimal Gauged U(1) Extension of the Standard Model with Classical Scale Invariance and Phenomenology

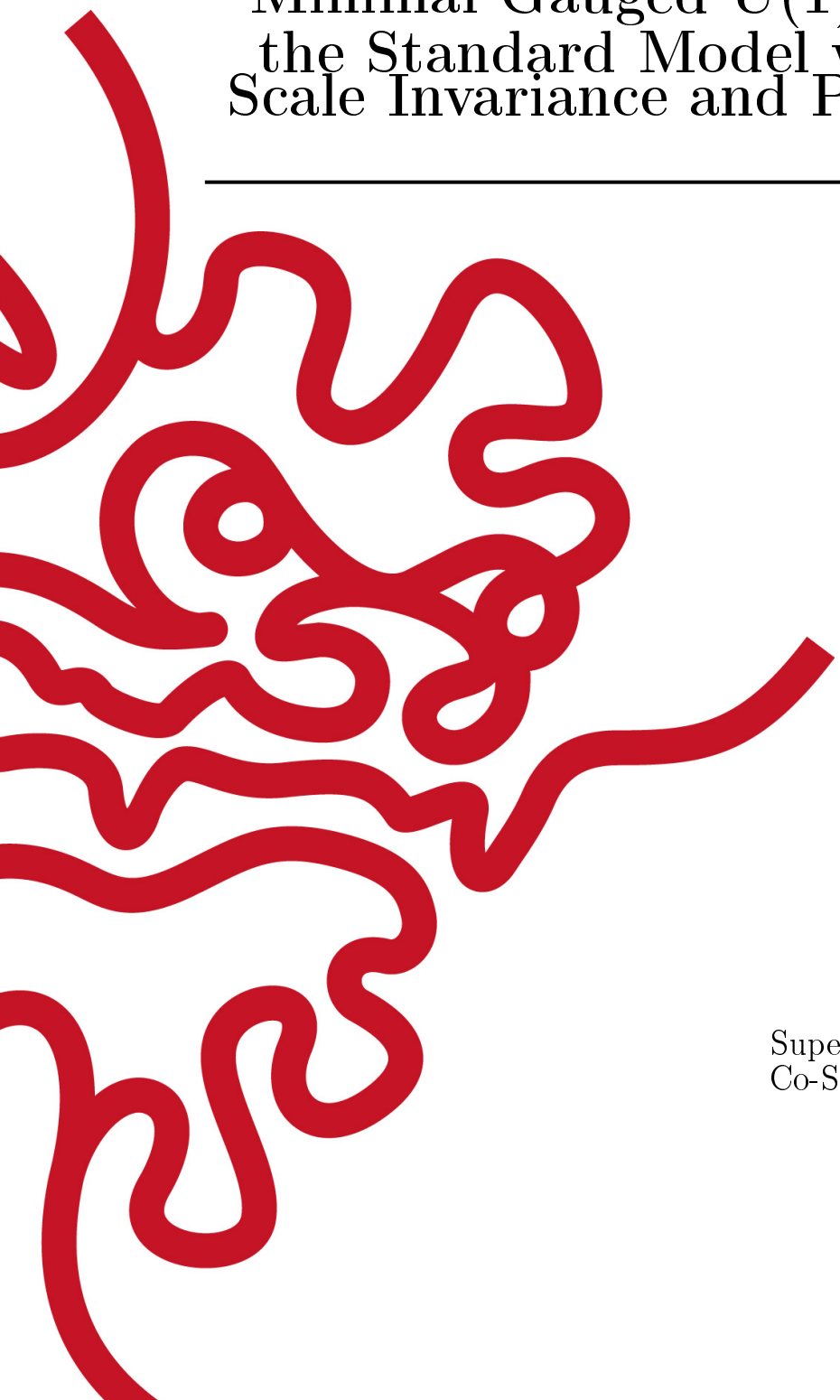

by

Dai-suke Takahashi

Supervisor: **Hirotaka Sugawara**
Co-Supervisor: **Shinobu Hikami**

December, 2017

Declaration of Original and Sole Authorship

I, Dai-suke Takahashi, declare that this thesis entitled *Minimal Gauged U(1) Extension of the Standard Model with Classical Scale Invariance and Phenomenology* and the data presented in it are original and my own work.

I confirm that:

- No part of this work has previously been submitted for a degree at this or any other university.
- References to the work of others have been clearly acknowledged. Quotations from the work of others have been clearly indicated, and attributed to them.
- In cases where others have contributed to part of this work, such contribution has been clearly acknowledged and distinguished from my own work.
- None of this work has been previously published elsewhere, with the exception of the following: (provide list of publications or presentations, or delete this part). (If the work of any co-authors appears in this thesis, authorization such as a release or signed waiver from all affected co-authors must be obtained prior to publishing the thesis. If so, attach copies of this authorization to your initial and final submitted versions, as a separate document for retention by the Graduate School, and indicate on this page that such authorization has been obtained).

Date: December, 2017
Signature:

Abstract

Minimal Gauged U(1) Extension of the Standard Model with Classical Scale Invariance and Phenomenology

Although the Standard Model (SM) is the best theory in describing phenomena among elementary particles, it suffers from several problems, such as the gauge hierarchy problem, origin of the electroweak symmetry breaking, non-zero neutrino mass, and no candidate of dark matter. For solving these problems, we consider minimal U(1) extension of the SM with the classically conformal invariance, where an anomaly-free U(1) gauge symmetry is introduced along with a U(1) Higgs field and three right-handed neutrinos (RHNs) for the seesaw mechanism generating neutrino masses. With no mass term allowed by the classically conformal invariance, the U(1) gauge symmetry is broken through the Coleman-Weinberg mechanism, which subsequently triggers the electroweak symmetry breaking. We perform parameter scan and identify regions resolving the SM Higgs vacuum instability, while satisfying the LHC Run-2 bound on the U(1) gauge boson production and the naturalness constraint. We also investigate cosmological aspects of the model. Introducing Z_2 parity, one RHN being an unique parity-odd particle in the model serves as dark matter. A successful inflation scenario is possible by identifying the U(1) Higgs boson with inflaton and introducing its non-minimal gravitational coupling. Interestingly, the LHC physics and cosmological observations are complementary narrowing down the model parameter space.

Acknowledgment

I would like to express my sincere gratitude to my advisor Prof. Hirotaka Sugawara for his continuous support of my Ph. D study and research, and for his comment, immense knowledge, and patience. I also would like to thank my co-supervisor Prof. Shinobu Hikami for all his supports during my stay at his unit.

Besides my advisors, I especially thank my collaborator Prof. Nobuchika Okada for his insightful discussions and supports. I have learned many things from him through the discussions and his lectures. I thank Arindam Das and Digesh Raut, my collaborators, for supportive discussions with my stays at the United States.

Dr. Hirohiko Shimada, Dr. Hiroaki Ueda always support me since early years of my Ph. D course. I really appreciate for their insightful discussions and encouragement to broaden my research from various perspectives.

I also never forget my gratitude toward Prof. Eiki Senaha, Prof. David Dorfan, Prof. Jonathan Dorfan and Prof. Jeff Wickens provided me an opportunity to research at OIST. My sincere thanks also go to Prof. Ulf Skoglund, my academic mentor, who always encourages me by his nice and warm messages for surviving in academic. Although the space is limited here to list all people to express my gratitude, it would be difficult to complete the thesis without them.

Finally, I would like to express my gratitude to my family.

Abbreviations

BBC	Bing Bang Cosmology
CKM	Cabibbo-Kobayashi-Maskawa
CMB	Cosmic Microwave Background
CW	Coleman-Weinberg
DE	dark energy
DM	dark matter
EM	electromagnetic
EW	electroweak
GUT	grand unified theory
LEP	Large Electron-Positron collider
LHC	Large Hadron Collider
QCD	Quantum Chromodynamics
QFT	quantum field theory
RG	renormalization group
RGE	renormalization group equation
RHN	right-handed neutrino
RW	Robertson-Walker
SM	Standard Model
VEV	vacuum expectation value
WINP	weakly interacting massive particle

Notations and Conventions

Units

In this thesis, we use the "God-given" units:

$$\hbar \;=\; c \;=\; 1, \tag{1}$$

which provide the relations among the fundamental quantities as follows:

$$[\text{mass}] \;=\; [\text{energy}] \;=\; \left[\frac{1}{\text{time}}\right] \;=\; \left[\frac{1}{\text{length}}\right]. \tag{2}$$

Pauli sigma matrices $\boldsymbol{\tau^i}$ $\boldsymbol{(i = 1, 2, 3)}$

The the fundamental representation of $\mathrm{SU}(2)_L$ is defined as $T^i = \tau^i/2$, where

$$\tau^1 \;=\; \begin{pmatrix} 0 & 1 \\ 1 & 0 \end{pmatrix}, \qquad \tau^2 \;=\; \begin{pmatrix} 0 & -i \\ i & 0 \end{pmatrix}, \qquad \tau^3 \;=\; \begin{pmatrix} 1 & 0 \\ 0 & -1 \end{pmatrix}. \tag{3}$$

Gell-Mann matrices $\boldsymbol{\lambda^a}$ $\boldsymbol{(a = 1, \cdots, 8)}$

The the fundamental representation of $\mathrm{SU}(3)_C$ is defined as $T^a_C = \lambda^a/2$, where

$$\begin{aligned}
\lambda^1 \;&=\; \begin{pmatrix} 0 & 1 & 0 \\ 1 & 0 & 0 \\ 0 & 0 & 0 \end{pmatrix}, \qquad \lambda^2 \;=\; \begin{pmatrix} 0 & -i & 0 \\ i & 0 & 0 \\ 0 & 0 & 0 \end{pmatrix}, \qquad \lambda^3 \;=\; \begin{pmatrix} 1 & 0 & 0 \\ 0 & -1 & 0 \\ 0 & 0 & 0 \end{pmatrix}, \\
\lambda^4 \;&=\; \begin{pmatrix} 0 & 0 & 1 \\ 0 & 0 & 0 \\ 1 & 0 & 0 \end{pmatrix}, \qquad \lambda^5 \;=\; \begin{pmatrix} 0 & 0 & -i \\ 0 & 0 & 0 \\ i & 0 & 0 \end{pmatrix}, \qquad \lambda^6 \;=\; \begin{pmatrix} 0 & 0 & 0 \\ 0 & 0 & 1 \\ 0 & 1 & 0 \end{pmatrix}, \\
\lambda^7 \;&=\; \begin{pmatrix} 0 & 0 & 0 \\ 0 & 0 & -i \\ 0 & i & 0 \end{pmatrix}, \qquad \lambda^8 \;=\; \frac{1}{\sqrt{3}} \begin{pmatrix} 1 & 0 & 0 \\ 0 & 1 & 0 \\ 0 & 0 & -2 \end{pmatrix}.
\end{aligned} \tag{4}$$

Nomenclature

c	Speed of light (2.998×10^{10} cm s^{-1})
$\hbar$	Planck constant (6.589×10^{-22} MeV s)
G_N	Gravitational constant (6.709×10^{-39} GeV^{-2})
$M_{\mathrm{Pl}} = \frac{1}{\sqrt{G_N}}$	Planck mass (1.22×10^{19} GeV)
$M_{\mathrm{P}} = \frac{M_{\mathrm{Pl}}}{\sqrt{8\pi}}$	Reduced Planck mass (2.44×10^{18} GeV)
G_F	Fermi constant (1.166×10^{-5} GeV^{-2})
$v_h = \frac{1}{\sqrt{\sqrt{2}G_F}}$	Standard model Higgs vacuum expectation value (246 GeV)
$\sin^2\theta_{\mathrm{w}}$	Weak mixing angle θ_{w} (0.23)
m_W	W-boson mass (80.384 GeV)
m_Z	Z-boson mass (91.189 GeV)
m_h	Higgs boson mass (129.09 GeV)
m_t	Top quark mass (173.34 GeV)
s_0	Entropy density of the present Universe (2890 cm^{-3})
ρ_c/h^2	Critical density (1.05×10^{-5} GeV cm^{-3})

“ The power of instruction is seldom of much efficacy
except in those happy dispositions
where it is almost superfluous. ”

Gibbons

Contents

List of Figures

List of Tables

Introduction

The standard model (SM) is a well-established model which can provide precise predictions for experiments. However, the SM still has several problems, such as the gauge hierarchy problem, origin of the electroweak symmetry breaking, non-zero neutrino mass, and no candidate of dark matter.

One of the most serious problems in the SM is the so-called gauge hierarchy problem, which has been motivating us to seek new physics beyond the SM for decades. The problem originates from the fact that quantum corrections to the self-energy of the SM Higgs doublet field quadratically diverge, and this divergence, once cut off by a physical new physics scale being much higher than the electroweak scale, must be canceled by a fine-tuning of the Higgs mass parameter at the tree level. Because of the chiral nature of the SM, the SM Lagrangian possesses the conformal (scale) invariance at the classical level, except for the Higgs mass term. It has been argued in [1] that once the classically conformal invariance and its minimal violation by quantum anomalies are imposed on the SM, it could be free from the quadratic divergences; hence, the classically conformal invariance might provide us with a solution to the gauge hierarchy problem. This picture nicely fits a setup first investigated by Coleman and Weinberg [2], namely, a U(1) gauge theory with a massless Higgs field. In this setup, it has been shown that the U(1) gauge symmetry is radiatively broken in the Coleman-Weinberg effective potential (Coleman-Weinberg mechanism).

Although it is tempting to apply this Coleman-Weinberg mechanism to the SM Higgs sector, this cannot work with the observed values of top quark and weak boson masses, since the Coleman-Weinberg potential for the SM Higgs field is found to be unbounded from below [3]. Therefore, in order to pursue this scheme, it is necessary to extend the SM. Among several new physics model proposals (see, for example, [4–39]), classically conformal $\mathrm{U}(1)_{B-L}$ extended SM proposed in [40, 41] is a very simple and well-motivated model. The $B - L$ (baryon number minus lepton number) is a unique anomaly-free global symmetry in the SM, and it can be easily gauged. Associated with gauging the $\mathrm{U}(1)_{B-L}$ symmetry, three generation of right-handed neutrinos and a $\mathrm{U}(1)_{B-L}$ Higgs field are introduced to make the model free from all gauge and gravitational anomalies, and to break the $\mathrm{U}(1)_{B-L}$ gauge symmetry. Once the $\mathrm{U}(1)_{B-L}$ gauge symmetry is broken, the $\mathrm{U}(1)_{B-L}$ gauge field (Z' boson) and the right-handed (Majorana) neutrinos obtain their masses. With the Majorana heavy neutrinos, the seesaw mechanism [42–47] is automatically implemented. In [40, 41], under a requirement of the classically conformal invariance, the radiative $\mathrm{U}(1)_{B-L}$ symmetry breaking by the Coleman-Weinberg mechanism has been investigated. The $\mathrm{U}(1)_{B-L}$ gauge symmetry breaking also triggers the electroweak symmetry breaking by generating a negative

mass squared for the SM Higgs doublet.

In this thesis, we introduce the classically conformal U(1)′ extension of the SM [48, 49], where in addition to the SM particle content, three generations of right-handed neutrinos and a U(1)′ Higgs field are introduced. By assigning generation-independent U(1)′ charges for fermions, making the model free from all gauge and gravitational anomalies, and reproducing the Yukawa structure in the SM, it turns out that the U(1)′ gauge symmetry is identified as a linear combination of the SM $U(1)_Y$ and the $U(1)_{B-L}$ gauge groups [50]. Hence, our model is a generalization on the classically conformal $U(1)_{B-L}$ extension of the SM proposed in [40, 41]. The U(1)′ gauge symmetry is radiatively broken by the Coleman-Weinberg mechanism, and the U(1)′ gauge field (Z' boson) and the right-handed (Majorana) neutrinos acquire their masses. A mixing quartic coupling between the U(1)′ Higgs and the SM Higgs doublet fields generates a negative mass squared for the SM Higgs doublet field, and the electroweak symmetry breaking is driven. Therefore, the radiative U(1)′ gauge symmetry is the sole origin of the mass scale in this model. With the Majorana heavy neutrinos, the seesaw mechanism [42–47] is also automatically implemented, and tiny active neutrino masses and their flavor mixing are generated after the electroweak symmetry breaking.

The SM Higgs boson has been discovered at the Large Hadron Collider (LHC), and this marks the beginning of the experimental confirmation of the SM Higgs sector. The observed Higgs boson mass of $m_h = 125.09 \pm 0.21(\text{stat.}) \pm 0.11(\text{syst.})$ GeV from a combined analysis by the ATLAS and the CMS [51] indicates that the electroweak vacuum is unstable [52] since the SM Higgs quartic coupling becomes negative far below the Planck mass, for the top quark pole mass $m_t = 173.34 \pm 0.76$ from the combined measurements by the Tevatron and the LHC experiments [53]. Practically, this instability may not be a problem in the SM, since the lifetime of our electroweak vacuum is estimated to be much longer than the age of the universe [54]. However, in the presence of the U(1)′ Higgs field, our Higgs potential is a function of two Higgs fields, and there might be a flat path around high mountains of the potential toward the true vacuum and make the lifetime of our electroweak vacuum very short. Because of a lack of field theoretical technology for analyzing the effective scalar potential with multiscalars in a wide range of field values, it would be the best way to solve the electroweak vacuum instability problem in the context of our model.

In chapter 2, we investigate the electroweak vacuum stability in the classically conformal U(1)′ extended SM by the renormalization group equations (RGEs) at the two-loop level, and present a complete result for the parameter scan. We also investigate the constraints on the model parameters by taking into account the LHC Run-2 2015 results for the search for Z' boson resonances [55, 56]. We find that the LHC Run-2 2015 results dramatically improve those obtained from the Run-1 results. In addition, we calculate the SM Higgs self-energy corrections from the effective potential involving the heavy states, the right-handed neutrinos and the Z' boson, after the U(1)′ symmetry breaking, and derive the naturalness bounds to reproduce the right electroweak scale for a fine-tuning level better than 10%.

Other important missing pieces in the SM are, for example, a candidate for the dark matter (DM), and tiny neutrino masses and their flavor mixings. The SM should be extended so as to supplement these missing pieces. The so-called seesaw mechanism is a natural way to reproduce the tiny neutrino masses [42–47], where heavy Majorana

right-handed neutrinos (RHNs) are introduced. The minimal gauged $B-L$ model [57–62] is one of the simplest extensions of the SM with an extra gauge symmetry, in which the accidentally anomaly-free global $B-L$ in the SM is gauged. Three RHNs play an essential roll to cancel the gauge and gravitational anomalies of the model. Associated with the $\mathrm{U}(1)_{B-L}$ symmetry breaking, the RHNs acquire their Majorana masses, and hence the seesaw mechanism is automatically implemented. The minimal $B-L$ model can be generalized to the so-called minimal $\mathrm{U}(1)'$ model [50]. Here, the $\mathrm{U}(1)'$ gauge group is defined as a linear combination of the $\mathrm{U}(1)_{B-L}$ and the SM $\mathrm{U}(1)_Y$ gauge groups, so that the $\mathrm{U}(1)'$ model is anomaly-free. In Refs. [48, 49], we have investigated the minimal $\mathrm{U}(1)'$ model with classically conformal invariance.

The so-called weakly interacting massive particle (WIMP) is one of the most promising candidates of the DM in our Universe, which is in thermal equilibrium in the early Universe. Among many possibilities, a simple way to introduce a WIMP DM in the minimal $\mathrm{U}(1)'$ model has been proposed in [63] (see also [64]), where Z_2-parity is introduced and an odd-parity is assigned to one RHN, while all the other particles is assigned to be Z_2-even. We adapt this scheme in our minimal $\mathrm{U}(1)'$ model with the classically conformal invariance, and the Z_2-odd RHN is a DM candidate, while the other two RHNs are utilized for the seesaw mechanism. Note that only two RHNs are sufficient to reproduce the neutrino oscillation data, and the observed baryon asymmetry in the Universe through leptogenesis [65]. This system is called the minimal seesaw [66, 67]. In our model, there are two ways for the RHN DM to interact with the SM particles. One is mediated by the Z' boson (Z'-portal) and the other is by the two Higgs bosons (Higgs portal) which are two mass eigenstates consisting of the SM Higgs and the $\mathrm{U}(1)'$ Higgs bosons. Recently, the Z'-portal DM scenarios [68–96] have been intensively investigated, while the Higgs portal RHN DM scenarios [63, 97, 98] have been analyzed in detail.

In chapter 3, we introduce the classically conformal $\mathrm{U}(1)'$ extended SM with the RHN DM [99]. In Refs. [48, 49], the allowed parameter regions in the classically conformal model are severely constrained in order to solve the electroweak vacuum instability problem, and to satisfy the LHC limits from the search for Z' boson resonance. In addition to these constraints, we investigate the RHN DM physics. Because of the nature of classical conformality, we find the mass mixing between the SM Higgs and the $\mathrm{U}(1)'$ Higgs bosons is very small, so that the RHN DM pair annihilation process mediated by the Higgs bosons is highly suppressed. Therefore, we focus on the study of the Z'-portal RHN DM [85, 94], and identify allowed parameter regions to reproduce the observed DM relic density from the Planck 2015 result [100]. We show that the DM physics, LHC phenomenology, and the electroweak vacuum stability condition complementarily work to narrow down the allowed parameter regions. For the identified allowed regions, we also calculate the spin-independent cross section of the RHN DM with nucleons and compare our results with the current upper bounds from the direct DM search experiments.

In the cosmological point of view, cosmological inflation [101–104] needs to provide not only solutions to problems in the Standard Big Bang Cosmology, such as the flatness and horizon problems, but also the primordial density fluctuations which are necessary for the formation of the large scale structure observed in the present universe. In a simple inflationary scenario known as the slow-roll inflation, inflation is driven

by a single scalar field (inflaton) while inflaton is slowly rolling down its potential to the minimum. During the slow-roll, the inflaton potential energy dominates the energy density of the universe, and the universe undergoes an accelerated expansion era, namely, cosmological inflation. The inflation ends when the kinetic energy of inflaton starts dominating over its potential energy, and the inflaton eventually decays into particles in the Standard Model (SM). The universe is reheated by relativistic particles created from the inflaton decay and continues to the Standard Big Bang Cosmology.

The Planck 2015 results [105] have set an upper bound on the tensor-to-scalar ratio as $r \lesssim 0.1$, while the best fit value for the spectral index (n_s) is 0.9655 ± 0.0062 at 68% CL. Hence, the chaotic inflation models with simple inflaton (ϕ) potentials such as $V \propto \phi^4$ and $V \propto \phi^2$ are disfavored because of their predictions for r being too large. Among many inflation models, quartic inflation with non-minimal gravitational coupling is a very simple model, which can satisfy the constraints from the Planck 2015 results for a non-minimal gravitational coupling $\xi \gtrsim 0.001$ [106, 107].

In the view point of particle physics, we may think that an inflation model is more compelling if the inflaton also plays an important role in the model. The Higgs inflation scenario[108–120] is a well-known example, in which the SM Higgs field is identified with the inflaton. Also, we may consider a unified scenario between inflaton and dark matter particle [121–126]. When the SM is extended with some extra or unified gauge groups, such extensions always include an extra Higgs field in addition to the SM Higgs field, which is necessary to spontaneously break the gauge symmetry down to the SM one. Similarly to the Higgs inflation scenario, we may identify the extra Higgs field with the inflaton.

In chapter 4, we introduce the quartic inflation with non-minimal gravitational coupling in the context of the minimal U(1)$'$ extension of the SM with the conformal invariance at the classical level [127]. Here, we identify the U(1)$'$ Higgs field as the inflaton. Because of the symmetry breaking via the Coleman-Weinberg mechanism, the quartic (self-)coupling of the U(1)$'$ Higgs field relates to the U(1)$'$ gauge coupling, in other words, we have a relation between the inflaton mass and the Z' boson mass. Since the inflationary predictions are controlled by the inflaton quartic coupling in the quartic inflation with non-minimal gravitational coupling, we have a correlation between the inflationary predictions and Z' boson physics. Assuming the Z' boson mass in the range of $\mathcal{O}(10\text{ GeV})-\mathcal{O}(10\text{ TeV})$, we investigate complementarities between the inflationary predictions and the constraints from the Z' boson resonance search at the LHC Run-2 2017 [128] as well as the prospect of the search for the Z' boson and the right-handed neutrinos at the future collider experiments.

This thesis is organized as follows: In chapter 1, we briefly explain the basics of the SM. In chapter 2, we introduce our U(1)$'$ extended SM with the classically conformal invariance, and investigate the electroweak vacuum instability problem in the SM. In chapter 3, we discuss the DM physics in the context of our U(1)$'$ model, where the Z_2-odd RHN serves as a DM candidate. In chapter 4, we consider an inflation scenario in our U(1)$'$ model, where the U(1)$'$ Higgs field is identified as the inflaton. The last chapter is devoted to conclusions. Formulas we used in our analysis are listed in the appendices.

Chapter 1

Standard Model

In this chapter, we briefly review the Standard Model (SM), especially focusing on the topics which are relevant to studies in this thesis (for more details, see, for example, Ref. [129]). The SM is one of the quantum field theory (QFT) which is based on the theory of relativity and the quantum mechanics. Because of the properties of the QFT, the possible form (terms) of the Lagrangian in the SM should be restricted by strong constraints, such as Lorentz invariance, renormalizability, and Chiral anomaly free nature. In addition to the property of the QFT, in the SM, gauge invariance and spontaneous symmetry breaking (Higgs mechanism) are important extra ingredients.

This chapter is organized as follows: In Sec. 1.1, we briefly explain the minimal SM, including the particle contents of the SM and its Lagrangian. In Sec. 1.2, we explain the Higgs mechanism, in which the masses are generated through the electroweak symmetry breaking. In Sec. 1.3, the renormalization group equation is explained. Although the SM is a well-established theory in describing phenomena among elementary particles, it has still several problems. We list these problems in Sec. 1.4.

1.1 The minimal Standard Model

The SM is a QFT which is based on a gauge group (local and internal symmetry group),

$$\mathrm{SU}(3)_C \times \mathrm{SU}(2)_L \times \mathrm{U}(1)_Y. \tag{1.1}$$

The $\mathrm{SU}(3)_C$ and $\mathrm{SU}(2)_L \times \mathrm{U}(1)_Y$ describe the Quantum Chromodynamics (QCD) and the electroweak (EW) interactions. The particle contents of the SM are shown in Table 1.1. The Weyl two-component spinors describe the quark (u^i and d^i) and lepton (ν^i and e^i) matter fields with three generations ($i = 1, 2, 3$). The L and R in the particle contents indicate right- and left-chirality. It is very interesting that only left-handed particles of the SM are involved in the EW interactions, so that the left-handed matter fields are described by doublet ones. In addition, only quarks interact with the QCD, then it behaves as color triplets. In the SM, a scalar doublet field (H) is introduced, which is called the Higgs field.

As being satisfied the properties of the QFT and the SM, the Lagrangian of the minimal SM, such that there are no CP-violating term and gravity, has a unique form:

$$\mathcal{L}_{\mathrm{SM}} = \mathcal{L}_{\mathrm{gauge}} + \mathcal{L}_{\mathrm{fermion}} + \mathcal{L}_{\mathrm{Yukawa}} + \mathcal{L}_{\mathrm{scalar}}, \tag{1.2}$$

	$\mathrm{SU}(3)_c$	$\mathrm{SU}(2)_L$	$\mathrm{U}(1)_Y$
q_L^i	**3**	**2**	$+\frac{1}{6}$
u_R^i	**3**	**1**	$+\frac{2}{3}$
d_R^i	**3**	**1**	$-\frac{1}{3}$
ℓ_L^i	**1**	**2**	$-\frac{1}{2}$
e_R^i	**1**	**1**	-1
H	**1**	**2**	$+\frac{1}{2}$

Table 1.1: Particle contents of the Standard Model (SM). u^i (d^i) are the up-type (down-type) quarks, and ν^i and e^i are the leptons (neutrinos and electrons), where $i = 1, 2, 3$ denotes the generation index. The L and R indicate right- and left-chirality, H is the SM Higgs doublet field.

where

$$\begin{aligned}
\mathcal{L}_{\text{gauge}} &= -\frac{1}{4}G^a_{\mu\nu}G^{a\mu\nu} - \frac{1}{4}W^i_{\mu\nu}W^{i\mu\nu} - \frac{1}{4}B_{\mu\nu}B^{\mu\nu}, \\
\mathcal{L}_{\text{fermion}} &= \overline{q^i_L}(i\not{D})q^i_L + \overline{u^i_R}(i\not{D})u^i_R + \overline{d^i_R}(i\not{D})d^i_R + \overline{\ell^i_L}(i\not{D})\ell^i_L + \overline{e^i_R}(i\not{D})e^i_R, \\
\mathcal{L}_{\text{Yukawa}} &= -Y_u^{ij}\overline{q^i_L}\tilde{H}u^j_R - Y_d^{ij}\overline{q^i_L}Hd^j_R - Y_e^{ij}\overline{\ell^i_L}He^j_R + \text{h.c.}, \\
\mathcal{L}_{\text{scalar}} &= |D_\mu H|^2 - V(H).
\end{aligned} \tag{1.3}$$

Here, the field strengths, $G^a_{\mu\nu}$, $W^i_{\mu\nu}$ and $B_{\mu\nu}$, are defined as

$$\begin{aligned}
G^a_{\mu\nu} &= \partial_\mu G^a_\nu - \partial_\nu G^a_\mu + g_3 f^{abc} G^b_\mu G^c_\nu, \\
W^i_{\mu\nu} &= \partial_\mu W^i_\nu - \partial_\nu W^i_\mu + g_2 \epsilon^{ijk} W^j_\mu W^j_\nu, \\
B_{\mu\nu} &= \partial_\mu B_\nu - \partial_\nu B_\mu,
\end{aligned} \tag{1.4}$$

and the covariant derivative is defined as

$$D_\mu \equiv \partial_\mu - ig_3 T^a_C G^a_\mu - ig_2 T^i W^i_\mu - ig_1 Y B_\mu, \tag{1.5}$$

where G^a_μ, W^i_μ, and B_μ correspond to the $\mathrm{SU}(3)_C$, $\mathrm{SU}(2)_L$, and $\mathrm{U}(1)_Y$ gauge field, respectively, and g_3, g_2, and g_1 also correspond to the couplings of each gauge group. f^{abc} (ϵ^{ijk}) are the structure constants of the $\mathrm{SU}(3)_C$ ($\mathrm{SU}(2)_L$) gauge group, which are satisfied the commutation relations

$$\begin{aligned}
\left[T^a_C, T^b_C\right] &= if^{abc}T^c_C, \\
\left[T^i, T^j\right] &= i\epsilon^{ijk}T^k.
\end{aligned} \tag{1.6}$$

For the generation-independent $\mathrm{U}(1)_Y$ charges of the fermions, the SM is completely free from of the gauge and gravitational anomalies:

$$\begin{aligned}
\mathrm{U}(1)_Y \times [\mathrm{SU}(3)_C]^2 \ : \quad & 2\left(\frac{1}{6}\right) - \left(\frac{2}{3}\right) - \left(-\frac{1}{3}\right) = 0, \\
\mathrm{U}(1)_Y \times [\mathrm{SU}(2)_L]^2 \ : \quad & 3\left(\frac{1}{6}\right) + \left(-\frac{1}{2}\right) = 0, \\
[\mathrm{U}(1)_Y]^3 \ : \quad & 6\left(\frac{1}{6}\right)^3 - 3\left(\frac{2}{3}\right)^3 - 3\left(-\frac{1}{3}\right)^3 + 2\left(-\frac{1}{2}\right)^3 - (-1)^3 = 0, \\
\mathrm{U}(1)_Y \times [\mathrm{grav.}]^2 \ : \quad & 6\left(\frac{1}{6}\right) - 3\left(\frac{2}{3}\right) - 3\left(-\frac{1}{3}\right) + 2\left(-\frac{1}{2}\right) - (-1) = 0. \quad (1.7)
\end{aligned}$$

Y_u^{ij}, Y_u^{ij} and Y_u^{ij} in the Yukawa Lagrangian of Eq. (1.3) are Yukawa couplings, and $\tilde{H} \equiv i\tau^2 H^*$. These interaction terms have the gauge invariance elegantly. All terms are also renormalizable, and accidentally has the $B - L$ (baryon number minus lepton number) global symmetry. The Higgs field (particle) also plays an important role of the unitarity when the symmetry is broken. The Higgs potential $V(H)$ in Eq. (1.3) is also determined by the gauge symmetry and renormalizability:

$$V(H) = \lambda_H (H^\dagger H)^2 - \mu^2 H^\dagger H. \quad (1.8)$$

In the next section, we briefly explain the Higgs mechanism (spontaneous symmetry breaking), and we can see how the fermions acquire their masses through the Yukawa terms with the non-zero Higgs vacuum expectation value (VEV).

1.2 Electroweak Symmetry Breaking (Higgs Mechanism)

Because of the chiral nature of the SM, all fermions should be massless. However, the fermions at current temperature of universe have their non-zero masses. In order to explain the mass generation from the original massless theory, there should be, at least, a mechanism for mass generation. If there is a scalar (Higgs) field in a model, it is possible to explain the mass generation through the EW symmetry breaking with non-zero vacuum expectation value (VEV) of the scalar field, even though the theory is originally massless.

This mechanism of the symmetry breaking with mass generation for vector fields, is called "the Higgs mechanism." In the SM, the EW gauge group breaks down spontaneously into the electromagnetic (EM) gauge group,

$$\mathrm{SU}(2)_L \times \mathrm{U}(1)_Y \ \rightarrow \ \mathrm{U}(1)_{\mathrm{EM}}, \quad (1.9)$$

by the complex scalar (Higgs) which is doublet field $H = (H^+,\ H^0)^T$ with hypercharge $1/2$ in the particle content (Table 1.1).

By using the unitary gauge,

$$H = \frac{1}{\sqrt{2}} \begin{pmatrix} 0 \\ h \end{pmatrix}, \quad (1.10)$$

the Higgs potential in Eq. (1.8) becomes

$$V(h) \;=\; \frac{\lambda_H}{4}h^4 - \frac{\mu^2}{2}h^2. \tag{1.11}$$

Because of the shape of Mexican-hat Higgs potential, the stationary condition $V'|_{h=v_h} = 0$ leads to produce a non-vanishing Higgs VEV v_h ($\equiv \langle h \rangle$)

$$v_h \;=\; \sqrt{\frac{\mu^2}{\lambda_H}} \tag{1.12}$$

which is determined by the strength of the weak interaction G_F (fermi constant) as

$$v_h \;=\; \frac{1}{\sqrt{\sqrt{2}G_F}} \;=\; 246 \text{ GeV}. \tag{1.13}$$

The fluctuating around the Higgs VEV provide the Higss mass, which is the curvature of the Higgs potential at the Higgs VEV

$$m_h^2 \;=\; \left.\frac{d^2V}{dh^2}\right|_{h=v_h} \;=\; 2\mu^2 \;=\; 2\lambda_H v_h^2. \tag{1.14}$$

The observed Higgs boson mass is $m_h = 125.09 \pm 0.21(\text{stat.}) \pm 0.11(\text{syst.})$ GeV from a combined analysis by the ATLAS and the CMS [51].

The gauge boson mass terms come from $|D_\mu H|^2$ term of $\mathcal{L}_{\text{scalar}}$ in Eq. (1.3), evaluated at the Higgs VEV $\langle H \rangle = 1/\sqrt{2}\,(0,\; v_h)^T$,

$$\begin{aligned}
|D_\mu \langle H \rangle|^2 &= \frac{v_h^2}{2} \cdot \frac{1}{4}\left[g_2^2 \left|W_\mu^1 - iW_\mu^2\right|^2 + \left(-g_2 W_\mu^3 + g_1 B_\mu\right)^2\right] \\
&= \left(\frac{g_2}{2}v_h\right)^2 \left|\frac{W_\mu^1 - iW_\mu^2}{\sqrt{2}}\right|^2 + \frac{1}{2}\left(\frac{\sqrt{g_2^2+g_1^2}}{2}v_h\right)^2 \left(\frac{g_2 W_\mu^3 - g_1 B_\mu}{\sqrt{g_2^2+g_1^2}}\right)^2 \\
&\equiv m_W^2 W_\mu^+ W^{-\mu} + \frac{1}{2}m_Z^2 Z_\mu Z^\mu,
\end{aligned} \tag{1.15}$$

where in the last expression, three massive gauge bosons ($W_\mu^\pm$, Z_μ) and one massless gauge boson (A_μ) appear as following:

$$\begin{aligned}
W_\mu^\pm &= \frac{1}{\sqrt{2}}(A_\mu^1 \mp iA_\mu^2), \\
Z_\mu &= \frac{1}{\sqrt{g_2^2+g_1^2}}(g_2 A_\mu^3 - g_1 B_\mu) \;\equiv\; \cos\theta_{\text{w}} \cdot A_\mu^3 - \sin\theta_{\text{w}} \cdot B_\mu, \\
A_\mu &= \frac{1}{\sqrt{g_2^2+g_1^2}}(g_1 A_\mu^3 + g_2 B_\mu) \;\equiv\; \sin\theta_{\text{w}} \cdot A_\mu^3 + \cos\theta_{\text{w}} \cdot B_\mu,
\end{aligned} \tag{1.16}$$

with masses

$$\begin{aligned}
m_W &= \frac{g_2}{2}v_h \;\left(=\; m_Z \cos\theta_{\text{w}}\right), \\
m_Z &= \frac{\sqrt{g_2^2+g_1^2}}{2}v_h, \\
m_A &= 0.
\end{aligned} \tag{1.17}$$

Here, A_μ is identified with the massless electromagnetic field, and $\theta_{\rm w}$ is called the weak mixing angle defined as

$$\cos\theta_{\rm w} = \frac{g_2}{\sqrt{g_2^2+g_1^2}}, \qquad \sin\theta_{\rm w} = \frac{g_1}{\sqrt{g_2^2+g_1^2}}, \tag{1.18}$$

which transforms the two bases between $(W_\mu^3,\, B_\mu)$ and $(Z_\mu,\, A_\mu)$ as in Eq. (1.16), and $\sin^2\theta_{\rm w} = 0.23$ from the experiments. By comparing the effective Lagrangian for the weak interaction, there is a relation between G_F and v_h as

$$\frac{G_F}{\sqrt{2}} = \frac{g_2^2}{8m_W^2} = \frac{1}{2v_h^2}, \tag{1.19}$$

which has been used to calculate v_h in Eq. (1.13).

In term of these mass eigenstate fields, the covariant derivative in Eq. (1.5) can be written in a more convenient way as a following:

$$\begin{aligned} D_\mu &= \partial_\mu - ig_3 T_C^a G_\mu^a - i\frac{g_2}{\sqrt{2}}(W_\mu^+ T^+ + W_\mu^- T^-) \\ &\quad - i\frac{1}{\sqrt{g_2^2+g_1^2}} Z_\mu (g_2^2 T^3 - g_1^2 Y) - i\frac{g_2 g_1}{\sqrt{g_2^2+g_1^2}} A_\mu (T^3+Y) \\ &= \partial_\mu - ig_3 T_C^a G_\mu^a - i\frac{g_2}{\sqrt{2}}(W_\mu^+ T^+ + W_\mu^- T^-) \\ &\quad - i\frac{g_2}{\cos\theta_{\rm w}} Z_\mu (T^3 - \sin^2\theta_{\rm w}\cdot Q) - ieA_\mu Q \end{aligned} \tag{1.20}$$

where $T^\pm \equiv T^1 \pm iT^2$, the electron charge is defined as

$$e = \frac{g_2 g_1}{\sqrt{g_2^2+g_1^2}} = g_2 \sin\theta_{\rm w}, \tag{1.21}$$

and the electric charge quantum number is $Q = T^3 + Y$. Now, we see that only two parameters of e and $\theta_{\rm w}$ decide the strength of the weak interaction. Because W and Z boson masses are connected by the $\theta_{\rm w}$ in Eq. (1.17), the exchange processes of the W and Z at tree level can be described by these three fundamental parameters, e, $\theta_{\rm w}$, and m_W.

Once the Higgs VEV has non-zero value, it simultaneously produces the mass of fermions through Yukawa terms in Eq. (1.3), evaluated at the Higgs VEV $\langle H\rangle = 1/\sqrt{2}\,(0,\ v_h)^T$,

$$\begin{aligned} \mathcal{L}_{\rm Yukawa}|_{H=\langle H\rangle} &= -Y_u^{ij}\overline{q_L^i}\langle\tilde{H}\rangle u_R^j - Y_d^{ij}\overline{q_L^i}\langle H\rangle d_R^j - Y_e^{ij}\overline{\ell_L^i}\langle H\rangle e_R^j + \text{h.c.} \\ &= -\overline{u_L^i}\left(\frac{Y_u^{ij}}{\sqrt{2}}v_h\right)u_R^j - \overline{d_L^i}\left(\frac{Y_d^{ij}}{\sqrt{2}}v_h\right)d_R^j - \overline{e_L^i}\left(\frac{Y_e^{ij}}{\sqrt{2}}v_h\right)e_R^j + \text{h.c.} \\ &\equiv -\overline{u_L^i} m_u^{ij} u_R^j - \overline{d_L^i} m_d^{ij} d_R^j - \overline{e_L^i} m_e^{ij} e_R^j + \text{h.c.} \\ &= -\left(\overline{u_L}U_u\right)^i \left(U_u^\dagger m_u W_u\right)^{ij} \left(W_u^\dagger u_R\right)^j - \left(\overline{d_L}U_d\right)^i \left(U_d^\dagger m_d W_d\right)^{ij} \left(W_d^\dagger d_R\right)^j \\ &\qquad - \left(\overline{e_L}U_e\right)^i \left(U_e^\dagger m_e W_e\right)^{ij} \left(W_e^\dagger e_R\right)^j + \text{h.c.} \\ &\equiv -\overline{u_L'^i}\, m_u'^{ij}\, u_R'^j - \overline{d_L'^i}\, m_d'^{ij}\, d_R'^j - \overline{e_L'^i}\, m_e'^{ij}\, e_R'^j + \text{h.c.} \end{aligned} \tag{1.22}$$

where in the third expression, mass matrices for u, d, and e are defined as

$$m_u^{ij} = \frac{Y_u^{ij}}{\sqrt{2}} v_h, \qquad m_d^{ij} = \frac{Y_d^{ij}}{\sqrt{2}} v_h, \qquad m_e^{ij} = \frac{Y_e^{ij}}{\sqrt{2}} v_h, \tag{1.23}$$

in the fourth expression, U_f and W_f (f denotes u, d, and e) are unitary matrices to diagonalize the mass matrices in Eq. (1.23). In the last expression of Eq. (1.22), the mass eigenstates (u', d', and e') are related to the gauge symmetric eigenstates (u, d, and e) by unitary transformations[1]:

$$\begin{aligned} u_L^i &= U_u^{ij} u_L'^j, & d_L^i &= U_d^{ij} d_L'^j, & e_L^i &= U_e^{ij} e_L'^j, \\ u_R^i &= W_u^{ij} u_R'^j, & d_R^i &= W_d^{ij} d_R'^j, & e_R^i &= W_e^{ij} e_R'^j, \end{aligned} \tag{1.24}$$

and the diagonalized mass matrices, m_u', m_d', and m_e', are defined as

$$\begin{aligned} m_u'^{ij} &= U_u^{\dagger\, ik} m_u^{kl} W_u^{lj} = \frac{v_h}{\sqrt{2}} \cdot U_u^{\dagger\, ik} Y_u^{kl} W_u^{lj}, \\ m_d'^{ij} &= U_d^{\dagger\, ik} m_d^{kl} W_d^{lj} = \frac{v_h}{\sqrt{2}} \cdot U_d^{\dagger\, ik} Y_d^{kl} W_d^{lj}, \\ m_e'^{ij} &= U_e^{\dagger\, ik} m_e^{kl} W_e^{lj} = \frac{v_h}{\sqrt{2}} \cdot U_e^{\dagger\, ik} Y_e^{kl} W_e^{lj}, \end{aligned} \tag{1.25}$$

and the fermion masses are given by

$$m_u^i = m_u'^{ii}, \qquad m_d^i = m_d'^{ii}, \qquad m_e^i = m_e'^{ii}. \tag{1.26}$$

1.3 Renormalization Group Equation

Quantum Correction

In our universe, there are three constants having dimensions, the speed of light c, the Planck constant h, and the gravitational constant G_N. The units in the study of particle physics

$$\hbar = c = 1, \tag{1.27}$$

where $\hbar \equiv h/(2\pi)$, provide the relations among the fundamental units:

$$[\text{mass}] = [\text{energy}] = \left[\frac{1}{\text{time}}\right] = \left[\frac{1}{\text{length}}\right]. \tag{1.28}$$

The short time scale is equivalent to the high energy one, by which virtual particles are allowed to be created. The virtual particle creations play important roles in the perturbative theoretical calculation for finding the probability, "amplitude," of happening that interactions. The particle interactions can be generally described by a "n-point function" in a word of "Feynman diagram," in which all possible diagram corresponding

[1] The charge-changing weak interactions link the three u_L^i quarks with a unitary rotation of the triplet of d_L^i quarks. This rotation is given by using the unitary matrices in Eq. (1.24) as $V_{\text{CKM}} = U_u^\dagger U_d$, which is known as the Cabibbo-Kobayashi-Maskawa (CKM) mixing matrix.

to a considered energy scale should be taken into account in terms of orders of the coupling constant. However, once we consider all contributions from all energy scale, the number of diagrams are infinity, which causes the result of non-physical infinite value ("ultraviolet divergence") in the QFT, unless the series is to converge fortunately.

The meaningful physical quantities must be ones which have been already subtracted by the such divergence systematically, whose method is called "renormalization."

Callan-Symanzik Equation and Beta-function

Particle interactions can be described by the Green's function. In a language of the renormalization, if two theories are the same, their bare Green's functions with bare couplings and cutoff should be the same one. In general, when the energy scale by which the system is described is shifted, the renormalized n-point Green's function with n-external legs connected diagrams

$$G^{(n)}(x_1, \cdots, x_n) = \langle \Omega \, | T\phi(x_1)\phi(x_2)\phi(x_3)\cdots\phi(x_n) | \, \Omega \rangle_{\text{connected}} \tag{1.29}$$

keeps its bare Green's function the same. By shifting the field, $\phi \to (\phi + \delta\eta)\phi$, $G^{(n)}$ becomes $(1 + n\delta\eta)G^{(n)}$. If the Green's function is the function of a scale μ and a coupling λ,

$$dG^{(n)} = \frac{\partial G^{(n)}}{\partial \mu}\delta\mu + \frac{\partial G^{(n)}}{\partial \lambda}\delta\lambda = n\delta\eta G^{(n)}, \tag{1.30}$$

which finally means

$$\left[\mu\frac{\partial}{\partial \mu} + \beta(\lambda)\frac{\partial}{\partial \lambda} + n\gamma(\lambda)\right] G^{(n)}(x_1, x_2, x_3, \cdots ; \, \mu, \lambda) = 0. \tag{1.31}$$

This is called the Callan-Symanzik equation which insists that the Green's function is invariant under the change of the scale μ, where the coupling λ and the field ϕ are also simultaneously shifted through the β and γ functions

$$\begin{aligned} \beta &\equiv \mu\frac{d}{d\mu}\lambda, \\ \gamma &\equiv -\mu\frac{d}{d\mu}\eta. \end{aligned} \tag{1.32}$$

Thus the β function explains the behavior of the change of the renormalized coupling at the scale μ corresponding to a fixed bare coupling.

Running Coupling Constant

As explained, the strength of the interaction changes with respect to their distance, which means the coupling constant varies with respect to the energy scale (the running coupling constant). The behavior for the running of the coupling is described by the

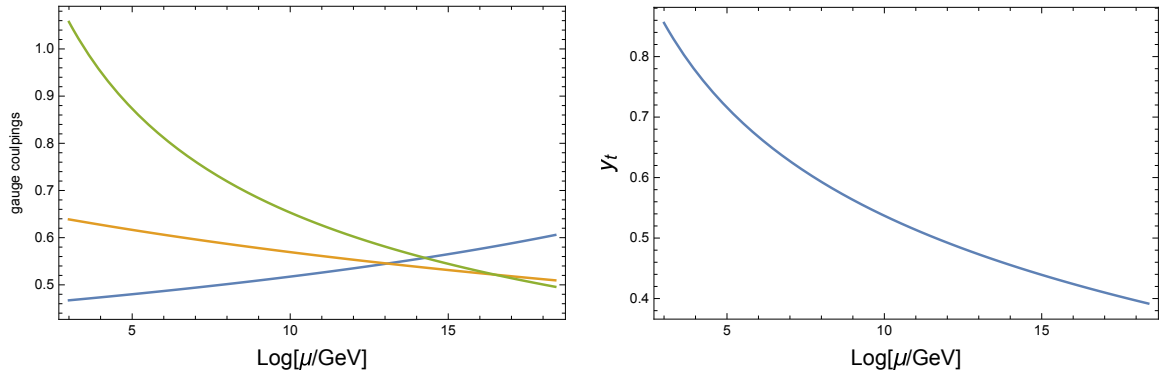

(a) (b)

Figure 1.1: (a) The RG evolutions of the gauge couplings g_1 (blue), g_2 (orange), and g_3 (green) for the inputs $m_t = 173.34$ GeV and $m_h = 125.09$ GeV. (b) The RG evolution of the top Yukawa coupling y_t.

words of renormalization, "Renormalization Group Equation (RGE)." The running couplings of the SM are governed by the corresponding RGEs. In order to know the behavior of the SM couplings, simultaneous differential equations for the SM RGEs should be solved [52]. In Fig. 1.1(a), For the inputs $m_t = 173.34$ GeV and $m_h = 125.09$ GeV, we plot the RG evolutions of the gauge couplings g_1 (blue), g_2 (orange), and g_3 (green) in Fig. 1.1(a), the top Yukawa coupling y_t in Fig. 1.1(b), and the SM Higgs quartic coupling λ_H in Fig. 1.2, in which the large top quark mass (Higgs mass) contributes the RGE negatively (positively). When the energy scale is increased, as we see from the Fig. 1.1(a), the Abelian gauge coupling g_1 is increased, which corresponds $\beta > 0$ (Screening effect). On the other hand, the non-Abelian gauge ones, g_3 and g_2, are decreased with $\beta < 0$ (Anti-screening effect), especially, the theory with a coupling constant going to zero at a logarithmic rate is called the "asymptotically free" theory.

1.4 Problems of the SM

The SM is a well-established theory to explain the phenomenology of the particle physics at low energy scale. However, the SM has several (serious) problems. For example, in the model, there are two different fundamental energy scale, the EW symmetry breaking scale 10^2 GeV and the Planck mass scale 10^19 GeV. The difference is really large about 10^17 which is a so-called “gauge hierarchy problem (Naturalness Problem).” The EW symmetry breaking scale also depends on the shape of Higgs potential. Adding quartic mass term in the Higgs potential is ad-hoc. The origin of the EW symmetry breaking, which also related to the Naturalness Problem, is not known within the framework of the SM. The shape of the Higgs effective potential dominantly depends on the top quark and the Higgs masses. As we discuss later, it is known that the current experimental data of the center values of these masses gives the negative Higgs quartic coupling around 10^10 GeV energy scale, which brings another problem of the EW vacuum instability.

The SM does not provide an answer to the question, why the neutrino mass is so

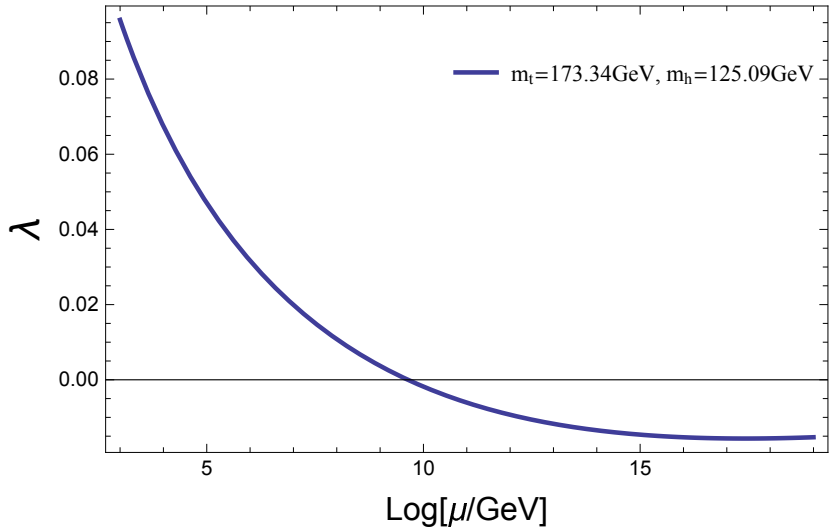

Figure 1.2: The evolution of the SM Higgs quartic coupling λ_H for the inputs $m_t = 173.34$ GeV and $m_h = 125.09$ GeV.

small comparing to other fermion masses (tiny neutrino mass problem). The smallness for the θ as a coefficient of a renormalizable $F\tilde{F}$ term is also one of the issue in the SM which related to the CP violation. This is called "strong CP problem."

From the cosmological observation, such as gravitational lens effect, the speed in the Galactic plane, and Cosmic Background Microwave (CMB), there exist Dark Matter (DM) and Dark Energy (DE) which are not ingredients of the SM. In addition, our universe consists of particles, not anti-particles, meaning "Baryon asymmetry" which cannot also be derived through the framework of the SM.

The SM is a gauge theory of $\mathrm{SU}(3)_C \times \mathrm{SU}(2)_L \times \mathrm{U}(1)_Y$ in which each gauge group has an independent parameter of coupling. In terms of the symmetry breaking, it is natural to think that the SM could be an effective theory which can be derived from higher rank gauge group, Grand Unified Theory (GUT) in which all three gauge coupling could have the same value at the GUT scale. The same sort of discussion can be said for the charges in the SM which cannot also take any arbitrary values in the framework of the SM. The SM does not also include gravitational effect in the Lagrangian. Some extensions with gravity should be implemented at high energy scale.

In the following subsections, we briefly review of the some issues which are mainly related to the studies of this thesis.

1.4.1 Instability of the Electroweak Vacuum with LHC Run-2 Results

In the SM, the RG evolution of the the Higgs quartic coupling is sensitive with the Higgs and the top quark masses. In the current experimental results from the Large Hadron Collider (LHC), the Higgs boson mass and top quark pole mass are reported by the ATLAS and CMS combined measurements [51] and the Tevatron and the LHC

combined measurements [53] as

$$\begin{aligned} m_h &= 125.09\ \text{GeV}, \\ m_t &= 173.34\ \text{GeV}, \end{aligned} \tag{1.33}$$

respectively. This indicates that the SM Higgs quartic coupling λ_H goes to negative around the $\mu = 10^{10}$ GeV scale, as we see in Fig. 1.2. The potential of the Higgs field becomes instable with the negative λ_H, where the effective potential of the Higgs field has a true vacuum at the high energy scale comparing to the EW one. In this Higgs potential, our vacuum will transit to the true vacuum with transitional time. This is called the EW vacuum instability problem. This might not be a problem in the framework of the SM if the life time of the universe is smaller than the time of vacuum transition which is proportional to the inverse of the decay rate. However, this does not work straightforwardly as we discuss in the context of the extension of the SM, in which our model has an extra Higgs field. With the extra Higgs field and the current experimental results of the masses of Higgs boson and top quark, the effective potential by the two Higgs fields should be a two-dimensional potential, where there might be a flat path toward to the true vacuum around the concave downward potential. In such case, the EW vacuum becomes instable.

1.4.2 Dark Matter

The energy budget of the universe is precisely determined by the Planck 2015 measurement [105],

$$\begin{aligned} \text{Dark Enargy}: &\quad 69\% \\ \text{Dark Matter}: &\quad 26\% \\ \text{Baryon}: &\quad 5\% \end{aligned} \tag{1.34}$$

Because there is no suitable dark matter (DM) candidate in the SM, which explains cosmological phenomena, such as the velocity distribution of the rotating Galaxy and the observed gravitational lens effect, the SM should be extended or revised in some way of the form including and/or connecting to the DM sector.

In general, it is known that the properties of the DM particle are electrically neutral, no interaction with the strong force, and non-relativistic. If the DM is a "weakly interacting massive particle (WIMP)," its mass may be considered around from the EW scale to the TeV scale, which can be detectable by the collider experiment after creating the DMs directly. If the the energy scale of the DM is close to that of the Higgs boson, the DM physics and the Higgs one are not irrelevant, in which it is possible that the DMs interact with the SM particles only through the Higgs mediation. The model is called the 'Higgs portal' scenario which has s-channel and t-channel processes. Later, the direct and the indirect detection will be discussed on the both channels.

1.4.3 Inflation (Problem of the Standard Big Bang Cosmology)

The Hubble's discovery on 1929 [130] about the relation between distance (d) and radial velocity (v) among extra-galactic nebulae, which provides an evidence of that

our universe is expanding by finding a following equation, the Hubble's law,

$$v = H \times d, \tag{1.35}$$

where H is the Hubble constant. In another words, our early universe is in a state of high temperature and high pressure.

The gravitational dynamics of the universe is governing by the Einstein equation,

$$G_{\mu\nu} = R_{\mu\nu} - \frac{1}{2} g_{\mu\nu} R + \Lambda g_{\mu\nu} = \frac{1}{M_{\rm P}^2} T_{\mu\nu} \tag{1.36}$$

with the reduced Planck mass $M_{\rm P} = M_{\rm Pl}/\sqrt{8\pi} = 2.44 \times 10^{18}$ GeV and the Planck mass $M_{\rm Pl} = 1/\sqrt{G_N} = 1.22 \times 10^{19}$ GeV, where $R_{\mu\nu}$ is the Ricci curvature tensor, R is the scalar curvature, $g_{\mu\nu}$ is the metric tensor, G_N is the Newton's gravitational constant, $T_{\mu\nu}$ is the stress-energy tensor. The left hand side defined by $G_{\mu\nu}$ shows the distortion of space-time. On the other hand, the right hand side $T_{\mu\nu}$ represents the energy of matter. Although the cosmological constant Λ is added by hand so as to make our universe dynamically static by Einstein, as we seen in the energy budget of the universe, Λ has become the necessary ingredient for describing dark energy.

In addition, the discovery of the Cosmic Microwave Background (CMB) also supports the Hubble's law. In the picture of the expanding universe, the necleosynthesis of each step depending on the temperature can naturally be explained. This is a called the "Big Bang Cosmology (BBC)" in which the "Big Bang Nucleosynthesis" occurs.

However, the standard BBC has several issues, such as the horizon problem, the flatness problem, the origin of the primordial density fluctuations, and unwanted relics from the grand unified theory (GUT), ex. monopole problem. The horizon problem indicated by Misner [131] is as following. In the standard BBC, the horizon means the distance where the light released from the big bang travels. This is the area having causality. However, the CMB indicates the flatness in all observed area which is exceeded from the area of horizon, which contradicts the causality. The flatness problem is firstly pointed out by Dicke in 1979. The spatial curvature of the current Universe is found to be very close to zero [105] (95% confidence level):

$$|\Omega_K| < 0.005, \tag{1.37}$$

where the Ω_K is the density parameter of the spacial curvature K, which satisfies the relation

$$\Omega_{\rm radiation} + \Omega_{\rm matter} + \Omega_\Lambda + \Omega_K = 1. \tag{1.38}$$

Because the Ω is proportional to $1/\dot{a}^2$, where a is a scale factor and a dot denotes a derivative with respect to time t, the initial value of the Ω grows gradually faster with the evolution of time. In order to generate the current tiny value of Ω_K, the initial value of it should be much smaller than the current one. This brings about unnatural "super- tunning" at the early universe.

Another problem is coming from the symmetry breaking of the GUT, in which there is an extremely heavy and stable monopole mass around 10^{16} GeV. This is an unwanted relics needed to be diluted. In addition, to create the observed large structure of the

universe, its origin should generate the primordial density fluctuations. Among these problems, introducing a long-term period of acceleration at the early universe, which is called the "inflation" can provide a solution. In the framework of the inflation, the points inside the horizon can be separated beyond the horizon, and the density parameter of spacial curvature Ω_K can go to zero (flat). In a same way, during the inflational expansion of the early universe, the number density of the monopole decreases exponentially, in which the probability of finding of the monopole is astronomically small.

Chapter 2

Classically conformal U(1)′ extended SM

In this chapter, we consider the minimal U(1)′ extension of the standard model (SM) with the classically conformal invariance, where an anomaly-free U(1)′ gauge symmetry is introduced along with three generations of right-handed neutrinos and a U(1)′ Higgs field. Since the classically conformal symmetry forbids all dimensional parameters in the model, the U(1)′ gauge symmetry is broken by the Coleman-Weinberg mechanism, generating the mass terms of the U(1)′ gauge boson (Z' boson) and the right-handed neutrinos. Through a mixing quartic coupling between the U(1)′ Higgs field and the SM Higgs doublet field, the radiative U(1)′ gauge symmetry breaking also triggers the breaking of the electroweak symmetry. In this model context, we first investigate the electroweak vacuum instability problem in the SM. Next we interpret the ATLAS and CMS search limits at the LHC Run-2 2015 for the sequential Z' boson to constrain the parameter region in our model. We also calculate self-energy corrections to the SM Higgs doublet field through the heavy states, the right-handed neutrinos and the Z' boson.

This chapter is organized as follows: The classically conformal U(1)′ extended SM is defined in Sec. 2.1. In Sec. 2.2, we discuss the radiative U(1)′ symmetry breaking through the Coleman-Weinberg mechanism. The electroweak symmetry breaking triggered by the radiative U(1)′ gauge symmetry breaking is discussed in Sec. 2.3. In Sec. 2.4, we analyze the renormalization group (RG) evolutions of the couplings at the two-loop level and find a region in three dimensional parameter space which can resolve the electroweak vacuum instability and keep all parameters in the perturbative regime up to the Planck mass. In Sec. 2.5, we analyze the collider bounds of the model parameters; in particular, the ATLAS and CMS results of the search for the Z' boson resonance at the LHC Run-2 2015 are interpreted in the Z' boson case of our model. In Sec. 2.6, we evaluate self-energy corrections to the SM Higgs doublet from the effective potential and derive the naturalness bounds to reproduce the electroweak scale for a fine-tuning level better than 10%. We summarize our results in Sec. 2.7.

	$\mathrm{SU}(3)_c$	$\mathrm{SU}(2)_L$	$\mathrm{U}(1)_Y$	$\mathrm{U}(1)'$		
q_L^i	**3**	**2**	$+1/6$	x_q	$=$	$\frac{1}{3}x_H + \frac{1}{6}x_\Phi$
u_R^i	**3**	**1**	$+2/3$	x_u	$=$	$\frac{4}{3}x_H + \frac{1}{6}x_\Phi$
d_R^i	**3**	**1**	$-1/3$	x_d	$=$	$-\frac{2}{3}x_H + \frac{1}{6}x_\Phi$
ℓ_L^i	**1**	**2**	$-1/2$	x_ℓ	$=$	$-x_H - \frac{1}{2}x_\Phi$
ν_R^i	**1**	**1**	0	x_ν	$=$	$-\frac{1}{2}x_\Phi$
e_R^i	**1**	**1**	-1	x_e	$=$	$-2x_H - \frac{1}{2}x_\Phi$
H	**1**	**2**	$+1/2$	x_H	$=$	x_H
Φ	**1**	**1**	0	x_Φ	$=$	x_Φ

Table 2.1: Particle contents. In addition to the SM particle contents, the right-handed neutrino ν_R^i ($i = 1, 2, 3$ denotes the generation index) and a complex scalar Φ are introduced.

2.1 Classically conformal U(1)′ extended SM

The model we investigate is the anomaly-free $\mathrm{U}(1)'$ extension of the SM with the classically conformal invariance, which is based on the gauge group $\mathrm{SU}(3)_C \times \mathrm{SU}(2)_L \times \mathrm{U}(1)_Y \times \mathrm{U}(1)'$. The particle contents of the model are listed in Table 2.1. In addition to the SM particle content, three generations of right-hand neutrinos ν_R^i and a $\mathrm{U}(1)'$ Higgs field Φ are introduced. The covariant derivatives relevant to $\mathrm{U}(1)_Y \times \mathrm{U}(1)'$ are defined as

$$D_\mu \equiv \partial_\mu - i \begin{pmatrix} Y_1 & Y_X \end{pmatrix} \begin{pmatrix} g_1 & g_{1X} \\ g_{X1} & g_X \end{pmatrix} \begin{pmatrix} B_\mu \\ B'_\mu \end{pmatrix}, \tag{2.1}$$

where Y_1 (Y_X) are $\mathrm{U}(1)_Y$ ($\mathrm{U}(1)'$) charge of a particle, and the gauge couplings g_{X1} and g_{1X} are introduced associated with a kinetic mixing between the two U(1) gauge bosons.

For generation-independent charge assignments, the $\mathrm{U}(1)'$ charges of the fermions are defined to satisfy the gauge and gravitational anomaly-free conditions:

$$\begin{aligned}
\mathrm{U}(1)' \times [\mathrm{SU}(3)_C]^2 &: & 2x_q - x_u - x_d &= 0, \\
\mathrm{U}(1)' \times [\mathrm{SU}(2)_L]^2 &: & 3x_q + x_\ell &= 0, \\
\mathrm{U}(1)' \times [\mathrm{U}(1)_Y]^2 &: & x_q - 8x_u - 2x_d + 3x_\ell - 6x_e &= 0, \\
[\mathrm{U}(1)']^2 \times \mathrm{U}(1)_Y &: & x_q^2 - 2x_u^2 + x_d^2 - x_\ell^2 + x_e^2 &= 0, \\
[\mathrm{U}(1)']^3 &: & 6x_q^3 - 3x_u^3 - 3x_d^3 + 2x_\ell^3 - x_\nu^3 - x_e^3 &= 0, \\
\mathrm{U}(1)' \times [\mathrm{grav.}]^2 &: & 6x_q - 3x_u - 3x_d + 2x_\ell - x_\nu - x_e &= 0.
\end{aligned} \tag{2.2}$$

In order to reproduce observed fermion masses and flavor mixings, we introduce the following Yukawa interactions:

$$\mathcal{L}_{\mathrm{Yukawa}} = -Y_u^{ij} \overline{q_L^i} \tilde{H} u_R^j - Y_d^{ij} \overline{q_L^i} H d_R^j - Y_\nu^{ij} \overline{\ell_L^i} \tilde{H} \nu_R^j - Y_e^{ij} \overline{\ell_L^i} H e_R^j - Y_M^i \Phi \overline{\nu_R^{ic}} \nu_R^i + \mathrm{h.c.}, \tag{2.3}$$

(x_H, x_Φ)	the U(1)′ extended SM
$(0, 2)$	the $\mathrm{U}(1)_{B-L}$ model
$(-1, 2)$	the $\mathrm{U}(1)_R$ model
$(-16/41, 2)$	the orthogonal model

Table 2.2: Model chart of the U(1)′ extended SM in the (x_H, x_Φ) parameter space. x_H and x_Φ are the U(1)′ charges of H and Φ, respectively.

where $\tilde{H} \equiv i\tau^2 H^*$, and the third and fifth terms on the right-hand side are for the see-saw mechanism to generate neutrino masses. These Yukawa interaction terms impose

$$\begin{aligned} x_H &= -x_q + x_u = x_q - x_d = -x_\ell + x_\nu = x_\ell - x_e, \\ x_\Phi &= -2x_\nu. \end{aligned} \tag{2.4}$$

Solutions to these conditions are listed in Table 2.1 and are controlled by only two parameters, x_H and x_Φ. The two parameters reflect the fact that the U(1)′ gauge group can be defined as a linear combination of the SM $\mathrm{U}(1)_Y$ and the $\mathrm{U}(1)_{B-L}$ gauge groups. Since the U(1)′ gauge coupling g_X is a free parameter of the model and it always appears as a product $x_\Phi g_X$ or $x_H g_X$, we fix $x_\Phi = 2$ without loss of generality throughout this thesis. This convention excludes the case in which the U(1)′ gauge group is identical to the SM $\mathrm{U}(1)_Y$. In Table 2.2, some typical U(1)′ extended SMs determined by the choice of (x_H, x_Φ) parameters are listed. The choice of $(x_H, x_\Phi) = (0, 2)$ corresponds to the $\mathrm{U}(1)_{B-L}$ model. Another example is $(x_H, x_\Phi) = (-1, 2)$, which corresponds to the SM with the so-called $\mathrm{U}(1)_R$ symmetry. When we choose $(x_H, x_\Phi) = (-16/41, 2)$, the beta function of g_{X1} (g_{1X}) at the 1-loop level only has terms proportional to g_{X1} (g_{1X}) (see Appendix B.1). This is the orthogonal condition between the $\mathrm{U}(1)_Y$ and U(1)′ at the 1-loop level, under which g_{X1} and g_{1X} do not evolve once we have set $g_{X1} = g_{1X} = 0$ at an energy scale. Although it is slightly modified (x_H becomes slightly larger than $-16/41$), we find that the choice of $(x_H, x_\Phi) = (-16/41, 2)$ is a good approximation even at the 2-loop level[1].

Imposing the classically conformal invariance, the scalar potential is given by

$$V = \lambda_H \left(H^\dagger H\right)^2 + \lambda_\Phi \left(\Phi^\dagger \Phi\right)^2 + \lambda_{\mathrm{mix}} \left(H^\dagger H\right)\left(\Phi^\dagger \Phi\right), \tag{2.5}$$

where the mass terms are forbidden by the conformal invariance. If λ_{mix} is negligibly small, we can analyze the Higgs potential separately for Φ and H as a good approximation. This will be justified in the following sections. When the Majorana Yukawa couplings Y_M^i are negligible compared to the U(1)′ gauge coupling, the Φ sector is identical to the original Coleman-Weinberg model [2], so the radiative U(1)′ symmetry breaking will be achieved. Once Φ develops a vacuum expectation value (VEV) through the Coleman-Weinberg mechanism, the tree-level mass term for the SM Higgs

[1] Even if we choose $(x_H, x_\Phi) = (-16/41, 2)$ and calculate the RG evolution of g_{X1} (g_{1X}) at the 2-loop level, g_{X1} (g_{1X}) evolves less than $\mathcal{O}(10^{-5})$ at the Planck scale once we have set $g_{X1} = g_{1X} = 0$ at $v_\phi \gtrsim 10$ TeV.

is effectively generated through $\lambda_{\rm mix}$ in Eq. (2.5). Taking $\lambda_{\rm mix}$ to be negative, the induced mass squared for the Higgs doublet is negative and, as a result, the electroweak symmetry breaking is driven in the same way as in the SM.

2.2 Radiative U(1)′ gauge symmetry breaking

Assuming $\lambda_{\rm mix}$ is negligibly small, we first analyze the U(1)′ Higgs sector. Without mass terms, the Coleman-Weinberg potential [2] at the 1-loop level is found to be

$$V(\phi) = \frac{\lambda_\Phi}{4}\phi^4 + \frac{\beta_\Phi}{8}\phi^4\left(\ln\left[\frac{\phi^2}{v_\phi^2}\right] - \frac{25}{6}\right), \tag{2.6}$$

where $\phi/\sqrt{2} = \Re[\Phi]$ which extracts a real part of Φ, and we have chosen the renormalization scale to be the VEV of Φ ($\langle\phi\rangle = v_\phi$). Here, the coefficient of the 1-loop quantum corrections is given by

$$\begin{aligned}\beta_\Phi &= \frac{1}{16\pi^2}\left[20\lambda_\Phi^2 + 6x_\Phi^4\left(g_{X1}^2 + g_X^2\right)^2 - 16\sum_i (Y_M^i)^4\right] &(2.7)\\ &\simeq \frac{1}{16\pi^2}\left[6\left(x_\Phi g_X\right)^4 - 16\sum_i (Y_M^i)^4\right], &(2.8)\end{aligned}$$

where in the last expression, we have used $\lambda_\Phi^2 \ll (x_\Phi g_X)^4$ as usual in the Coleman-Weinberg mechanism and set $g_{X1} = g_{1X} = 0$ at $\langle\phi\rangle = v_\phi$, for simplicity. The stationary condition $dV/d\phi|_{\phi=v_\phi} = 0$ leads to

$$\lambda_\Phi = \frac{11}{6}\beta_\Phi, \tag{2.9}$$

and this λ_Φ is nothing but a renormalized self-coupling at v_ϕ defined as

$$\lambda_\Phi = \frac{1}{3!}\left.\frac{d^4V(\phi)}{d\phi^4}\right|_{\phi=v_\phi}. \tag{2.10}$$

For more detailed discussion, see [19].

Associated with this radiative U(1)′ symmetry breaking (as well as the electroweak symmetry breaking), the U(1)′ gauge boson (Z' boson) and the right-handed Majorana neutrinos acquire their masses as

$$m_{Z'} = \sqrt{(x_\Phi g_X v_\phi)^2 + (x_H g_X v_h)^2} \simeq x_\Phi g_X v_\phi, \quad m_{N^i} = \sqrt{2}Y_M^i v_\phi, \tag{2.11}$$

where $v_h = 246$ GeV is the SM Higgs VEV, and we have used $x_\Phi v_\phi \gg x_H v_h$, which will be verified below. In this chapter, we assume degenerate masses for the three Majorana neutrinos, $Y_M^i = y_M$ (equivalently, $m_{N^i} = m_N$) for all $i = 1, 2, 3$, for simplicity. The U(1)′ Higgs boson mass is given by

$$\begin{aligned}m_\phi^2 &= \left.\frac{d^2V}{d\phi^2}\right|_{\phi=v_\phi} = \beta_\Phi v_\phi^2 \simeq \frac{3}{8\pi^2}\left(\left(x_\Phi g_X\right)^4 - 8y_M^4\right)v_\phi^2\\ &\simeq \frac{3}{8\pi^2}\frac{m_{Z'}^4 - 2m_N^4}{v_\phi^2} \simeq \frac{6}{\pi}\alpha_{g_X} m_{Z'}^2\left(1 - 2\left(\frac{m_N}{m_{Z'}}\right)^4\right), &(2.12)\end{aligned}$$

where $\alpha_{g_X} = g_X^2/(4\pi)$. When the Yukawa coupling is negligibly small, this equation reduces to the well-known relation derived in the original paper by Coleman-Weinberg [2]. For a sizable Majorana mass, this formula indicates that the potential minimum disappears for $m_N > m_{Z'}/2^{1/4}$, so there is an upper bound on the right-handed neutrino mass for the U(1)′ symmetry to be broken radiatively. This is in fact the same reason why the Coleman-Weinberg mechanism in the SM Higgs sector fails to break the electroweak symmetry when the top Yukawa coupling is large, as observed. In order to avoid the destabilization of the U(1)′ Higgs potential, we simply set $m_{Z'}^4 \gg m_N^4$ in the following analysis. Note that this condition does not mean that the Majorana neutrinos must be very light, even though a factor difference between $m_{Z'}$ and m_N is enough to satisfy the condition. For simplicity, we set $y_M = 0$ at v_ϕ in the following RG analysis.

2.3 Electroweak symmetry breaking

Let us now consider the SM Higgs sector. In our model, the electroweak symmetry breaking is achieved in a very simple way. Once the U(1)′ symmetry is radiatively broken, the SM Higgs doublet mass is generated through the mixing quartic term between H and Φ in the scalar potential in Eq. (2.5),

$$V(h) = \frac{\lambda_H}{4} h^4 + \frac{\lambda_{\rm mix}}{4} v_\phi^2 h^2, \tag{2.13}$$

where we have replaced H by $H = 1/\sqrt{2}\,(0,\, h)^T$ in the unitary gauge. Choosing $\lambda_{\rm mix} < 0$, the electroweak symmetry is broken in the same way as in the SM [40, 41]. However, we should note that a crucial difference from the SM is that in our model the electroweak symmetry breaking originates from the radiative breaking of the U(1)′ gauge symmetry. At the tree level, the stationary condition $V'|_{h=v_h} = 0$ leads to the relation $|\lambda_{\rm mix}| = 2\lambda_H (v_h/v_\phi)^2$, and the Higgs boson mass m_h is given by

$$m_h^2 = \left.\frac{d^2 V}{dh^2}\right|_{h=v_h} = |\lambda_{\rm mix}| v_\phi^2 = 2\lambda_H v_h^2. \tag{2.14}$$

In the following RG analysis, this is used as the boundary condition for $\lambda_{\rm mix}$ at the renormalization scale $\mu = v_\phi$. Note that since $\lambda_H \sim 0.1$ and $v_\phi \gtrsim 10$ TeV by the large electron-positron collider (LEP) constraint [132–135], $|\lambda_{\rm mix}| \lesssim 10^{-5}$, which is very small.

In our discussion about the U(1)′ symmetry breaking, we neglected $\lambda_{\rm mix}$ by assuming it to be negligibly small. Here we justify this treatment. In the presence of $\lambda_{\rm mix}$ and the Higgs VEV, Eq. (2.9) is modified as

$$\lambda_\Phi = \frac{11}{6}\beta_\Phi + \frac{|\lambda_{\rm mix}|}{2}\left(\frac{v_h}{v_\phi}\right)^2 \simeq \frac{1}{2v_\phi^4}\left(\frac{11}{8\pi^2} m_{Z'}^4 + m_h^2 v_h^2\right). \tag{2.15}$$

Considering the LHC Run-2 2015 bound from the search for Z' boson resonances [55, 56], $m_{Z'} \gtrsim 3$ TeV, we find that the first term in the parentheses in the last equality is 5 orders of magnitude greater than the second term, and therefore we can analyze the two Higgs sectors separately.

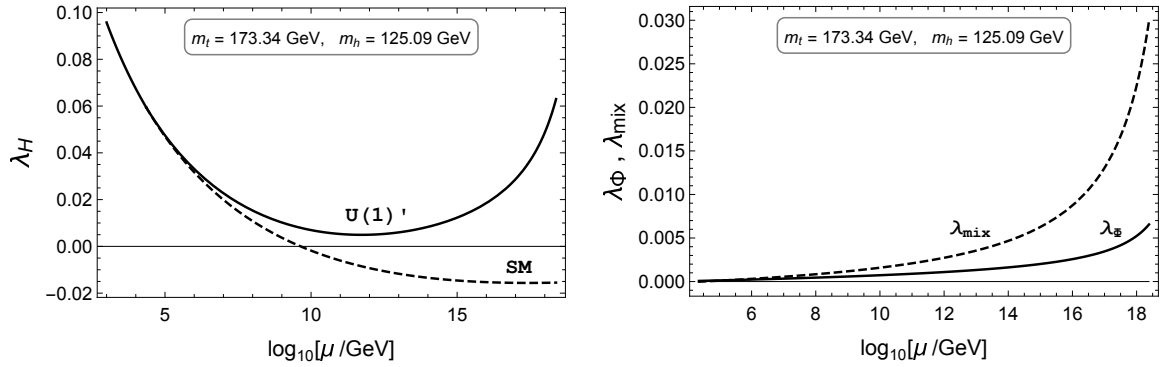

(a) (b)

Figure 2.1: (a) The evolutions of the Higgs quartic coupling λ_H (solid line) for the inputs $m_t = 173.34$ GeV and $m_h = 125.09$ GeV, along with the SM case (dashed line). (b) The RG evolutions of λ_Φ (solid line) and $\lambda_{\rm mix}$ (dashed line). Here, we have taken $x_H = 2$, $v_\phi = 23$ TeV and $g_X(v_\phi) = 0.09$.

2.4 Solving the SM Higgs vacuum instability

In the SM with the observed Higgs boson mass of $m_h = 125.09$ GeV, the RG evolution of the SM Higgs quartic coupling shows that the running coupling becomes negative at the intermediate scale $\mu \simeq 10^{10}$ GeV [52] for $m_t = 173.34$ GeV, and hence the electroweak vacuum is unstable. In this section, we investigate RG evolution of the Higgs quartic coupling and a possibility to solve the Higgs vacuum instability problem in our U(1)′ extended SM. Without the classical conformal invariance, Ref. [136, 137] (see also [138]) has considered the same problem, and identified parameter regions which can resolve the Higgs vacuum instability. A crucial difference in our model is that because of the classical conformal invariance and the symmetry breaking by the Coleman-Weinberg mechanism, the initial values of λ_Φ and $\lambda_{\rm mix}$ at v_ϕ are not free parameters. Therefore, it is nontrivial to resolve the Higgs vacuum instability in the present model. The Higgs vacuum stability has been investigated in [19] for the classically conformal extension of the SM with an extend gauge group and particle content including a dark matter candidate.

In our RGE analysis, we employ the SM RGEs at the 2-loop level [52] from the top pole mass to the U(1)′ Higgs VEV, and connect the RGEs to those of the U(1)′ extended SM at the 2-loop level, which are generated by using SARAH [139, 140]. RGEs used in our analysis are listed in the appendices. For inputs of the Higgs boson mass and top quark pole mass, we employ a central value of the ATLAS and CMS combined measurement $m_h = 125.09$ GeV [51], while $m_t = 173.34$ GeV is the central value of combined results of the Tevatron and the LHC measurements of top quark mass [53]. There are only three free parameters in our model, by which inputs at v_ϕ are determined: x_H, v_ϕ, and g_X.

In Fig. 2.1(a), we show the RG evolution of the SM Higgs quartic coupling in our model (solid line), along with the SM result (dashed line). Here, we have taken $x_H = 2$, $v_\phi = 23$ TeV, and $g_X(v_\phi) = 0.09$ as an example. Recall that we have fixed $x_\Phi = 2$ without loss of generality. The Higgs quartic coupling remains positive all the way

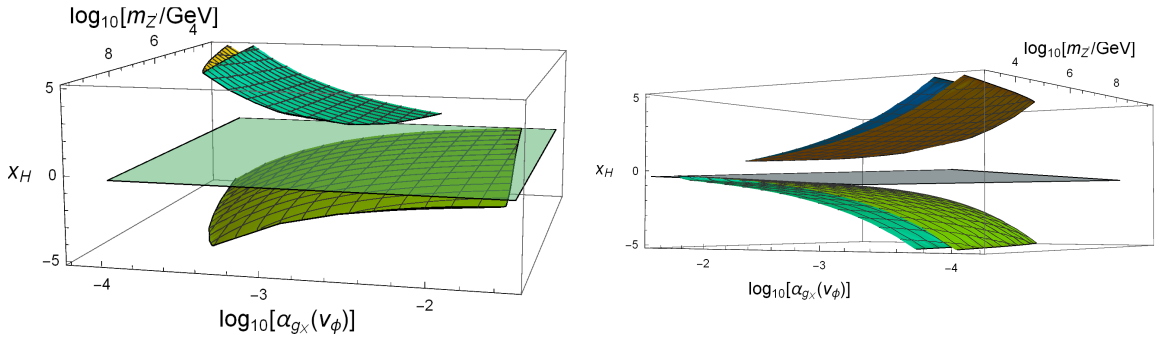

(a) (b)

Figure 2.2: (a) The result of the three-dimensional parameter scans for v_ϕ, g_X and x_H, shown in $(m_{Z'}(\mathrm{GeV}), \alpha_{g_X}, x_H)$ parameter space with $m_{Z'} \simeq x_\Phi g_X v_\phi$, by using the inputs $m_t = 173.34$ GeV and $m_h = 125.09$ GeV. As a reference, a horizontal plane for $x_H = -16/41$ is shown, which corresponds to the orthogonal case. There are two separated regions of solving the electroweak vacuum instability and satisfying the perturbative conditions inside very thin curved layers above and below the plane of the orthogonal case. (b) Same three-dimensional parameter scans as (a), but at a different angle.

up to the Planck mass, so the Higgs vacuum instability problem is solved. There are complex, synergetic effects in the coupled RGEs to resolve the Higgs vacuum instability (see the appendices for RGEs). For example, the $\mathrm{U}(1)_Y$ gauge coupling grows faster than the SM case in the presence of the mixing gauge couplings g_{X1} and g_{1X}, which makes the evolution of top Yukawa coupling decrease faster than in the SM case. The evolution of the mixing gauge coupling is controlled by the $\mathrm{U}(1)'$ gauge coupling. Both of them are asymptotic nonfree. The gauge couplings positively contribute to the beta function of the SM Higgs quartic coupling, while the top Yukawa coupling gives a negative contribution. As a result, the RG evolutions of the gauge and top Yukawa couplings work to change the sign of the beta function of the SM Higgs quartic coupling at $\mu \simeq 10^{12}$ GeV in Fig. 2.1(a). Figure 2.1(b) shows the RG evolutions of the other Higgs quartic couplings. Note that the input of λ_Φ and λ_{mix} is very small because of the radiative gauge symmetry breaking, and the two couplings remain very small even at the Planck mass. Thus, the positive contribution of λ_{mix} to the beta function of the SM Higgs quartic coupling is negligible. This is in sharp contrast to U(1) extended models without the conformal invariance, where λ_{mix} is a free parameter and we can take its input to give a large, positive contribution to the beta function; thus, the Higgs vacuum instability problem is relatively easier to solve.

In order to identify a parameter region to resolve the Higgs vacuum instability, we perform parameter scans for the free parameters x_H, v_ϕ and g_X. In this analysis, we impose several conditions on the running couplings at $v_\phi \leq \mu \leq M_P$ ($M_P = 2.44 \times 10^{18}$ GeV is the reduced Planck mass): stability conditions of the Higgs potential ($\lambda_H, \lambda_\Phi > 0$), and the perturbative conditions that all the running couplings remain in the perturbative regime, namely, g_i^2 $(i = 1, 2, 3)$, g_X^2, g_{X1}^2, $g_{1X}^2 < 4\pi$ and λ_H, λ_Φ, $\lambda_{\mathrm{mix}} < 4\pi$. For theoretical consistency, we also impose a condition that the 2-loop beta

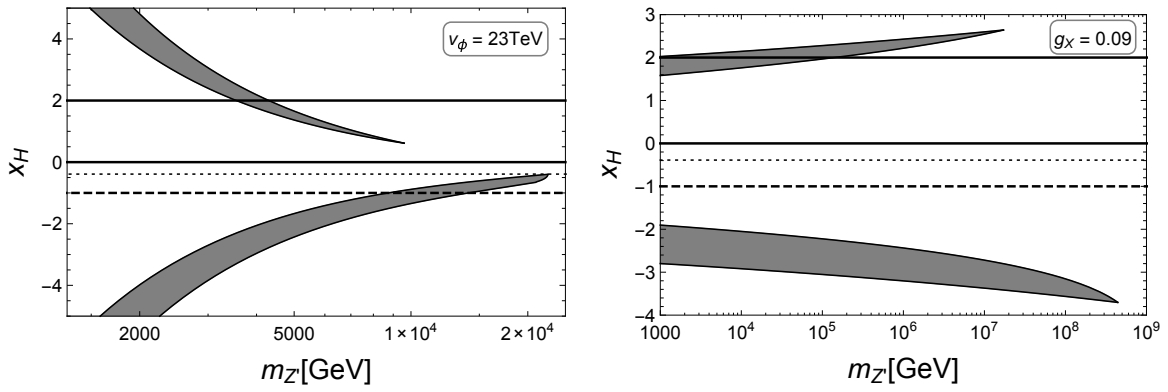

(a) (b)

Figure 2.3: (a) The result of parameter scan for x_H and g_X with a fixed $v_\phi = 23$ TeV, shown in the $(m_{Z'}, x_H)$ plane with $m_{Z'} \simeq x_\Phi g_X v_\phi$. The shaded regions depict the parameters to resolve the electroweak vacuum instability and satisfy the perturbative conditions. As a reference, horizontal lines are depicted for $x_H = 2$, 0 [$\mathrm{U}(1)_{B-L}$ case], $-16/41$ [orthogonal case], and -1 [$\mathrm{U}(1)_R$ case]. (b) Same as (a), but for a parameter scan for x_H and v_ϕ with a fixed $g_X = 0.09$.

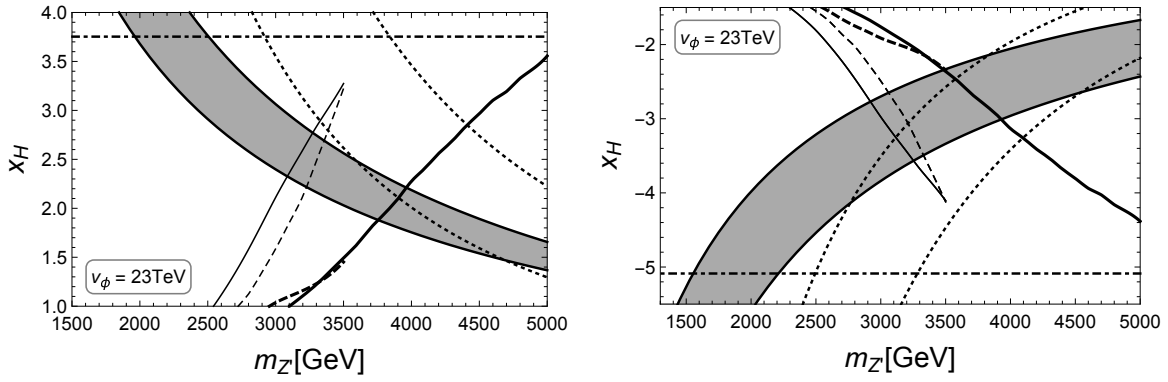

(a) (b)

Figure 2.4: (a) The allowed positive x_H region at the TeV scale in Fig. 2.3(a) is magnified, along with the LEP bound (dashed-dotted line), the LHC Run-1 CMS bound (thin dashed line), the LHC Run-1 ATLAS bound (thin solid line), the LHC Run-2 CMS 2015 bound (thick dashed line) and the LHC Run-2 ATLAS 2015 bound (thick solid line) from a direct search for Z' boson resonance. The region on the left side of the lines is excluded. Here, the naturalness bounds for 10% (right dotted line) and 30% (left dotted line) fine-tuning levels are also depicted. (b) Same as (a), but for the negative x_H region.

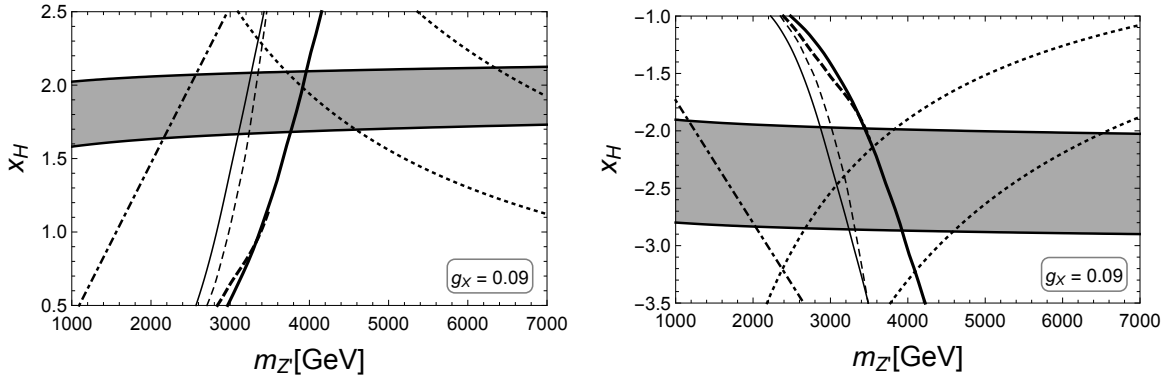

(a) (b)

Figure 2.5: (a) Same as Fig. 2.4(a), but magnifying Fig. 2.3(b). (b) Same as Fig. 2.4(b), but magnifying Fig. 2.3(b).

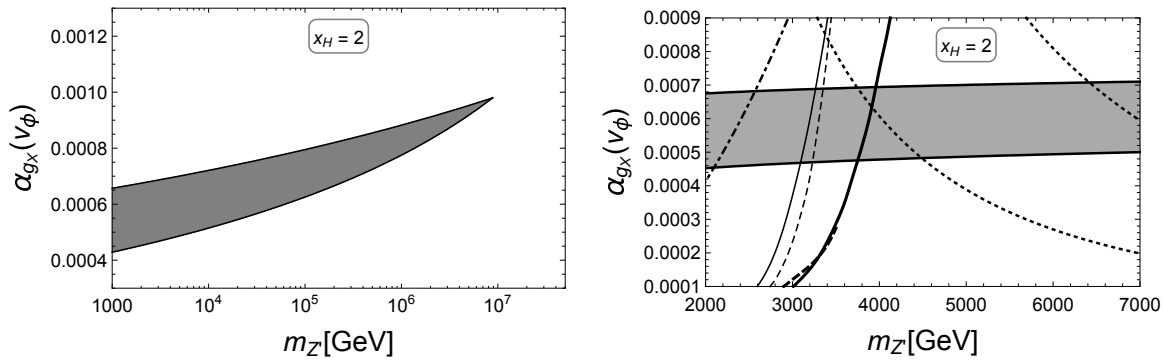

(a) (b)

Figure 2.6: (a) The result of parameter scan for v_ϕ and g_X with a fixed $x_H = 2$ in the $(m_{Z'}, \alpha_{g_X})$ plane. The shaded region depicts the parameters to resolve the electroweak vacuum instability and satisfy the perturbative conditions. (b) The allowed region at the TeV scale in (a) is magnified, along with the LEP bound (dashed-dotted line), the LHC Run-1 CMS bound (thin dashed line), the LHC Run-1 ATLAS bound (thin solid line), the LHC Run-2 CMS 2015 bound (thick dashed line) and the LHC Run-2 ATLAS 2015 bound (thick solid line) from direct search for Z' boson resonance. The region on the left side of the lines is excluded. Here, the naturalness bounds for 10% (right dotted line) and 30% (left dotted line) fine-tuning levels are also depicted.

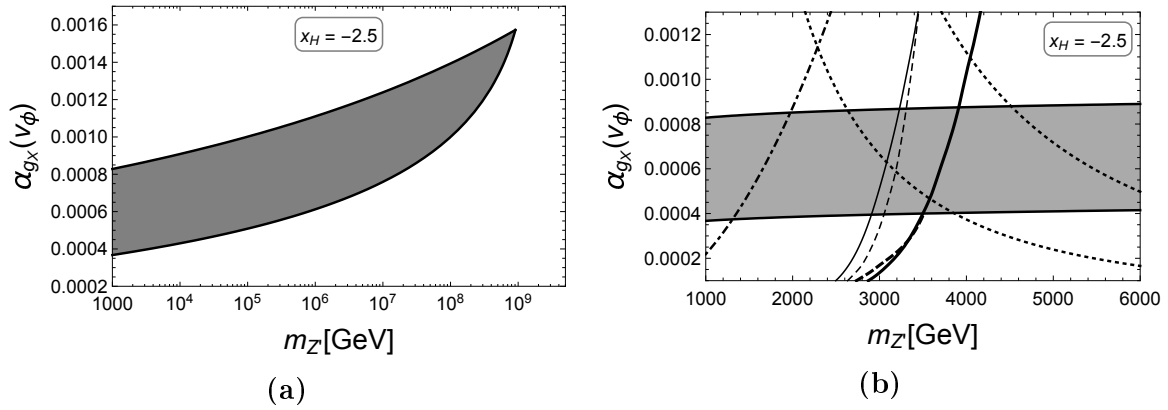

Figure 2.7: (a) Same as Fig. 2.6(a), but for $x_H = -2.5$. (b) Same as Fig. 2.6(b), but for $x_H = -2.5$.

functions are smaller than the 1-loop beta functions. In Fig. 2.2, we show the result of our parameter scans in the three-dimensional parameter space of $(m_{Z'}, \alpha_{g_X}, x_H)$, where $\alpha_{g_X} = g_X^2/(4\pi)$. As a reference, we show a horizontal plane corresponding to the orthogonal case $x_H = -16/41$. There are two separated regions of solving the electroweak vacuum instability and satisfying the perturbative conditions inside very thin curved layers above and below the plane of the orthogonal case. There is no overlapping of the plane with the resultant parameter regions to resolve the electroweak vacuum instability.

In order to discuss our results in detail, we show in Figs. 2.3-2.7 the parameter scan results on several two-dimensional hypersurfaces in the 3D plot of Fig. 2.2. The shaded regions in Figs. 2.3-2.7 depict the parameters to resolve the electroweak vacuum instability and satisfy the perturbative conditions. In Fig. 2.3, our results are shown for x_H and g_X with a fixed $v_\phi = 23$ TeV (a) and for x_H and v_ϕ with a fixed $g_X = 0.09$ (b) in the $(m_{Z'}, x_H)$ plane, along with the horizontal lines corresponding to $x_H =$ 2, 0 [U(1)$_{B-L}$ case], $-16/41$ [orthogonal case], and -1 [U(1)$_R$ case]. We can see that the resultant parameter space is very restricted. For example, the Higgs vacuum instability cannot be resolved in the classically conformal U(1)$_{B-L}$ extended SM or the classically conformal orthogonal U(1) extended SM, for the inputs $m_t = 173.34$ GeV and $m_h = 125.09$ GeV. The allowed regions at the TeV scale in Figs. 2.3(a) and 2.3(b) are magnified in Figs. 2.4 and 2.5, respectively. Here we also show the collider bounds, namely, the LEP bounds (dashed-dotted lines) [132–135], the CMS bounds at the LHC Run-1 (thin dashed lines) [141, 142], the ATLAS bounds at the LHC Run-1 (thin solid lines) [143], the CMS bounds at the LHC Run-2 2015 (thick dashed lines) [56], and the ATLAS bounds at the LHC Run-2 2015 (thick solid lines) [55], from the search for Z' boson mediated processes, which will be obtained in the next section. The region on the left side of the lines is excluded. Naturalness bounds (dotted lines), which will be obtained in Sec. 2.6, are also shown. These naturalness bounds for the 10% fine-tuning level are found to be compatible with the bounds obtained by the LHC Run-2 2015 results. The result of parameter scan for v_ϕ and α_{g_X} with a fixed $x_H = 2$ is depicted in Fig. 2.6(a), and the allowed region at the TeV scale is magnified in Fig. 2.6(b), along with the collider and naturalness bounds. Same plots as Fig. 2.6 but for $x_H = -2.5$

are shown in Fig. 2.7.

2.5 LHC bounds on the U(1)′ Z' boson

The ATLAS and the CMS Collaborations have searched for Z' boson resonance at the LHC Run-1 with $\sqrt{s} = 8$ TeV, and continued the search at the LHC Run-2 with $\sqrt{s} = 13$ TeV. The most stringent bounds on the Z' boson production cross section times branching ratio have been obtained by using the dilepton final state. For the so-called sequential SM Z' (Z'_{SSM}) model [144], where the Z'_{SSM} boson has exactly the same couplings with the SM fermions as those of the SM Z boson, the cross section bounds from the LHC Run-1 results lead to lower bounds on the Z'_{SSM} boson mass as $m_{Z'_{SSM}} \geq 2.90$ TeV in the ATLAS Run-1[2] results [143] and $m_{Z'_{SSM}} \geq 2.96$ TeV in the CMS Run-1[3] results [141, 142], respectively. In 2015, these bounds have been updated by the ATLAS and CMS analysis with the LHC Run-2 at $\sqrt{s} = 13$ TeV as $m_{Z'_{SSM}} \geq 3.4$ TeV (ATLAS 2015[4] [55]) and $m_{Z'_{SSM}} \geq 3.15$ TeV (CMS 2015[5] [56]), respectively. Furthermore, in 2016, the cross section bounds from the LHC Run-2 2016 results have continued to update lower bounds on the Z'_{SSM} boson mass as $m_{Z'_{SSM}} \geq 4.05$ TeV (ATLAS 2016[6] [145]) and $m_{Z'_{SSM}} \geq 4.0$ TeV (CMS 2016[7] [146]), respectively. In 2017, the cross section bound from the LHC Run-2 ATLAS 2017[8] results [128] leads to lower bounds on the Z'_{SSM} boson mass as $m_{Z'_{SSM}} \geq 4.5$ TeV. We interpret these ATLAS and CMS results in the U(1)′ Z' boson case and derive an upper bound on x_H or α_{g_X} as a function of $m_{Z'}$.

We calculate the dilepton production cross section for the process $pp \to Z' + X \to \ell^+\ell^- + X$. The differential cross section with respect to the invariant mass $M_{\ell\ell}$ of the final state dilepton is described as

$$\frac{d\sigma}{dM_{\ell\ell}} = \sum_{a,b} \int_{\frac{M^2_{\ell\ell}}{E^2_{\rm CM}}}^1 dx_1 \frac{2M_{\ell\ell}}{x_1 E^2_{\rm CM}} f_a(x_1, M^2_{\ell\ell}) f_b\left(\frac{M^2_{\ell\ell}}{x_1 E^2_{\rm CM}}, M^2_{\ell\ell}\right) \hat{\sigma}(\bar{q}q \to Z' \to \ell^+\ell^-), \quad (2.16)$$

where f_a is the parton distribution function for a parton a, and $E_{\rm CM} = 13$ TeV (8 TeV) is the center-of-mass energy of the LHC Run-2 (Run-1). In our numerical analysis, we employ CTEQ5M [147] for the parton distribution functions. In the case of the U(1)′

[2] ATLAS Run-1 denotes the search for Z' boson resonance in proton-proton (pp) collisions at $\sqrt{s} = 8$ TeV with the ATLAS detector, corresponding to an integrated luminosity of 20.3 fb^{-1} in the dielectron (ee) channel and 20.5 fb^{-1} in the dimuon ($\mu\mu$) channel.

[3] CMS Run-1 denotes the CMS results at $\sqrt{s} = 8$ TeV, 19.6 fb^{-1} (ee) and 20.6 fb^{-1} ($\mu\mu$).

[4] ATLAS 2015 denotes the ATLAS results at $\sqrt{s} = 13$ TeV, 3.2 fb^{-1} ($\ell\ell$).

[5] CMS 2015 denotes the CMS results at $\sqrt{s} = 13$ TeV, 2.6 fb^{-1} (ee) and 2.8 fb^{-1} ($\mu\mu$).

[6] ATLAS 2016 denotes the ATLAS results at $\sqrt{s} = 13$ TeV, 13.3 fb^{-1} ($\ell\ell$).

[7] CMS 2016 denotes the CMS results at $\sqrt{s} = 13$ TeV, 12.4 fb^{-1} (ee) and 13.0 fb^{-1} ($\mu\mu$).

[8] ATLAS 2017 denotes the ATLAS results at $\sqrt{s} = 13$ TeV, 36.1 fb^{-1} ($\ell\ell$).

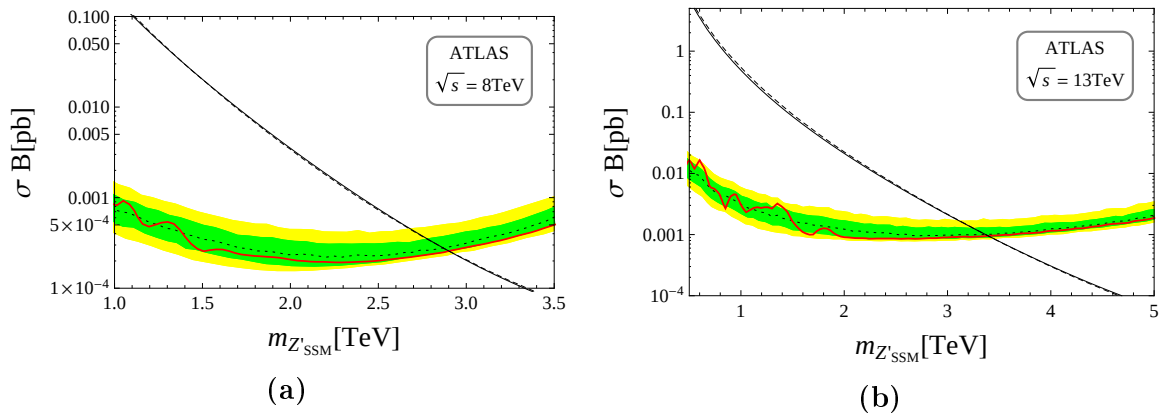

(a) (b)

Figure 2.8: (a) The cross section as a function of the Z'_{SSM} mass (solid line) with $k = 1.18$, along with the LHC Run-1 ATLAS result from the combined dielectron and dimuon channels in Ref. [143]. (b) Same as (a), but with $k = 1.19$, along with the LHC Run-2 ATLAS 2015 result in Ref. [55].

model, the cross section for the colliding partons with a fixed $x_\Phi = 2$ is given by

$$\begin{aligned}\hat{\sigma}(\bar{u}u \to Z' \to \ell^+\ell^-) &= \frac{\pi\alpha_{g_X}^2}{81}\frac{M_{\ell\ell}^2}{(M_{\ell\ell}^2 - m_{Z'}^2)^2 + m_{Z'}^2\Gamma_{Z'}^2} \\ &\quad \times (85x_H^4 + 152x_H^3 + 104x_H^2 + 32x_H + 4), \\ \hat{\sigma}(\bar{d}d \to Z' \to \ell^+\ell^-) &= \frac{\pi\alpha_{g_X}^2}{81}\frac{M_{\ell\ell}^2}{(M_{\ell\ell}^2 - m_{Z'}^2)^2 + m_{Z'}^2\Gamma_{Z'}^2} \\ &\quad \times (25x_H^4 + 20x_H^3 + 8x_H^2 + 8x_H + 4), \end{aligned} \tag{2.17}$$

where the total decay width of the Z' boson is given by

$$\begin{aligned}\Gamma_{Z'} &= \frac{\alpha_{g_X} m_{Z'}}{6}\Bigg[\frac{103x_H^2 + 86x_H + 37}{3} \\ &\quad + \frac{17x_H^2 + 10x_H + 2 + (7x_H^2 + 20x_H + 4)\frac{m_t^2}{m_{Z'}^2}}{3}\sqrt{1 - \frac{4m_t^2}{m_{Z'}^2}}\Bigg]. \end{aligned} \tag{2.18}$$

Here, we have neglected all SM fermion masses except for m_t, and we have assumed $m_N^i > m_{Z'}/2$ for simplicity. By integrating the differential cross section over a range of $M_{\ell\ell}$ set by the ATLAS and CMS analyses, respectively, we obtain the cross section as a function of x_H, α_{g_X} and $m_{Z'}$, which are compared with the lower bounds obtained by the ATLAS and CMS Collaborations.

In interpreting the ATLAS and the CMS results for the U(1)′ Z' boson, we follow the strategy in [85], where the minimal $U(1)_{B-L}$ model has been investigated and an upper bound on the $U(1)_{B-L}$ gauge coupling as a function of the Z' boson mass has been obtained from the ATLAS and the CMS results at the LHC Run-2. We first analyze the sequential SM Z' model to check the consistency of our analysis with the one by the ATLAS and the CMS Collaborations. With the same couplings as the SM, we calculate

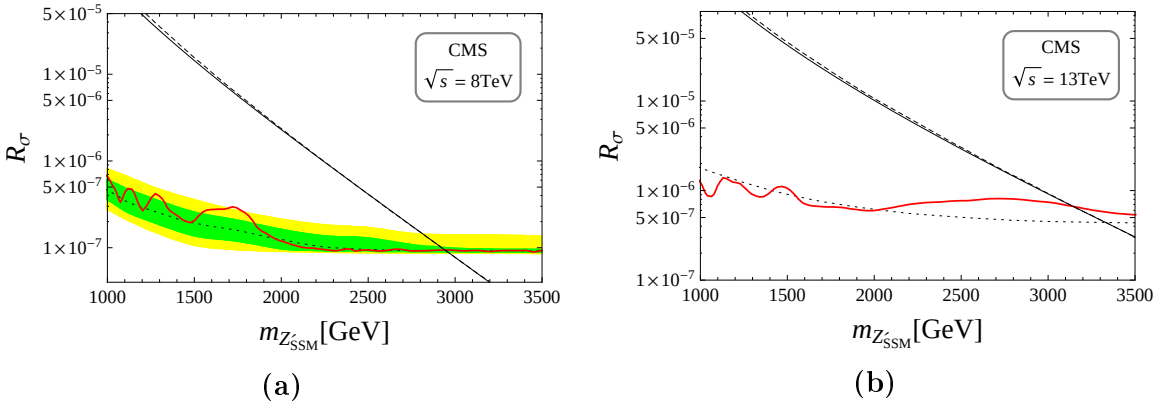

(a) (b)

Figure 2.9: (a) The cross section ratio as a function of the Z'_{SSM} mass (solid line) with $k = 1.01$, along with the LHC Run-1 CMS result from the combined dielectron and dimuon channels in Ref. [141, 142]. (b) Same as (a), but with $k = 1.65$, along with the LHC Run-2 CMS 2015 result in Ref. [56].

the differential cross section of the process $pp \to Z'_{SSM} + X \to \ell^+\ell^- + X$ like Eq. (2.16). According to the analysis by the ATLAS Collaboration at the LHC Run-1 (Run-2), we integrate the differential cross section for the range of 128 GeV$\leq M_{\ell\ell} \leq$ 4500 GeV [143] (128 GeV$\leq M_{\ell\ell} \leq$ 6000 GeV [55], 120 GeV $\leq M_{\ell\ell} \leq$ 6000 GeV [128, 145]) and obtain the cross section of the dilepton production process as a function of the Z'_{SSM} boson mass. Our results are shown as solid lines in Fig. 2.8(a) for the LHC ATLAS Run-1, Fig. 2.8(b) for the LHC Run-2 ATLAS 2015, Fig. 2.10(a) for the LHC Run-2 ATLAS 2016 and Fig. 2.11 for the LHC Run-2 ATLAS 2017, respectively, along with the plots presented by the ATLAS Collaborations at the LHC ATLAS Run-1 [143], the LHC Run-2 ATLAS 2015 [55], the ATLAS 2016 [145], and the ATLAS 2017 [128]. In Figs. 2.8(a), 2.8(b), 2.10(a), and 2.11 the experimental upper bounds on the Z' boson production cross section are depicted as the horizontal solid (red) curves. The theoretical Z' boson production cross section is shown as the diagonal dashed lines, and the lower limits of the Z'_{SSM} boson mass obtained by the ATLAS Collaborations are found to be 2.90 TeV for the LHC ATLAS Run-1, 3.4 TeV for the LHC Run-2 ATLAS 2015, 4.05 TeV for the LHC Run-2 ATLAS 2016, and 4.5 TeV for the LHC Run-2 ATLAS 2017, respectively, which can be read off from the intersection points of the theoretical predictions (diagonal dashed lines) and the experimental cross section bounds (horizontal solid (red) curves). In order to take into account the difference of the parton distribution functions used in the ATLAS analysis and our analysis and QCD corrections of the process, we have scaled our resultant cross sections by a factor $k = 1.18$ in Fig. 2.8(a), by $k = 1.19$ in Fig. 2.8(b), by $k = 1.16$ in Fig. 2.10(a), and by $k = 1.15$ in Fig. 2.11, with which we can obtain the same lower limits of the Z'_{SSM} boson mass as 2.90 TeV, 3.4 TeV, 4.05 TeV, and 4.5 TeV. We can see that our results (solid lines) in Figs. 2.8(a), 2.8(b), 2.10(a), and 2.11 with the factors of $k = 1.18$, $k = 1.19$, $k = 1.16$, and $k = 1.15$, respectively, are very consistent with the theoretical predictions (diagonal dashed lines) presented by the ATLAS Collaboration. We use these factors in the following analysis for the U(1)′ Z' production process.

Now we calculate the cross section of the process $pp \to Z' + X \to \ell^+\ell^- + X$ for

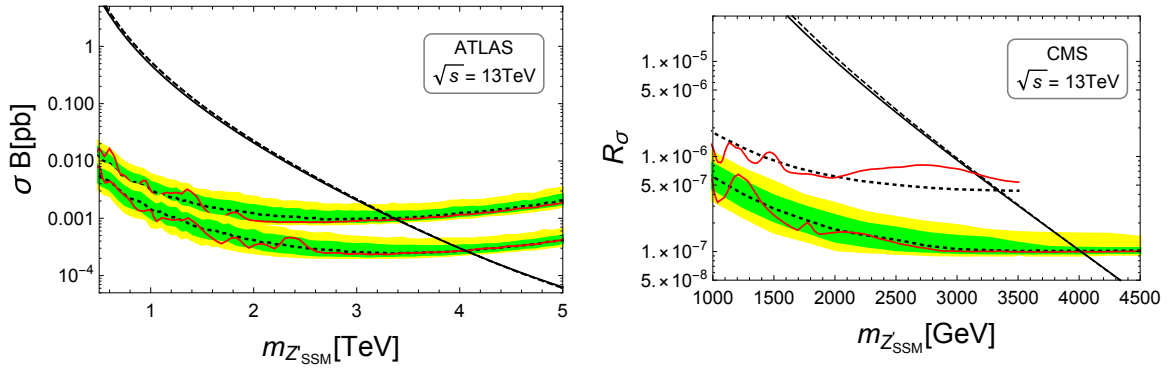

(a) (b)

Figure 2.10: (a) The cross section as a function of the Z'_{SSM} mass (solid line) with $k = 1.16$, along with the LHC Run-2 ATLAS 2016 result from the combined dielectron and dimuon channels in Ref. [145]. (Here we have also shown the ALTAS 2015 result [55] for comparison.) (b) The cross section ratio as a function of the Z'_{SSM} mass (solid line) with $k = 1.42$, along with the LHC Run-2 CMS 2016 result from the combined dielectron and dimuon channels in Ref. [146]. (Here we have also shown the CMS 2015 result [56] for comparison.)

various values of g_X, x_H and v_ϕ, and read off the constraints on these parameters from the cross section bounds given by the ATLAS Collaboration. In Figs. 2.4-2.7, our results from the ATLAS bounds at the LHC ATLAS Run-1 and Run-2 ATLAS 2015 are depicted as thin solid lines and thick solid lines, respectively. We can see that the LHC Run-2 ATLAS 2015 results have dramatically improved the bounds from those obtained by the LHC ATLAS Run-1 results. Our results from the LHC Run-2 ATLAS 2016 will be depicted as (red) dashed lines in Figs. 3.2-3.3, and the one from the LHC Run-2 ATLAS 2017 will be depicted as (red) solid lines in Figs. 4.2-4.3.

We apply the same strategy and compare our results for the Z'_{SSM} model with those in the LHC CMS Run-1 results [141, 142], the LHC Run-2 CMS 2015 results [56], and the LHC Run-2 CMS 2016 results [146]. According to the analysis by the CMS Collaboration at the LHC Run-1 (Run-2), we integrate the differential cross section for the range of $0.6\ m_{Z'_{SSM}} \leq M_{\ell\ell} \leq 1.4\ m_{Z'_{SSM}}$ [141, 142] ($0.97\ m_{Z'_{SSM}} \leq M_{\ell\ell} \leq 1.03\ m_{Z'_{SSM}}$ [56], $0.95\ m_{Z'_{SSM}} \leq M_{\ell\ell} \leq 1.05\ m_{Z'_{SSM}}$ [146]) and obtain the cross section. In the CMS analysis, the limits are set on the ratio of the Z'_{SSM} boson cross section to the Z/γ^* cross section:

$$R_\sigma \;=\; \frac{\sigma(pp \to Z' + X \to \ell\ell + X)}{\sigma(pp \to Z + X \to \ell\ell + X)}, \tag{2.19}$$

where the Z/γ^* production cross sections in the mass window of 60 GeV$\leq M_{\ell\ell} \leq$ 120 GeV are predicted to be 1117 pb at the LHC Run-1 [141, 142] and 1928 pb at the LHC Run-2 [56, 146], respectively. Our results for the Z'_{SSM} model are shown as the solid lines in Figs. 2.9(a), 2.9(b), and 2.10(b), along with the plots presented in Refs. [141, 142], [56], and [146], respectively. The analyses in these CMS papers lead to the lower limits of the Z'_{SSM} boson mass as 2.96 TeV for the LHC CMS Run-1, 3.15 TeV for the LHC Run-2 CMS 2015, and 4.0 TeV for the LHC Run-2 CMS 2016,

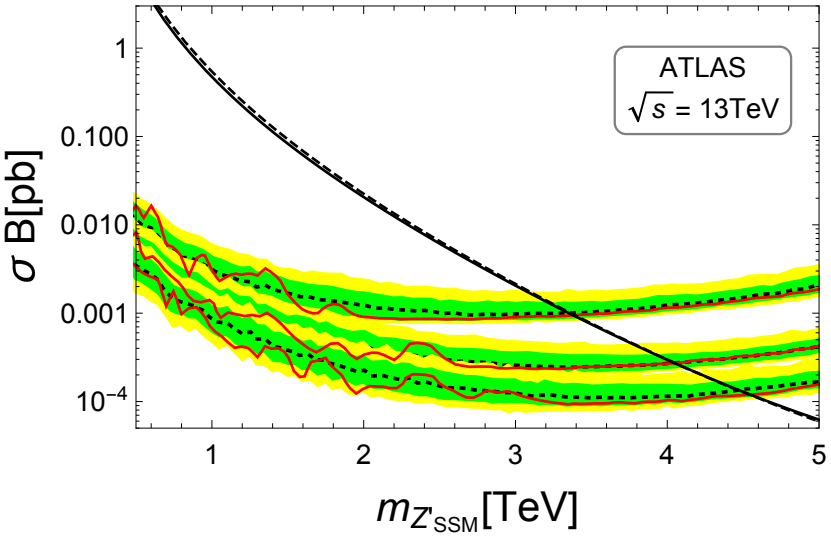

Figure 2.11: The cross section as a function of the Z'_{SSM} mass (solid line) with $k = 1.15$, along with the LHC Run-2 ATLAS 2017 result from the combined dielectron and dimuon channels in Ref. [128]. (Here we have also shown the ALTAS 2016 [145] and 2015 [55] results for comparison.)

which are read off from the intersection points of the theoretical predictions (diagonal dashed lines) and the experimental cross section bounds (horizontal solid (red) curves). In order to obtain the same lower mass limits, we have scaled our resultant cross sections by a factor $k = 1.01$ in Fig. 2.9(a), by $k = 1.65$ in Fig. 2.9(b), and by $k = 1.42$ in Fig. 2.10(b), respectively. With these k factors, our results (solid lines) are very consistent with the theoretical predictions (diagonal dashed lines) presented in Refs. [141, 142], [56], and [146]. We use these k factors in our analysis to interpret the CMS results for the U(1)′ Z' boson case. In Figs. 2.4-2.7, our results from the CMS bounds at the LHC CMS Run-1 and Run-2 CMS 2015 are depicted as thin dashed lines and thick dashed lines, respectively. We can see that the LHC Run-2 CMS 2015 results have dramatically improved the bounds obtained by the LHC CMS Run-1 results. We find that the ATLAS and the CMS bounds we have obtained are consistent with each other. For the LHC Run-2 2015 results, the ATLAS bounds are slightly more severe than the CMS bounds for $m_{Z'} \leq 3.5$ TeV and applicable up to $m_{Z'} = 5$ TeV, leading to the most severe LHC bound on the model parameters. In Figs. 3.2-3.3, our results from the LHC Run-2 CMS 2016 will be depicted as (red) solid lines.

The search for effective 4-Fermi interactions mediated by the Z' boson at the LEP leads to a lower bound on $m_{Z'}/g_X$ [132–135]. Employing the limits from the final LEP 2 data [134] at 95% confidence level, we follow [133] and derive a lower bound on $m_{Z'}/g_X$ as a function x_H. Our result is shown in Fig. 2.12. In Figs. 2.4-2.7, the LEP bounds are depicted as the dashed-dotted lines.

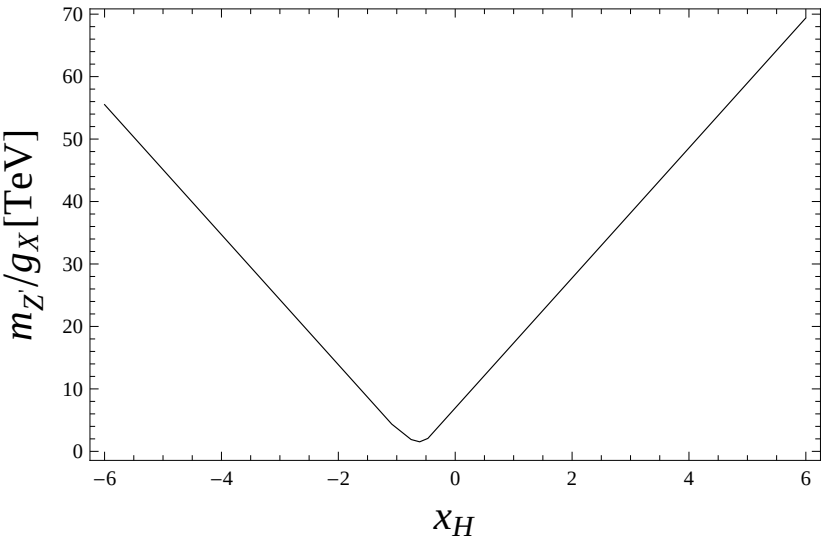

Figure 2.12: The lower bound on $m_{Z'}/g_X$ as a function of x_H (with a fixed x_Φ =2), obtained by the limits from the final LEP 2 data [134] at 95% confidence level.

2.6 Naturalness bounds from SM Higgs mass corrections

Once the classical conformal symmetry is radiatively broken by the Coleman-Weinberg mechanism, the masses for the Z' boson and the Majorana neutrinos are generated and they contribute to self-energy corrections of the SM Higgs doublet. If the U(1)′ gauge symmetry breaking scale is very large, the self-energy corrections may exceed the electroweak scale and require us to fine-tune the model parameters in reproducing the correct electroweak scale. See [148] for related discussions. We consider two heavy states, the right-handed neutrino and Z' boson, whose masses are generated by the U(1)′ gauge symmetry breaking.

Since the original theory is classically conformal and defined as a massless theory, the self-energy corrections to the SM Higgs doublet originate from corrections to the mixing quartic coupling $\lambda_{\rm mix}$. Thus, what we calculate to derive the naturalness bounds are quantum corrections to the term $\lambda_{\rm mix}h^2\phi^2$ in the effective Higgs potential

$$V_{\rm eff} \supset \frac{\lambda_{\rm mix}}{4}h^2\phi^2 + \frac{\beta_{\lambda_{\rm mix}}}{8}h^2\phi^2\left(\ln\left[\phi^2\right] + C\right), \tag{2.20}$$

where the logarithmic divergence and the terms independent of ϕ are all encoded in C. Here, the major contributions to quantum corrections are found to be

$$\beta_{\lambda_{\rm mix}} \supset -\frac{48|y_M|^2|Y_\nu|^2}{16\pi^2} + \frac{12x_H^2x_\Phi^2g_X^4}{16\pi^2} - \frac{4\left(19x_H^2 + 10x_Hx_\Phi + x_\Phi^2\right)x_\Phi^2y_t^2g_X^4}{\left(16\pi^2\right)^2}, \tag{2.21}$$

where the first term comes from the one-loop diagram involving the Majorana neutrinos, the second one is from the one-loop diagram involving the Z' boson, and the third one is from the two-loop diagram [40, 41] involving the Z' boson and the top quark.

By adding a counterterm, we renormalize the coupling $\lambda_{\rm mix}$ with the renormalization condition,

$$\frac{\partial^4 V_{\rm eff}}{\partial h^2 \partial \phi^2}\Big|_{h=0,\phi=v_\phi} = \lambda_{\rm mix}, \tag{2.22}$$

where $\lambda_{\rm mix}$ is the renormalized coupling. As a result, we obtain

$$V_{\rm eff} \supset \frac{\lambda_{\rm mix}}{4} h^2\phi^2 + \frac{\beta_{\lambda_{\rm mix}}}{8} h^2\phi^2 \left(\ln\left[\frac{\phi^2}{v_\phi}\right] - 3 \right). \tag{2.23}$$

Substituting $\phi = v_\phi$, we obtain the SM Higgs self-energy correction as

$$\begin{aligned} \Delta m_h^2 &= -\frac{3}{4}\beta_{\lambda_{\rm mix}} v_\phi^2 \\ &\sim \frac{9 m_\nu m_N^3}{4\pi^2 v_h^2} - \frac{9}{4\pi} x_H^2 \alpha_{g_X} m_{Z'}^2 + \frac{3 m_t^2}{32\pi^3 v_h^2}\left(19 x_H^2 + 20 x_H + 4\right)\alpha_{g_X} m_{Z'}^2 \end{aligned} \tag{2.24}$$

where we have used the seesaw formula, $m_\nu \sim Y_\nu^2 v_h^2/2m_N$ [42–47], and set $x_\Phi = 2$. For the stability of the electroweak vacuum, we impose $\Delta m_h^2 \lesssim m_h^2$ as the naturalness. For example, when the light neutrino mass scale is around $m_\nu \sim 0.1$ eV, we have an upper bound from the first term of Eq. (2.24) for the Majorana mass as $m_N \lesssim 3 \times 10^6$ GeV. This bound is much larger than the scale that we are interested in, $m_N \lesssim 1$ TeV. The most important contribution to Δm_h^2 is the second term of Eq. (2.24) generated through the one-loop diagram with the Z' gauge boson, and the third term becomes important in the case of the U(1)$_{B-L}$ model because the $x_H = 0$ condition makes the second term vanish.

If Δm_h^2 is much larger than the electroweak scale, we need a fine-tuning of the tree-level Higgs mass ($|\lambda_{\rm mix}| v_\phi^2/2$) to reproduce the correct SM Higgs VEV, $v_h = 246$ GeV. We simply evaluate a fine-tuning level as

$$\delta = \frac{m_h^2}{2|\Delta m_h^2|}. \tag{2.25}$$

Here, $\delta = 0.1$, for example, indicates that we need to fine-tune the tree-level Higgs mass squared at the 10% accuracy level. In Figs. 2.4-2.7, the naturalness bounds for 10% and 30% fine-tuning levels are plotted as the dotted lines. Interestingly, the naturalness bounds from the 30% fine-tuning level are found to be compatible with the ALTAS bounds from the LHC Run-2 2015.

2.7 Summary

In this chapter, we have considered the classically conformal U(1)$'$ extended SM with three right-handed neutrinos and a U(1)$'$ Higgs singlet field. The U(1)$'$ symmetry is radiatively broken by the Coleman-Weinberg mechanism, by which the Z' boson as well as the right-handed (Majorana) neutrinos acquire their masses. With the Majorana heavy neutrinos, the seesaw mechanism is automatically implemented. Through

a mixing quartic term between the U(1)′ Higgs and the SM Higgs doublet fields, a negative mass squared for the SM Higgs doublet is generated and, as a result, the electroweak symmetry breaking is triggered associated with the radiative U(1)′ gauge symmetry breaking. Therefore, all mass generations occur through the dimensional transmutation in our model.

In the context of the classically conformal U(1)′ model, we have investigated the possibility to resolve the electroweak vacuum instability. Since the gauge symmetry is broken by the Coleman-Weinberg mechanism, all quartic couplings in the Higgs potential, except the SM Higgs one, are very small, and hence their positive contributions to the U(1)′ model are not effective in resolving the SM Higgs vacuum instability. On the other hand, in the U(1)′ model, the SM Higgs doublet has a nonzero U(1)′ charge, and this gauge interaction positively contributes to the beta function. In addition, the U(1)′ gauge interaction negatively contributes to the beta function of the top Yukawa coupling, so the running top Yukawa coupling is decreasing faster than in the SM case, and its negative contribution to the beta function of the SM Higgs quartic coupling becomes milder. For three free parameters of the model, $m_{Z'}$, α_{g_X} and x_H, we have performed a parameter scan by analyzing the renormalization group evolutions of the model parameters at the two-loop level, and we have identified parameter regions which can solve the electroweak vacuum instability problem and keep all coupling values in the perturbative regime up to the Planck mass. We have found that the resultant parameter regions are very severely constrained, and also that the $U(1)_{B-L}$ model and the orthogonal model are excluded from having the electroweak vacuum stability with the current world average of the experimental data, $m_t = 173.34$ GeV [53] and $m_h = 125.09$ GeV [51].

We have also considered the collider bounds on the U(1)′ Z' boson mass from the ATLAS and CMS results at the LHC Run-2 2015 with $\sqrt{s} = 13$ TeV. We have interpreted the Z' boson resonance search results at the LHC Run-1 and Run-2 2015 to the U(1)′ Z' boson case and obtained the collider bound on the U(1)′ charge of the SM Higgs doublet x_H for a fixed U(1)′ gauge coupling, the collider bound on x_H for a fixed VEV of the U(1)′ Higgs, or the upper bound on the U(1)′ gauge coupling for a fixed x_H as a function of the U(1)′ Z' boson mass $m_{Z'}$. Combining the constraints from the electroweak vacuum stability and the LHC Run-2 2015 results, we find a bound on the Z' boson mass as $m_{Z'} \gtrsim 3.5$ TeV. The LEP results in the search for effective 4-Fermi interactions mediated by the U(1)′ Z' boson can also constrain the model parameter space, but the constraint is found to be weaker than those obtained from the LHC Run-2 2015 results.

Once the U(1)′ gauge symmetry is broken, the Z' boson and the right-handed neutrinos become heavy and contribute to the SM Higgs self-energy through quantum corrections. Therefore, the SM Higgs self-energy can exceed the electroweak scale, if the states are so heavy. Since the SM Higgs doublet has nonzero U(1)′ charge, the self-energy corrections from the Z' boson occur at the one-loop level. This is in sharp contrast to the classically conformal $U(1)_{B-L}$ model [40, 41], where the Higgs doublet has no $U(1)_{B-L}$ charge, and the self-energy corrections from the Z' boson occur at the two-loop level. We have evaluated the Higgs self-energy corrections and found the naturalness bounds to reproduce the right electroweak scale for the fine-tuning level better than 10%. We have found that the naturalness bounds for the 30% fine-tuning

level are compatible with the ALTAS constraint from the LHC Run-2 2015 results, and requiring a fine-tuning level $> 10\%$ leads to the upper bound on the U(1)$'$ Z' boson mass as $m_{Z'} \lesssim 7$ TeV.

Putting all our results together in Figs. 2.4-2.7, we have found that the U(1)$'$ Z' boson mass lies in the range of 3.5 TeV$\lesssim m_{Z'} \lesssim 7$ TeV.

Chapter 3

Dark Matter Physics

In this chapter, we consider the dark matter (DM) scenario in the context of the classically conformal U(1)$'$ extended standard model (SM) which is introduced in chapter 2, with three right-handed neutrinos (RHNs) and the U(1)$'$ Higgs field. The model is free from all the U(1)$'$ gauge and gravitational anomalies in the presence of the three RHNs. We introduce a Z_2-parity in the model, under which an odd-parity is assigned to one RHN, while all the other particles is assigned to be Z_2-even, and hence the Z_2-odd RHN serves as a DM candidate[1]. In this model, the U(1)$'$ gauge symmetry is radiatively broken through the Coleman-Weinberg mechanism, by which the electroweak symmetry breaking is triggered. As we have already mentioned in chapter 2, there are three free parameters in our model, the U(1)$'$ charge of the SM Higgs doublet (x_H), the new U(1)$'$ gauge coupling (g_X), and the U(1)$'$ gauge boson (Z') mass ($m_{Z'}$), which are severely constrained in order to solve the electroweak vacuum instability problem, and satisfy the LHC Run-2 bounds from the search for Z' boson resonance. In addition to these constraints, we investigate the RHN DM physics. Because of the nature of classical conformality, we find that a RHN DM pair mainly annihilates into the SM particles through the Z' boson exchange. This is the so-called Z'-portal DM scenario. We will combine these three constrains, the electroweak vacuum stability condition, the LHC Run-2 2016 bounds, and the cosmological constraint from the observed DM relic density, and find parameter regions to satisfy all three constraints. For the obtained allowed regions, we also calculate the spin-independent cross section of the RHN DM with nucleons.

This chapter is organized as follows: In Sec. 3.1, we briefly introduce the classically conformal U(1)$'$ extended SM with the Z_2-odd RHN DM. In Sec. 3.2, we calculate the relic density of the Z'-portal RHN DM. In Sec. 3.3, we combine all the constraints obtained from the RHN DM physics, collider phenomenology, and the electroweak vacuum stability, and narrow allowed regions. In Sec. 3.4, for the allowed parameter regions, we calculate the spin-independent cross section of the RHN DM with nucleons. We summarize our results in Sec. 3.5.

[1] Although we introduce this ad-hoc Z_2 parity, without introducing additional scalers, it is difficult to build a new model which has a stable DM candidate. In this point of view, we put ourselves in a position in which the existence of the DM implies a new parity.

	$SU(3)_c$	$SU(2)_L$	$U(1)_Y$	$U(1)'$			Z_2
q_L^i	**3**	**2**	$+1/6$	x_q	$=$	$\frac{1}{3}x_H + \frac{1}{6}x_\Phi$	$+$
u_R^i	**3**	**1**	$+2/3$	x_u	$=$	$\frac{4}{3}x_H + \frac{1}{6}x_\Phi$	$+$
d_R^i	**3**	**1**	$-1/3$	x_d	$=$	$-\frac{2}{3}x_H + \frac{1}{6}x_\Phi$	$+$
ℓ_L^i	**1**	**2**	$-1/2$	x_ℓ	$=$	$-x_H - \frac{1}{2}x_\Phi$	$+$
$\nu_R^{1,2}$	**1**	**1**	0	x_ν	$=$	$-\frac{1}{2}x_\Phi$	$+$
ν_R^3	**1**	**1**	0	x_ν	$=$	$-\frac{1}{2}x_\Phi$	$-$
e_R^i	**1**	**1**	-1	x_e	$=$	$-2x_H - \frac{1}{2}x_\Phi$	$+$
H	**1**	**2**	$+1/2$	x_H	$=$	x_H	$+$
Φ	**1**	**1**	0	x_Φ	$=$	x_Φ	$+$

Table 3.1: Particle contents of the $U(1)'$ extended SM with Z_2 parity. In addition to the SM particle contents, three generations of RHNs ν_R^i ($i = 1, 2, 3$ denotes the generation index) and $U(1)'$ Higgs field Φ are introduced. Under Z_2 parity, the only one RHN ν_R^3 is odd, while the other particles, including ν_R^1 and ν_R^2, are even.

3.1 The classically conformal $U(1)'$ extended SM with RHN DM

The model we will investigate is the anomaly-free $U(1)'$ extension of the SM with the classically conformal invariance, which is based on the gauge group $SU(3)_C \times SU(2)_L \times U(1)_Y \times U(1)'$ introduced in chapter 2. The particle contents of the model are listed in Table 3.1, where we also introduce the Z_2 parity [63], and assign an odd parity to one RHN ν_R^3, while the other particles, including ν_R^1 and ν_R^2, have even parity. The conservation of Z_2 parity ensures the stability of ν_R^3, which is a unique candidate of the DM in our model. By introducing the Z_2 parity, the Yukawa sector of the SM is extended to have

$$\mathcal{L}_{\text{Yukawa}} \supset -\sum_{i=1}^{3}\sum_{j=1}^{2} Y_\nu^{ij}\overline{\ell_L^i}\tilde{H}\nu_R^j - \sum_{i=1}^{3} Y_M^i \Phi \overline{\nu_R^{ic}}\nu_R^i + \text{h.c.}, \tag{3.1}$$

where $\tilde{H} \equiv i\tau^2 H^*$, and the terms in the right-handed side are for the seesaw mechanism to generate neutrino masses. Because of the Z_2 parity, only two generation RHNs are involved in the neutrino Dirac Yukawa couplings and hence the neutrino Dirac mass matrix is 2 by 3. Once the $U(1)'$ Higgs field Φ develops a VEV, the $U(1)'$ symmetry is broken and the Majorana mass terms for the RHNs are generated. After the electroweak symmetry breaking, the seesaw mechanism [42–47] is automatically implemented, except that only two generation RHNs are relevant. This system is the minimal seesaw [66, 67], which possesses a number of free parameters Y_ν^{ij} and Y_M^j ($i = 1, 2, 3$, $j = 1, 2$) enough to reproduce the neutrino oscillation data with a prediction of one massless eigenstate.

Associated with the radiative $U(1)'$ symmetry breaking (as well as the electroweak symmetry breaking), the $U(1)'$ gauge boson (Z' boson), the Majorana RHNs $\nu_R^{1,2}$, and

the RHN DM particle ν_R^3 acquire their masses as

$$\begin{aligned} m_{Z'} &= \sqrt{(x_\Phi g_X v_\phi)^2 + (x_H g_X v_h)^2} \simeq x_\Phi g_X v_\phi, \\ m_{N^{1,2}} &= \sqrt{2} Y_M^{1,2} v_\phi, \qquad m_{\rm DM} = \sqrt{2} Y_M^3 v_\phi, \end{aligned} \tag{3.2}$$

where $v_h = 246$ GeV is the SM Higgs VEV, and we have used $x_\Phi v_\phi \gg x_H v_h$. In this chapter, we assume degenerate masses for $\nu_R^{1,2}$, ($Y_M^1 = Y_M^2 = y_M$, equivalently, $m_{N^{1,2}} = m_N$), for simplicity. The U(1)$'$ Higgs boson mass is given by

$$\begin{aligned} m_\phi^2 &= \left.\frac{d^2 V}{d\phi^2}\right|_{\phi=v_\phi} = \beta_\Phi v_\phi^2 \simeq \frac{1}{8\pi^2}\left(3(x_\Phi g_X)^4 - 16 y_M^4 - 8 y_{\rm DM}^4\right) v_\phi^2 \\ &\simeq \frac{1}{8\pi^2}\frac{3m_{Z'}^4 - 4m_N^4 - 2m_{\rm DM}^4}{v_\phi^2}, \end{aligned} \tag{3.3}$$

where $y_{\rm DM} = Y_M^3$. For a sizable Majorana mass, this formula indicates that the potential minimum disappears, so that there is an upper bound on the RHN mass for the U(1)$'$ symmetry to be broken radiatively. In order to avoid the destabilization of the U(1)$'$ Higgs potential, we simply set $m_{Z'}^4 \gg m_N^4$ in the following analysis, while $m_{\rm DM} \simeq m_{Z'}/2$ as we will find in the next section. Note that this condition does not mean that the Majorana RHNs must be very light, even though a factor difference between $m_{Z'}$ and m_N is enough to satisfy the condition. For simplicity, we set $y_M = 0$ at v_ϕ in the following RG analysis as an approximation.

3.2 Relic density of the RHN DM

In this section, we calculate the thermal relic density of the RHN DM and identify the model parameter region to be consistent with the Planck 2015 measurement [100] (68% confidence level):

$$\Omega_{\rm DM} h^2 = 0.1198 \pm 0.0015. \tag{3.4}$$

Because of the nature of classical conformality, we find the mass mixing between the SM Higgs and the U(1)$'$ Higgs bosons is very small, so that the RHN DM pair annihilation process mediated by the Higgs bosons is highly suppressed. Therefore, in our model, the RHN DM particles mainly annihilate into the SM particles through the s-channel process mediated by the U(1)$'$ gauge boson Z'[2].

The Boltzmann equation of the RHN DM is given by

$$\frac{dY}{dx} = -\frac{xs\langle\sigma v\rangle}{H(m_{\rm DM})}(Y^2 - Y_{\rm EQ}^2), \tag{3.5}$$

[2] The freeze out temperature from the equilibrium state of the RHN DM is determined by a condition that the life time of the RHN DM nearly equals the life time of Universe ($1/\Gamma_{\rm DM} \sim 1/H$). Even if we consider a temperature $T \sim 100$ TeV, just above our targeted energy scale $m_{\rm DM} \sim \mathcal{O}(1\text{ TeV})$, the equilibrium condition $\Gamma_{\rm DM} > H$ is satisfied. Thus, the RHN DMs of our model are in the thermal equilibrium in the early Universe.

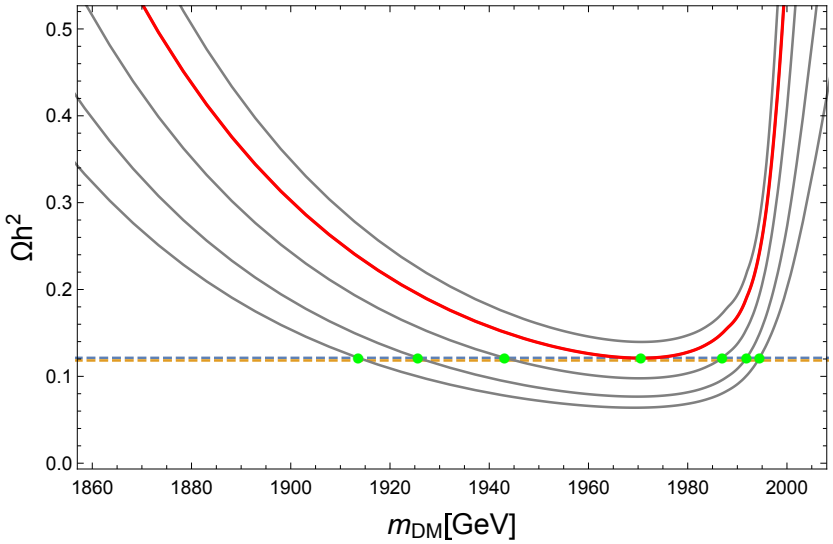

Figure 3.1: The relic density of the RHN DM as a function of its mass ($m_{\rm DM}$). We have fixed $x_H = -0.575$ and $m_{Z'} = 4$ TeV, and have shown the relic densities for various values of the gauge coupling, $\alpha_{g_X} = 0.002$, 0.00235, 0.003, 0.004 and 0.005 (solid lines from top to bottom). The two horizontal lines denote the range of the observed DM relic density, $0.1183 \leq \Omega_{\rm DM}h^2 \leq 0.1213$ in the Planck 2015 results [100].

where temperature of the Universe is normalized by the mass of the RHN DM $x = m_{\rm DM}/T$, $H(m_{\rm DM})$ is the Hubble parameter at $T = m_{\rm DM}$, s is the entropy density, $Y = n/s$ is the yield of the RHN DM which is defined by the ratio of the number density n to s, $Y_{\rm EQ}$ is the yield in the thermal equilibrium, and $\langle\sigma v\rangle$ is the thermal averaged product of the RHN DM annihilation cross section σ and relative velocity v. Explicit formulas of these are summarized as follows:

$$\begin{aligned} s &= \frac{2\pi^2}{45} g_* \frac{m_{\rm DM}^3}{x^3}, \\ H(m_{\rm DM}) &= \sqrt{\frac{\pi^2}{90} g_*} \frac{m_{\rm DM}^2}{M_{\rm P}}, \\ sY_{\rm EQ} &= \frac{g_{\rm DM}}{2\pi^2} \frac{m_{\rm DM}^3}{x} K_2(x), \end{aligned} \tag{3.6}$$

where $g_{\rm DM} = 2$ is the number of degrees of the freedom for the RHN DM, g_* is the effective total number of degrees of freedom for particles in thermal equilibrium (in this chapter, we set $g_* = 106.75$ for the SM particles), and K_2 is the modified Bessel function of the second kind. The thermally-averaged annihilation cross section times velocity is given by

$$\langle\sigma v\rangle = (sY_{\rm EQ})^{-2} g_{\rm DM}^2 \frac{m_{\rm DM}}{64\pi^4 x} \int_{4m_{\rm DM}^2}^{\infty} ds \hat{\sigma}(s) \sqrt{s} K_1\left(\frac{x\sqrt{s}}{m_{\rm DM}}\right), \tag{3.7}$$

where the reduced cross section is defined as $\hat{\sigma}(s) = 2(s - 4m_{\rm DM}^2)\sigma(s)$ with the total cross section $\sigma(s)$, K_1 is the modified Bessel function of the first kind. The total cross

section of the RHN DM annihilation process $\nu_R^3\nu_R^3 \to Z' \to f\bar{f}$ (f denotes the SM fermion)[3] is calculated as

$$\begin{aligned}\sigma(s) &= \frac{\pi}{3}\alpha_{gx}^2 \frac{\sqrt{s(s-4m_{\rm DM}^2)}}{(s-m_{Z'}^2)^2+m_{Z'}^2\Gamma_{Z'}^2} \\ &\times \left[\frac{103x_H^2+86x_H+37}{3}+\frac{17x_H^2+10x_H+2+(7x_H^2+20x_H+4)\frac{m_t^2}{s}}{3}\sqrt{1-\frac{4m_t^2}{s}}\right. \\ &\left. +18x_H^2\frac{(s-m_{Z'}^2)^2}{s(s-4m_{\rm DM}^2)}\frac{m_{\rm DM}^2 m_t^2}{m_{Z'}^4}\sqrt{1-\frac{4m_t^2}{s}}\right], \end{aligned} \tag{3.8}$$

where the total decay width of Z' boson is given by

$$\begin{aligned}\Gamma_{Z'} &= \frac{\alpha_{gx}m_{Z'}}{6}\left[\frac{103x_H^2+86x_H+37}{3}\right. \\ &+\frac{17x_H^2+10x_H+2+(7x_H^2+20x_H+4)\frac{m_t^2}{m_{Z'}^2}}{3}\sqrt{1-\frac{4m_t^2}{m_{Z'}^2}} \\ &\left.+2\left(1-\frac{4m_N^2}{m_{Z'}^2}\right)^{\frac{3}{2}}\theta\left(\frac{m_{Z'}^2}{m_N^2}-4\right)+\left(1-\frac{4m_{\rm DM}^2}{m_{Z'}^2}\right)^{\frac{3}{2}}\theta\left(\frac{m_{Z'}^2}{m_{\rm DM}^2}-4\right)\right]. \end{aligned} \tag{3.9}$$

Here, we have neglected all SM fermion masses except for the top quark mass m_t.

By solving the Boltzmann Eq. (3.5) numerically, we find the asymptotic value of the yield $Y(\infty)$, and the present DM relic density is given by

$$\Omega_{\rm DM}h^2 = \frac{m_{\rm DM}s_0Y(\infty)}{\rho_c/h^2}, \tag{3.10}$$

where $s_0 = 2890$ cm^{-3} is the entropy density of the present Universe, and $\rho_c/h^2 = 1.05\times10^{-5}$ GeV/cm^3 is the critical density. Our analysis involves four parameters, namely α_{gx}, $m_{Z'}$, $m_{\rm DM}$ and x_H. For $m_{Z'} = 4$ TeV and $x_H = -0.575$, we show in Fig. 3.1 the resultant RHN DM relic density as a function of the RHN DM mass $m_{\rm DM}$, along with the range of the observed DM relic density, $0.1183 \le \Omega_{\rm DM}h^2 \le 0.1213$ [100] (two horizontal dashed lines). The solid lines from top to bottom show the resultant RHN DM relic densities for various values of the gauge coupling, $\alpha_{gx} = 0.002$, 0.00235, 0.003, 0.004 and 0.005. The plots indicate the lower bound on $\alpha_{gx} \ge 0.00235$ for $m_{Z'} = 4$ TeV and $x_H = -0.575$ in order to reproduce the observed relic density. In addition, we can see that the enhancement of the RHN DM annihilation cross section via the Z' boson resonance is necessary to satisfy the cosmological constraint and hence, $m_{\rm DM} \simeq m_{Z'}/2$.

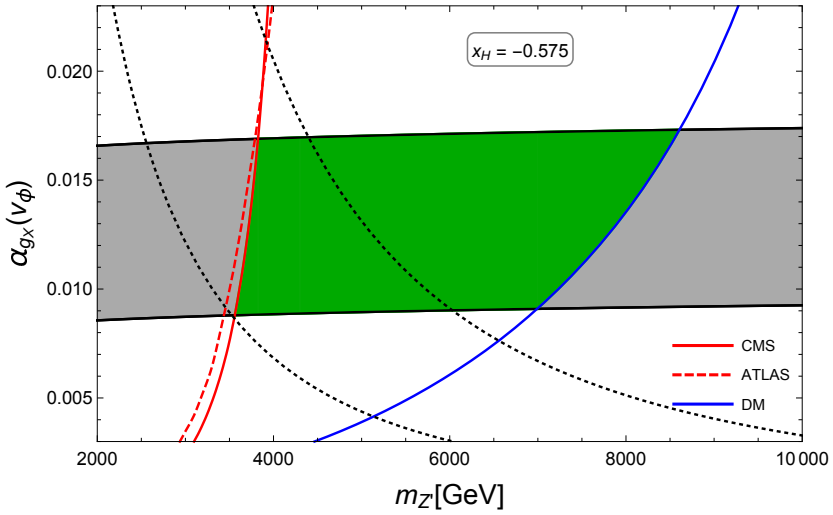

Figure 3.2: The allowed regions to solve the electroweak instability problem for $m_{Z'}$ and α_{g_X} with a fixed $x_H = -0.575$ at the TeV scale, along with the dark matter lower bound ((blue) right solid line) on α_{g_X}, the LHC Run-2 (2016) CMS upper bound ((red) solid line) on α_{g_X} and the LHC Run-2 ATLAS (2016) upper bound ((red) dashed line) on α_{g_X} from direct search for Z' boson resonance. The (green) shaded region in between two solid lines satisfies all constraints. Here, the naturalness bounds for 10% (right dotted line) and 30% (left dotted line) fine-tuning levels are also depicted, which have been discussed in Sec. 2.6.

3.3 Combined results

Now let us combine all the constraints that we have obtained in the previous sections from the RHN DM physics, collider phenomenology, and the electroweak vacuum stability. In Fig. 3.2, we show the allowed region in the ($m_{Z'}$, α_{g_X})-plane for fixed $x_H = -0.575$, as an example. The shaded region indicates the parameter space for solving the electroweak vacuum instability. The (blue) right solid line shows the lower bound on α_{g_X} as a function of $m_{Z'}$ to reproduce the observed DM relic density of the Planck result [100]. The (red) left solid (dashed) line shows the LHC Run-2 2016 upper bound on α_{g_X} obtained from the search results for Z' boson resonance by the CMS [146] (ATLAS [145]) Collaboration. The (green) shaded region in between two solid lines satisfies all constraints. These three constraints are complementary to narrow down the allowed region to be 4 TeV $\lesssim m_{Z'} \lesssim$ 8 TeV and $0.009 \lesssim \alpha_{g_X} \lesssim 0.017$. We also show the naturalness bounds for 10% (right dotted line) and 30% (left dotted line) fine-tuning levels, which have been discussed in Sec. 2.6.

In Fig. 3.3, we show allowed parameter regions in the (x_H, α_{g_X})-plane for various $m_{Z'}$ values. Fig. 3.3(a) is for $m_{Z'} = 4$ TeV. The shaded region indicates the parameter space for solving the electroweak vacuum instability. The (blue) convex-downward solid

[3] Although there are also other annihilation processes, such as $\nu_R^3\nu_R^3 \to \phi\phi$, $\nu_R^3\nu_R^3 \to \phi Z'$ and $\nu_R^3\nu_R^3 \to Z'Z'$ (see, for example, Ref. [149]), all these cross sections are estimated to be much less than 1 pb, which is a typical cross section to reproduce $\Omega_{\rm DM}h^2 \simeq 0.1$, for $\alpha_{g_X} \sim 0.01$ (see Figs. 3.2 and 3.3), $y_{\rm DM} \sim g_X$, and $m_{\rm DM} \sim 1$ TeV.

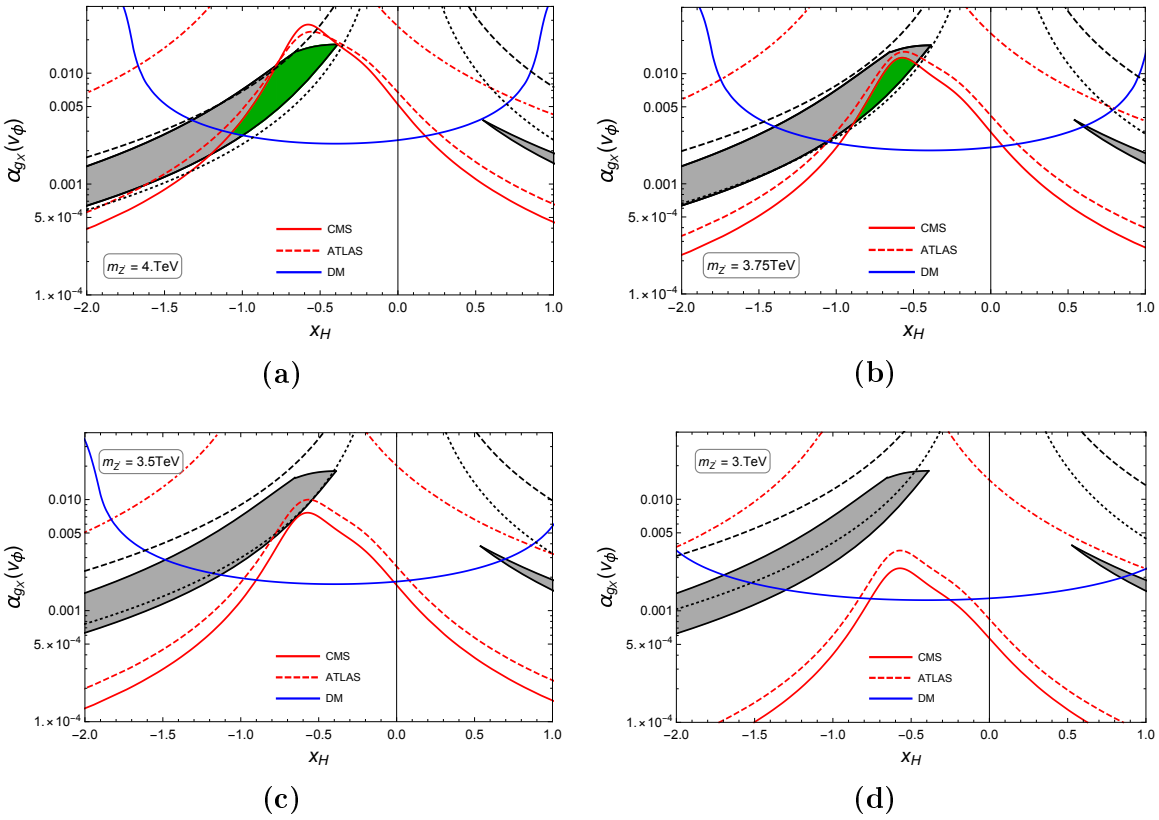

Figure 3.3: Allowed parameter regions in the (x_H, α_{g_X})-plane for various $m_{Z'}$ values. (a) is for $m_{Z'} = 4$ TeV. The shaded region indicates the parameter space for solving the electroweak vacuum instability. The (blue) convex-downward solid line shows the cosmological lower bound on α_{g_X} as a function of x_H. The (red) convex-upward solid (dashed) line shows the LHC Run-2 2016 upper bound on α_{g_X} obtained from the Z' boson search by the CMS [146] (ATLAS [145]) Collaboration, and the (red) dashed-dotted lines show the LEP upper bounds obtained from Fig. 2.12. The (green) shaded region in between two solid lines satisfies all constraints. Here, the naturalness bounds for 10% (dashed line) and 30% (dotted line) fine-tuning levels are also depicted, which have been discussed in Sec. 2.6. (b), (c) and (d) are the same as (a), but $m_{Z'} = 3.75$ TeV, 3.5 TeV and 3 TeV, respectively.

line shows the lower bound on α_{g_X} as a function of x_H to reproduce the observed DM relic density. The (red) convex-upward solid (dashed) line shows the LHC Run-2 2016 upper bound on α_{g_X} obtained from the search results for Z' boson resonance by the CMS [146] (ATLAS [145]) Collaboration[4], and the (red) dashed-dotted lines also show the LEP upper bounds obtained from Fig. 2.12 (for more details, see Sec. 2.5). The (green) shaded region in between two solid lines satisfies all constraints. These three constraints are complementary to narrow down the allowed region to be $-1.1 \lesssim x_H \lesssim -0.4$ and $0.002 \lesssim \alpha_{g_X} \lesssim 0.02$. We also show the naturalness bounds for 10% (dashed line) and 30% (dotted line) fine-tuning levels, which have been discussed in Sec. 2.6. Figs. 3.3(b), 3.3(c) and 3.3(d) are the same as Fig. 3.3(a), but $m_{Z'} = 3.75$ TeV, 3.5 TeV and 3 TeV, respectively. From Fig. 3.3(b), the allowed region to satisfy these three constraints indicates $-0.9 \lesssim x_H \lesssim -0.5$ and $0.003 \lesssim \alpha_{g_X} \lesssim 0.015$ for fixed $m_{Z'} = 3.75$ TeV. As $m_{Z'}$ decreases, the LHC upper bound lines are shifted downward, while the DM lower bound line remains almost the same (it slightly moves to downward). Therefore, the allowed region between the LHC upper bounds and the DM lower bound narrows. On the other hand, the shaded region remains almost the same, so that the (green) shaded region disappears for $m_{Z'} \lesssim 3.5$ TeV.

Finally, we roughly estimate the future Z' detections from the end of the LHC Run-2 with about 100 fb^{-1} luminosity and the full HL-LHC with about 3000 fb^{-1} one. The experimental cross section bound is inversely proportional to the luminosity, which can see from the Fig. 2.11. In addition, from Eqs. (2.16)-(2.18), we see that the cross section is proportional to α_{g_X} because the narrow width approximation can be applied here for high mass range of $m_{Z'}$. As a result, in Fig. 3.3, we see that the upper bound on α_{g_X} at the end of LHC Run-2 (100 fb^{-1}) will be decreased roughly 13.3 fb^{-1}/100 fb^{-1} times lower than one at the LHC Run-2 2016 (13.3 fb^{-1}), which means the all allowed (green) shaded region will be disappeared. The same can be said for the HL-LHC bound on α_{g_X}, which gives a more strong constraint and will exclude the allowed regions even if $m_{Z'} > 4$ TeV.

3.4 Direct detection of RHN DM

A variety of experiments are underway and also planned for directly detecting a DM particle through its elastic scattering off with nuclei.[5] In this section, we calculate the spin-independent elastic scattering cross section of the RHN DM particle via the Higgs bosons exchange,[6] and compare our results with the current experimental results and

[4] For the validity for the use of the narrow width approximation in the analysis of Fig. 3.3, we confirmed that the upper bound satisfying $\Gamma_{Z'} \lesssim m_{Z'}$ is far above the (red) collider upper bounds in Fig. 3.3 . Even the upper bound satisfying $\Gamma_{Z'} \lesssim 0.05\, m_{Z'}$ is still above the LHC Run-2 2016 bounds.

[5] We can also consider an indirect detection of the RHN DM through cosmic rays from a pair annihilation of the RHN DMs. However, using the parameters in the allowed regions shown in Sec. 3.3, we have found that the pair annihilation cross section is much smaller than the current upper bounds obtained from, for example, the Fermi-LAT experiments [150].

[6] There is another process for the RHN DM to scatter off with nuclei via Z'-boson exchange. Since the RHN DM is a Majorana particle, only its interaction with nuclei is spin-dependent. We have calculated this spin-dependent cross section to be $\sigma_{\rm SD} \sim 10^{-9}$ pb, which is far below the current upper bounds, $\sigma_{\rm SD} \lesssim 10^{-4}$ pb obtained from the LUX [151] and the IceCube [152] experiments.

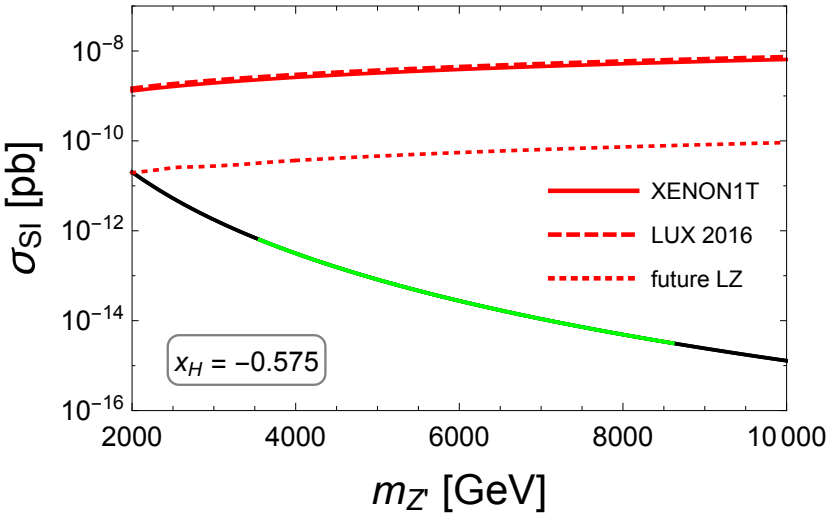

Figure 3.4: For a fixed $x_H = -0.575$, the resultant spin-independent cross section $\sigma_{\rm SI}$ as a function of $m_{Z'}$. Here, for a fixed $m_{Z'}$ value, α_{g_X} is taken from the shaded region in Fig. 3.2 to solve the electroweak vacuum instability problem. The (green) shaded region in between around 3.5 TeV and 9 TeV corresponds to the (green) shaded parameter region in Fig. 3.2, which satisfies all three constraints, the electroweak vacuum stability condition, the LHC Run-2 2016 bound, and the cosmological constraint from the observed RHN DM relic density. The (red) upper solid (dashed) line shows the XENON1T [153] (LUX 2016 [154]) upper bound on $\sigma_{\rm SI}$ as a function of $m_{Z'} \simeq 2m_{\rm DM}$, and the (red) dotted line shows the prospective reach for the upper bound on $\sigma_{\rm SI}$ in the next-generation successor of the LUX experiment, the LUX-ZEPLIN (LZ) DM experiment [155].

a prospective reach by future experiments.

From Eq. (3.2), the U(1)′ Higgs VEV v_ϕ is expressed as a function of $m_{Z'}$, α_{g_X} and x_H:

$$v_\phi^2 = \frac{m_{Z'}^2}{16\pi\alpha_{g_X}}\left[1 - 4\pi\alpha_{g_X}\left(\frac{x_H v_h}{m_{Z'}}\right)^2\right] \simeq \frac{m_{Z'}^2}{16\pi\alpha_{g_X}}. \tag{3.11}$$

In Sec. 3.2, we have also shown that $m_{\rm DM} \simeq m_{Z'}/2$ to satisfy the experimental relic density of the Z'-portal RHN DM, which means $y_{\rm DM} \simeq m_{Z'}/2\sqrt{2}v_\phi \simeq \sqrt{2\pi\alpha_{g_X}}$, and then Eq. (3.3) is approximately expressed as

$$m_\phi^2 \simeq \frac{1}{8\pi^2}\frac{23}{8}\frac{m_{Z'}^4}{v_\phi^2} \simeq \frac{23}{4\pi}\alpha_{g_X} m_{Z'}^2. \tag{3.12}$$

Using the SM Higgs boson mass in Eq. (2.14), the scalar mass matrix is found to be

$$\mathcal{M} = \begin{pmatrix} m_h^2 & -m_h^2\left(\frac{v_h}{v_\phi}\right) \\ -m_h^2\left(\frac{v_h}{v_\phi}\right) & m_\phi^2 \end{pmatrix}. \tag{3.13}$$

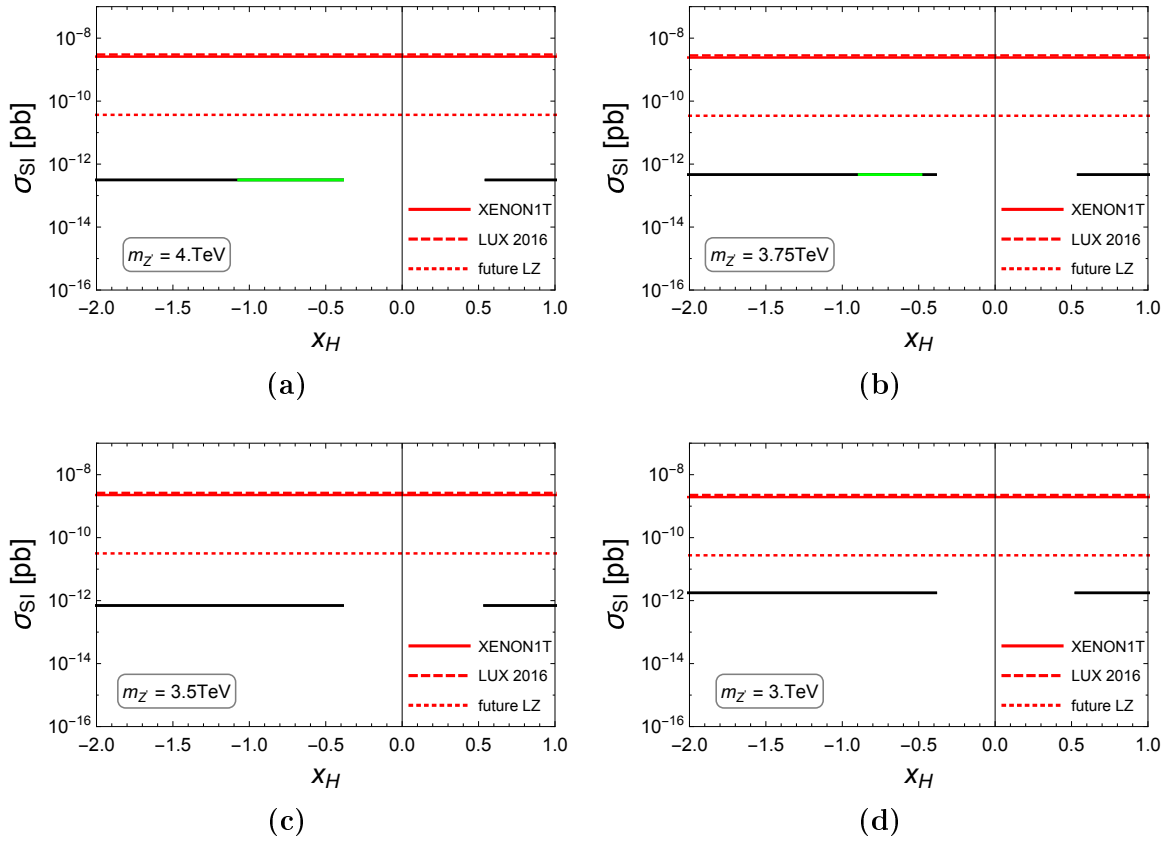

Figure 3.5: The resultant $\sigma_{\rm SI}$ in the (x_H, $\sigma_{\rm SI}$)-plane for various $m_{Z'}$ values, corresponding to the parameter regions shown in Fig. 3.3. (a) shows our results for $m_{Z'} = 4$ TeV. The shaded regions indicate the parameter space for solving the electroweak vacuum instability. The (green) shaded region in the range of $-1.1 \lesssim x_H \lesssim -0.4$ corresponds to the (green) shaded region in Fig. 3.3(a), which satisfies all three constraints, the electroweak vacuum stability condition, the LHC Run-2 2016 bound, and the cosmological constraint from the observed RHN DM relic density. The (red) upper solid (dashed) line shows the XENON1T [153] (LUX 2016 [154]) upper bound on $\sigma_{\rm SI}$, and the (red) dotted line shows the prospective reach for the upper bound on $\sigma_{\rm SI}$ in the LZ DM experiment [155]. Figs. (b), (c) and (d) are the same as (a), but for $m_{Z'} = 3.75$ TeV, 3.5 TeV and 3 TeV corresponding to Fig. 3.3(b), 3.3(c) and 3.3(d), respectively.

The mass eigenstates h' and ϕ' are defined as

$$\begin{pmatrix} h' \\ \phi' \end{pmatrix} = \begin{pmatrix} \cos\theta & -\sin\theta \\ \sin\theta & \cos\theta \end{pmatrix} \begin{pmatrix} h \\ \phi \end{pmatrix}, \tag{3.14}$$

with the mixing angle θ given by

$$\tan 2\theta = \frac{2m_h^2(v_h/v_\phi)}{m_h^2 - m_\phi^2}, \tag{3.15}$$

and their mass eigenvalues are given by

$$\begin{aligned} m_{h'}^2 &= m_h^2\cos^2\theta + m_\phi^2\sin^2\theta + 2m_h^2\frac{v_h}{v_\phi}\sin\theta\cos\theta \simeq m_h^2, \\ m_{\phi'}^2 &= m_h^2\sin^2\theta + m_\phi^2\cos^2\theta - 2m_h^2\frac{v_h}{v_\phi}\sin\theta\cos\theta \simeq m_\phi^2. \end{aligned} \tag{3.16}$$

Here, we have used the fact that except for the special case, $m_h^2 \simeq m_\phi^2$, the mixing angle is always small because of the suppression by v_h/v_ϕ with $v_h = 246$ GeV and $v_\phi \gtrsim 10$ TeV. Thus, the mass eigenstate h' is the SM-like Higgs boson, while ϕ' is the U(1)$'$-like Higgs boson.

The spin-independent elastic scattering cross section with nucleon is given by

$$\begin{aligned} \sigma_{\rm SI} &= \frac{1}{\pi}\left(\sqrt{2}y_{\rm DM}\sin\theta\cos\theta\right)^2\left(\frac{\mu_{\rm DM,N}}{v_h}\right)^2 f_N^2\left(\frac{1}{m_{h'}^2} - \frac{1}{m_{\phi'}^2}\right)^2 \\ &\simeq 4\theta^2\alpha_{g_X}\left(\frac{\mu_{\rm DM,N}}{v_h}\right)^2 f_N^2\left(\frac{1}{m_h^2} - \frac{1}{m_\phi^2}\right)^2, \end{aligned} \tag{3.17}$$

where $\mu_{\rm DM,N} = m_N m_{\rm DM}/(m_N + m_{\rm DM})$ is the reduced mass of the RHN DM-nucleon system with the nucleon mass $m_N = 0.939$ GeV, and

$$f_N = \left(\sum_{q=u,d,s} f_{T_q} + \frac{2}{9}f_{TG}\right) m_N \tag{3.18}$$

is the nuclear matrix element accounting for the quark and gluon contents of the nucleon. In evaluating f_{T_q}, we use the results from the lattice QCD simulation [156]: $f_{T_u} + f_{T_d} \simeq 0.056$ and $|f_{T_s}| \leq 0.08$. For conservative analysis, we take $f_{T_s} = 0$ in the following. Using the trace anomaly formula, $\sum_{q=u,d,s} f_{T_q} + f_{TG} = 1$ [157–161], we obtain $f_N^2 \simeq 0.0706\ m_N^2$. Using Eqs. (3.11), (3.12) and (3.15), $\sigma_{\rm SI}$ is expressed as a function of only two free parameters: α_{g_X} and $m_{Z'}$.

For a fixed $x_H = -0.575$, the resultant spin-independent cross section $\sigma_{\rm SI}$ as a function of $m_{Z'}$ is depicted in Fig. 3.4. Here, for a fixed $m_{Z'}$ value, α_{g_X} is taken from the shaded region in Fig. 3.2 to solve the electroweak vacuum instability problem. The (green) shaded region in between around 3.5 TeV and 9 TeV corresponds to the (green) shaded parameter region in Fig. 3.2, which satisfies all three constraints, the electroweak vacuum stability condition, the LHC Run-2 2016 bound, and the cosmological constraint from the observed RHN DM relic density. The (red) upper solid

(dashed) line shows the XENON1T [153] (LUX 2016 [154]) upper bound on $\sigma_{\rm SI}$ as a function of $m_{Z'} \simeq 2m_{\rm DM}$, and the (red) dotted line shows the prospective reach for the upper bound on $\sigma_{\rm SI}$ in the next-generation successor of the LUX experiment, the LUX-ZEPLIN (LZ) DM experiment [155]. Our resultant spin-independent cross section appears below the future reach.

In Fig. 3.5, we show the resultant $\sigma_{\rm SI}$ in the (x_H, $\sigma_{\rm SI}$)-plane for various $m_{Z'}$ values, corresponding to the parameter regions shown in Fig. 3.3. Fig. 3.5(a) shows our results for $m_{Z'} = 4$ TeV. The shaded regions indicate the parameter space for solving the electroweak vacuum instability. The (green) shaded region in the range of $-1.1 \lesssim x_H \lesssim -0.4$ corresponds to the (green) shaded region in Fig. 3.3(a), which satisfies all three constraints, the electroweak vacuum stability condition, the LHC Run-2 2016 bound, and the cosmological constraint from the observed RHN DM relic density. The (red) upper solid (dashed) line shows the XENON1T [153] (LUX 2016 [154]) upper bound on $\sigma_{\rm SI}$, and the (red) dotted line shows the prospective reach for the upper bound on $\sigma_{\rm SI}$ in the LZ DM experiment [155]. Figs. 3.5(b), 3.5(c) and 3.5(d) are the same as Fig. 3.5(a), but for $m_{Z'} = 3.75$ TeV, 3.5 TeV and 3 TeV corresponding to Fig. 3.3(b), 3.3(c) and 3.3(d), respectively. Fig. 3.5(b) has a (green) shaded region in the range of $-0.9 \lesssim x_H \lesssim -0.5$ to satisfy the three constraints, while Figs. 3.5(c) and 3.5(d) have no such region.

3.5 Summary

In this chapter, we have considered the DM scenario in the context of the classically conformal U(1)$'$ extended SM, with three RHNs and the U(1)$'$ Higgs field. The model is free from all the U(1)$'$ gauge and gravitational anomalies in the presence of the three RHNs. We have introduced a Z_2-parity in the model, under which an odd-parity is assigned to one RHN, while all the other particles are assigned to be Z_2-even. In our model, the Z_2-odd RHN serves as a stable DM candidate, while the other two RHNs are utilized for the the minimal seesaw mechanism in order to reproduce the neutrino oscillation data and the observed baryon asymmetry in the Universe through leptogenesis. In this model, the U(1)$'$ gauge symmetry is radiatively broken through the CW mechanism, by which the electroweak symmetry breaking is triggered. There are three free parameters in our model, the U(1)$'$ charge of the SM Higgs doublet (x_H), the new U(1)$'$ gauge coupling (α_{g_X}), and the U(1)$'$ gauge boson (Z') mass ($m_{Z'}$).

In this model context, we have first investigated a possibility to resolve the electroweak vacuum instability with the current world average of the experimental data, $m_t = 173.34$ GeV and $m_h = 125.09$ GeV. By using the same strategy in chapter 2. we have found that the resultant parameter regions are very severely constrained. Next, we have calculated the thermal relic density of the RHN DM and identified the model parameter region to reproduce the observed DM relic density of the Planck 2015 measurement. In our model, the RHN DM particles mainly annihilate into the SM particles through the s-channel process mediated by the Z' boson. We have obtained the lower bound on α_{g_X} as a function of $m_{Z'}$ and x_H from the observed DM relic density. We have also considered the LHC Run-2 2016 bounds from the search for the Z' boson resonance by the ATLAS and CMS analysis, which lead to the upper bounds on α_{g_X}

as a function of $m_{Z'}$ and x_H. The LEP results from the search for effective 4-Fermi interactions mediated by the Z' boson can also constrain the model parameter space, but the LEP constraints are found to be weaker than those obtained from the LHC Run-2 2016 results. Finally, we have combined all the constraints. The cosmological constraint on the RHN DM yields the lower bound on α_{g_X} as a function of $m_{Z'}$ and x_H, while the upper bound on α_{g_X} is obtained from the LHC Run-2 2016 results, so that these constraints are complementary to narrow the allowed parameter regions. We have found that only small portions in these allowed parameter regions can solve the electroweak vacuum instability problem. In particular, no allowed region to satisfy all constraints exists for $m_{Z'} \lesssim 3.5$ TeV. For the obtained allowed regions, we have calculated the spin-independent cross section of the RHN DM with nucleons. We have found that the resultant cross section well below the experimental (XENON1T [153] and LUX 2016 [154]) upper bounds.

Chapter 4

Inflation

In this chapter, we propose quartic inflation with non-minimal gravitational coupling in the context of the classically conformal U(1)′ extension of the Standard Model (SM), which is introduced in chapter 2. In this model, the U(1)′ gauge symmetry is radiatively broken through the Coleman-Weinberg mechanism, by which the U(1)′ gauge boson (Z' boson) and the right-handed Majorana neutrinos acquire their masses. We consider their masses in the range of $\mathcal{O}(10\text{ GeV})-\mathcal{O}(10\text{ TeV})$, which are accessible to high energy collider experiments. As we have already mentioned in chapter 2, the radiative U(1)′ gauge symmetry breaking also generates a negative mass squared for the SM Higgs doublet, and the electroweak symmetry breaking occurs subsequently. We identify the U(1)′ Higgs field with inflaton and calculate the inflationary predictions. Due to the Coleman-Weinberg mechanism, the inflaton quartic coupling during inflation, which determines the inflationary predictions, is correlated to the U(1)′ gauge coupling. With this correlation, we investigate complementarities between the inflationary predictions and the constraint from the Z' boson resonance search at the LHC Run-2 2017 as well as the prospect of the search for the Z' boson and the right-handed neutrinos at the future collider experiments.

This chapter is organized as follows: In Sec. 4.1, we review the basics of the quartic inflation with non-minimal gravitational coupling and the constraints on the inflationary predictions from the Planck 2015 results [105]. In Sec. 4.2, identifying the U(1)′ Higgs field in the classically conformal U(1)′ extended SM as an inflaton, we investigate the quartic inflation with non-minimal gravitational coupling. Because of the radiative U(1)′ symmetry breaking, the inflaton quartic coupling during inflation relates to the U(1)′ gauge coupling at low energies through the renormalization group evolutions. In Sec. 4.3, we discuss the LHC Run-2 2017 constraints on the Z' production cross section [128] and the future prospects of the search for the Z' boson and the right-handed neutrinos. Here, we emphasize complementarities between the collider physics and the inflationary predictions. In Sec. 4.4, for completion of our inflation scenario, we also discuss reheating after inflation. We summarize our results in Sec. 4.5.

4.1 Non-minimal quartic inflation

In this section, we introduce the quartic inflation with non-minimal gravitational coupling (non-minimal quartic inflation). We define the inflation scenario by the following action in the Jordan frame:

$$\mathcal{S}_J = \int d^4x\sqrt{-g}\left[-\frac{1}{2}(1+\xi\phi^2)\mathcal{R} + \frac{1}{2}g^{\mu\nu}\left(\partial_\mu\phi\right)\left(\partial_\nu\phi\right) - \frac{\lambda}{4}\phi^4\right], \tag{4.1}$$

where the reduced Planck mass, $M_P = 2.44\times10^{18}$ GeV, is set to be 1 (Planck unit), ϕ is a real scalar (inflaton), $\xi > 0$ is a dimensionless and real parameter of the non-minimal gravitational coupling, and λ is a quartic coupling of the inflaton. In the limit $\xi \to 0$, the model is reduced to the minimal quartic inflation.

In the Einstein frame with a canonical gravity sector, we describe the action with a new inflaton field (σ) with a canonical kinetic term. The relation between the new inflaton σ and the original inflaton ϕ is given by

$$\left(\frac{d\sigma}{d\phi}\right)^2 = \frac{1+\xi(6\xi+1)\phi^2}{\left(1+\xi\phi^2\right)^2}. \tag{4.2}$$

The action in the Einstein frame is then given by

$$S_E = \int d^4x\sqrt{-g_E}\left[-\frac{1}{2}\mathcal{R}_E + \frac{1}{2}g_E^{\mu\nu}\left(\partial_\mu\sigma\right)\left(\partial_\nu\sigma\right) - V_E(\sigma(\phi))\right], \tag{4.3}$$

where the inflaton potential in terms of the original ϕ is described as

$$V_E = \frac{\lambda}{4}\frac{\phi^4}{(1+\xi\phi^2)^2}. \tag{4.4}$$

We express the slow-roll parameters in terms of ϕ as follows:

$$\begin{aligned}
\epsilon(\phi) &= \frac{1}{2}\left(\frac{V_E'}{V_E\,\sigma'}\right)^2, \\
\eta(\phi) &= \frac{V_E''}{V_E\,(\sigma')^2} - \frac{V_E'\,\sigma''}{V_E\,(\sigma')^3}, \\
\zeta(\phi) &= \left(\frac{V_E'}{V_E\,\sigma'}\right)\left(\frac{V_E'''}{V_E\,(\sigma')^3} - 3\frac{V_E''\,\sigma''}{V_E\,(\sigma')^4} + 3\frac{V_E'\,(\sigma'')^2}{V_E\,(\sigma')^5} - \frac{V_E'\,\sigma'''}{V_E\,(\sigma')^4}\right),
\end{aligned} \tag{4.5}$$

where a prime denotes a derivative with respect to ϕ. The amplitude of the curvature perturbation $\Delta_\mathcal{R}$ is given by

$$\Delta_\mathcal{R}^2 = \left.\frac{V_E}{24\pi^2\epsilon}\right|_{k_0}, \tag{4.6}$$

which should satisfy $\Delta_\mathcal{R}^2 = 2.195\times10^{-9}$ from the Planck measurements [105] with the pivot scale chosen at $k_0 = 0.002$ Mpc^{-1}. The number of e-folds is given by

$$N_0 = \frac{1}{\sqrt{2}}\int_{\phi_e}^{\phi_0} d\phi\frac{\sigma'}{\sqrt{\epsilon(\phi)}} \tag{4.7}$$

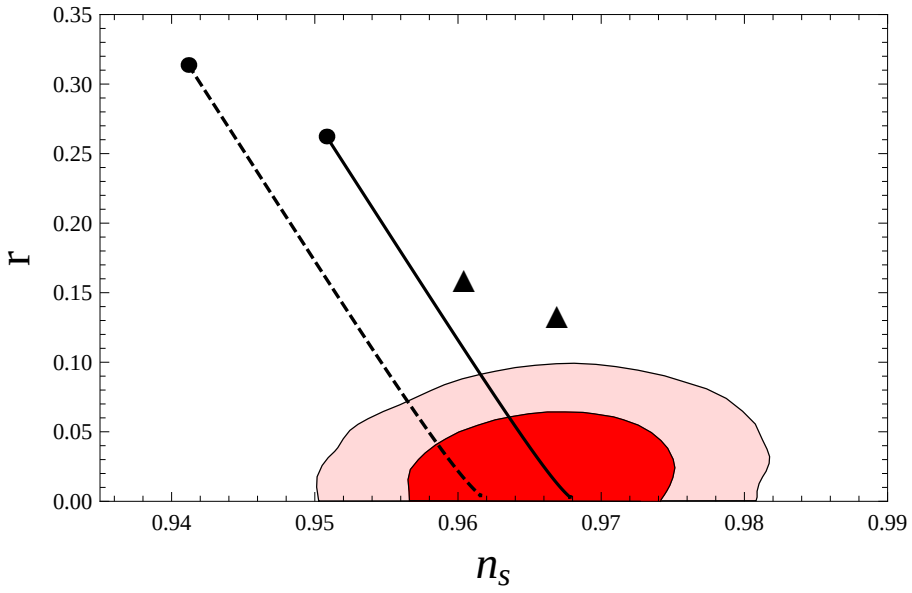

Figure 4.1: The inflationary predictions (n_s and r) in the non-minimal quartic inflation for various values of $\xi \geq 0$, along with the contours for the limits at the confidence levels of 68% (inner) and 95% (outer) obtained by the Planck measurements (*Planck* TT+lowP+BKP) [105]. The solid and the dashed diagonal lines correspond to the inflationary predictions for $N_0 = 60$ and $N_0 = 50$, respectively. The predictions of the minimal quartic inflation ($\xi = 0$) for $N_0 = 60$ and $N_0 = 50$ are depicted by the right and left black points, respectively. Here, we also show the predictions of the quadratic inflation for $N_0 = 60$ and $N_0 = 50$ as the right and left triangles, respectively. As ξ is increased, the predicted r values approach their asymptotic values $r \simeq 0.00296$ and 0.00419 for $N_0 = 60$ and $N_0 = 50$, respectively.

where ϕ_0 is the inflaton value at horizon exit of the scale corresponding to k_0, and ϕ_e is the inflaton value at the end of inflation, which is defined by $\epsilon(\phi_e) = 1$. The value of N_0 depends logarithmically on the energy scale during inflation as well as on the reheating temperature, and we take its typical value to be $N_0 = 50 - 60$ in order to solve the horizon and flatness problems.

The slow-roll approximation is valid as long as the conditions $\epsilon \ll 1$, $|\eta| \ll 1$ and $\zeta \ll 1$ hold. In this case, the inflationary predictions, the scalar spectral index n_s, the tensor-to-scalar ratio r, and the running of the spectral index $\alpha = \frac{dn_s}{d\ln k}$, are given by

$$n_s = 1 - 6\epsilon + 2\eta, \quad r = 16\epsilon, \quad \alpha = 16\epsilon\eta - 24\epsilon^2 - 2\zeta. \tag{4.8}$$

Here, the inflationary predictions are evaluated at $\phi = \phi_0$. Under the constraint of $\Delta^2_{\mathcal{R}} = 2.195 \times 10^{-9}$ from the Planck measurements [105], once N_0 is fixed, all the inflationary predictions as well as the quartic coupling λ are determined as a function of ξ. In Fig. 4.1, we show the inflationary predictions (n_s and r) for various values of $\xi \geq 0$, along with the contours for the limits at the confidence levels of 68% (inner) and 95% (outer) obtained by the Planck measurements (*Planck* TT+lowP+BKP) [105]. The solid and the dashed diagonal lines correspond to the inflationary predictions for

$N_0 = 60$						
ξ	ϕ_0	ϕ_e	n_s	r	$\alpha(10^{-4})$	λ
0	22.1	2.83	0.951	0.262	-8.06	1.43×10^{-13}
0.00333	22.00	2.79	0.961	0.1	-7.03	3.79×10^{-13}
0.0689	18.9	2.30	0.967	0.01	-5.44	6.69×10^{-12}
1	8.52	1.00	0.968	0.00346	-5.25	4.62×10^{-10}
10	2.89	0.337	0.968	0.00301	-5.24	4.01×10^{-8}
100	0.920	0.107	0.968	0.00297	-5.23	3.95×10^{-6}
1000	0.291	0.0340	0.968	0.00296	-5.23	3.94×10^{-4}
$N_0 = 50$						
ξ	ϕ_0	ϕ_e	n_s	r	$\alpha(10^{-4})$	λ
0	20.2	2.83	0.941	0.314	-11.5	2.45×10^{-13}
0.00527	20.0	2.77	0.955	0.1	-9.74	7.83×10^{-13}
0.119	15.8	2.07	0.961	0.01	-7.70	1.96×10^{-11}
1	7.82	1.00	0.961	0.00489	-7.51	6.56×10^{-10}
10	2.65	0.337	0.962	0.00426	-7.49	5.70×10^{-8}
100	0.844	0.107	0.962	0.00420	-7.48	5.61×10^{-6}
1000	0.267	0.0340	0.962	0.00419	-7.48	5.60×10^{-4}

Table 4.1: Inflationary predictions for various values of ξ in the non-minimal quartic inflation for fixed $N_0 = 60$ and 50. Here, ϕ_0 and ϕ_e are evaluated in the Planck units ($M_P = 1$).

$N_0 = 60$ and $N_0 = 50$, respectively. The predictions of the minimal quartic inflation ($\xi = 0$) for $N_0 = 60$ and $N_0 = 50$ are depicted by the right and left black points, respectively. Here, we also show the predictions of the quadratic inflation for $N_0 = 60$ and $N_0 = 50$ as the right and left triangles, respectively. As ξ is increased, the inflationary predictions approach their asymptotic values, $n_s \simeq 0.968$, $r \simeq 0.00296$ and $\alpha \simeq -5.23 \times 10^{-4}$ for $N_0 = 60$ ($n_s \simeq 0.962$, $r \simeq 0.00419$ and $\alpha \simeq -7.48 \times 10^{-4}$ for $N_0 = 50$). In Fig. 4.1, we find a lower bound on $\xi \geq 0.00385$, which corresponds to $r \leq 0.0913$ for $N_0 = 60$, from the limit at 95% confidence level. We have summarized in Table 4.1 the numerical values of the inflationary predictions for various ξ values and fixed $N_0 = 60$ and 50.

4.2 Non-minimal quartic inflation with the U(1)′ Higgs field

The model we will investigate is the minimal U(1)′ extension of the SM with classically conformal invariance [48, 49], which is based on the gauge group $\mathrm{SU}(3)_c \times \mathrm{SU}(2)_L \times \mathrm{U}(1)_Y \times \mathrm{U}(1)'$ introduced in chapter 2. The particle content of the model is listed in Table 2.1. In the following, the real part of the U(1)′ Higgs filed Φ is identified with the inflaton in the non-minimal quartic inflation. In the original Jordan frame action,

we introduce the non-minimal gravitational coupling of

$$-\xi \left(\Phi^\dagger \Phi\right) \mathcal{R}, \tag{4.9}$$

which leads to the non-minimal gravitational coupling in Eq. (4.1) for the inflaton/Higgs filed defined as $\phi = \sqrt{2}\Re[\Phi]$. The scalar potential in Eq. (4.1) is replaced by the effective potential in Eq. (2.6). Since the inflaton value $\phi \gg v_\phi$ during inflation, we can neglect the effects of the VEV v_ϕ for the non-minimal coupling as well as the inflaton potential. In our inflation analysis, we employ the renormalization group (RG) improved effective potential of the form [162],

$$V(\phi) = \frac{1}{4}\lambda_\Phi(\phi)\phi^4, \tag{4.10}$$

where $\lambda(\phi)$ is the solution to the RG equation with identifying the renormalization scale as ϕ along the inflation trajectory.

As we have discussed in Sec. 4.1, the inflationary predictions are determined by the parameter ξ of the non-minimal gravitational coupling. From the view point of the unitarity arguments [163–166] of the non-minimal quartic inflation scenario, we may take $\xi \lesssim 10$ to make our analysis valid. This means from Table 4.1 that the inflaton quartic coupling is very small, $\lambda \lesssim 4 \times 10^{-8}$ for $N_0 = 60$. Note that the stationary condition of Eq. (2.9) derived from the Coleman-Weinberg mechanism requires the quartic coupling to be very small. Hence, one may consider it natural to realize the non-minimal quartic inflation with a small ξ in the context of our classically conformal model. Because of the stationary condition and $\lambda_\Phi \ll 1$, the U(1)′ gauge and the Majorana Yukawa couplings must be very small, $g_X, y_M \ll 1$. Thus, the RG evolutions of all couplings in our model are very mild, and we calculate the inflationary predictions with a constant quartic coupling, $\lambda_\Phi(\phi_0)$, evaluated at the inflaton value $\phi = \phi_0$. Our results for the inflationary predictions in the non-minimal quartic inflation are presented in Sec. 4.1. In the following analysis, we identify λ in Sec. 4.1 with $\lambda = \lambda_\Phi(\phi_0)$.

We evaluate the inflaton quartic coupling at $\phi = \phi_0$ by extrapolating the gauge, the Majorana Yukawa, and the Higgs quartic couplings at v_ϕ through their RG equations. Since all couplings are very small, the RG equations at the one-loop level are approximately given by

$$\begin{aligned}
\frac{d\lambda_\Phi}{d\ln\phi} &= \beta_{\lambda_\Phi} \simeq 96\alpha_{g_X}^2 - 48\alpha_{y_M}^2, \\
\frac{d\alpha_{g_X}}{d\ln\phi} &= \beta_{g_X} = \frac{18 + 32x_H + 41x_H^2}{3\pi}\alpha_{g_X}^2, \\
\frac{d\alpha_{y_M}}{d\ln\phi} &= \beta_{y_M} = \frac{1}{\pi}\alpha_{y_M}\left(5\alpha_{y_M} - 3\alpha_{g_X}\right),
\end{aligned} \tag{4.11}$$

where $\alpha_{g_X} = g_X^2/(4\pi)$ and $\alpha_{y_M} = y_M^2/(4\pi)$. In the leading-log approximation, we have the solutions of the RG equations for α_{g_X} and α_{y_M} as

$$\alpha_{g_X}(\phi) \simeq \overline{\alpha_{g_X}} + \overline{\beta_{g_X}} \ln\left[\frac{\phi}{v_\phi}\right], \quad \alpha_{y_M}(\phi) \simeq \overline{\alpha_{y_M}} + \overline{\beta_{y_M}} \ln\left[\frac{\phi}{v_\phi}\right], \tag{4.12}$$

where $\overline{\alpha_{g_X}} \equiv \alpha_{g_X}(v_\phi)$, $\overline{\alpha_{y_M}} \equiv \alpha_{y_M}(v_\phi)$, and $\overline{\beta_{g_X}}$ and $\overline{\beta_{y_M}}$ are the beta functions in Eq. (4.11) evaluated with $\overline{\alpha_{g_X}}$ and $\overline{\alpha_{y_M}}$. Using these solutions, we obtain

$$\beta_{\lambda_\Phi} \simeq 96\alpha_{g_X}^2 - 48\alpha_{y_M}^2 \simeq \overline{\beta_{\lambda_\Phi}} + 2\left(96\,\overline{\alpha_{g_X}}\,\overline{\beta_{g_X}} - 48\,\overline{\alpha_{y_M}}\,\overline{\beta_{y_M}}\right)\ln\left[\frac{\phi}{v_\phi}\right], \tag{4.13}$$

where $\overline{\beta_{\lambda_\Phi}} = 96\,\overline{\alpha_{g_X}} - 48\,\overline{\alpha_{y_M}}$. Finally, we arrived at an approximate solution as

$$\begin{aligned}\lambda_\Phi(\phi) &\simeq \overline{\lambda_\Phi} + \overline{\beta_{\lambda_\Phi}}\ln\left[\frac{\phi}{v_\phi}\right] + \left(96\,\overline{\alpha_{g_X}}\,\overline{\beta_{g_X}} - 48\,\overline{\alpha_{y_M}}\,\overline{\beta_{y_M}}\right)\left(\ln\left[\frac{\phi}{v_\phi}\right]\right)^2 \\ &= \left(\frac{11}{6} + \ln\left[\frac{\phi}{v_\phi}\right]\right)\overline{\beta_{\lambda_\Phi}} + \left(96\,\overline{\alpha_{g_X}}\,\overline{\beta_{g_X}} - 48\,\overline{\alpha_{y_M}}\,\overline{\beta_{y_M}}\right)\left(\ln\left[\frac{\phi}{v_\phi}\right]\right)^2, \end{aligned} \tag{4.14}$$

where $\overline{\lambda_\Phi} \equiv \lambda_\Phi(v_\phi)$, and we have used Eq. (2.9) in the second line.

In the next section, we will discuss the collider physics for the Z' boson and the heavy Majorana neutrinos. For our discussion, it is convenient to adopt the Z' boson mass ($m_{Z'}$) and the degenerate heavy Majorana neutrino mass (m_N) as free parameters, instead of the U(1)$'$ Higgs VEV v_ϕ and $\overline{y_M}$. In our analysis, we have 5 free parameters, namely, ξ, x_H, $\overline{g_X}$, $m_{Z'}$, and m_N, after replacing v_ϕ and $\overline{y_M}$ by using the relations, $v_\phi = m_{Z'}/(2\,\overline{g_X})$ and $\overline{y_M} = m_N/\sqrt{2}\,v_\phi = \sqrt{2}\;\overline{g_X}\,(m_N/m_{Z'})$. As has been discussed in Sec. 4.1, once ξ is fixed, not only the inflationary predictions but also ϕ_0, ϕ_e and $\lambda_\Phi(\phi_0)$ are all determined. When ξ, $m_{Z'}$ and m_N values are fixed, we obtain $\overline{g_X}$ as a function of x_H from Eq. (4.14). In Fig. 4.2, we show $\overline{\alpha_{g_X}}\,x_H^2$ as a function of x_H for various values of ξ for (a) $m_{Z'} = 3$ TeV and $x_H > 0$, (b) $m_{Z'} = 3$ TeV and $x_H < 0$, (c) $m_{Z'} = 4$ TeV and $x_H > 0$, and (d) $m_{Z'} = 4$ TeV and $x_H < 0$. In Figs. 4.2(a)-(d), the diagonal (black) lines correspond to $\xi = 10$, 1, 0.0689, and 0.00333 from left to right. Here, we have fixed $m_N = m_{Z'}/3$ (see the next section), for simplicity. The results for $x_H > 0$ and $x_H < 0$ are well overlapped and indistinguishable.

4.3 Complementarity between collider physics and inflation

Realizing the non-minimal quartic inflation in the context of the classically conformal U(1)$'$ model, we have obtained a relation between the U(1)$'$ gauge coupling and the inflationary predictions once x_H, $m_{Z'}$ and m_N are fixed. If $m_{Z'} \lesssim 10$ TeV, the Z' boson in our U(1)$'$ model can be produced at the high-energy colliders, which has been discussed in Sec. 2.5. Since the production cross section of the Z' boson depends on its mass, the gauge coupling and x_H, we have in our model a correlation between the collider physics on Z' boson and the inflationary predictions.

By following the same strategy in Sec. 2.5, we interpret the LHC Run-2 ATLAS 2017 results [128] on the Z'_{SSM} boson into the U(1)$'$ Z' boson case. In Fig. 4.2, the horizontal (red) lines show the upper bounds on $\overline{\alpha_{g_X}}\,x_H^2$ as a function of x_H from the ATLAS 2017 results on the search for a narrow resonance with the combined dielectron and dimuon channels [128]. As we can see the cross section formula, the horizontal (red) lines in Figs. 4.2(a) and 4.2(b) (Figs. 4.2(c) and 4.2(d)) approach to a constant

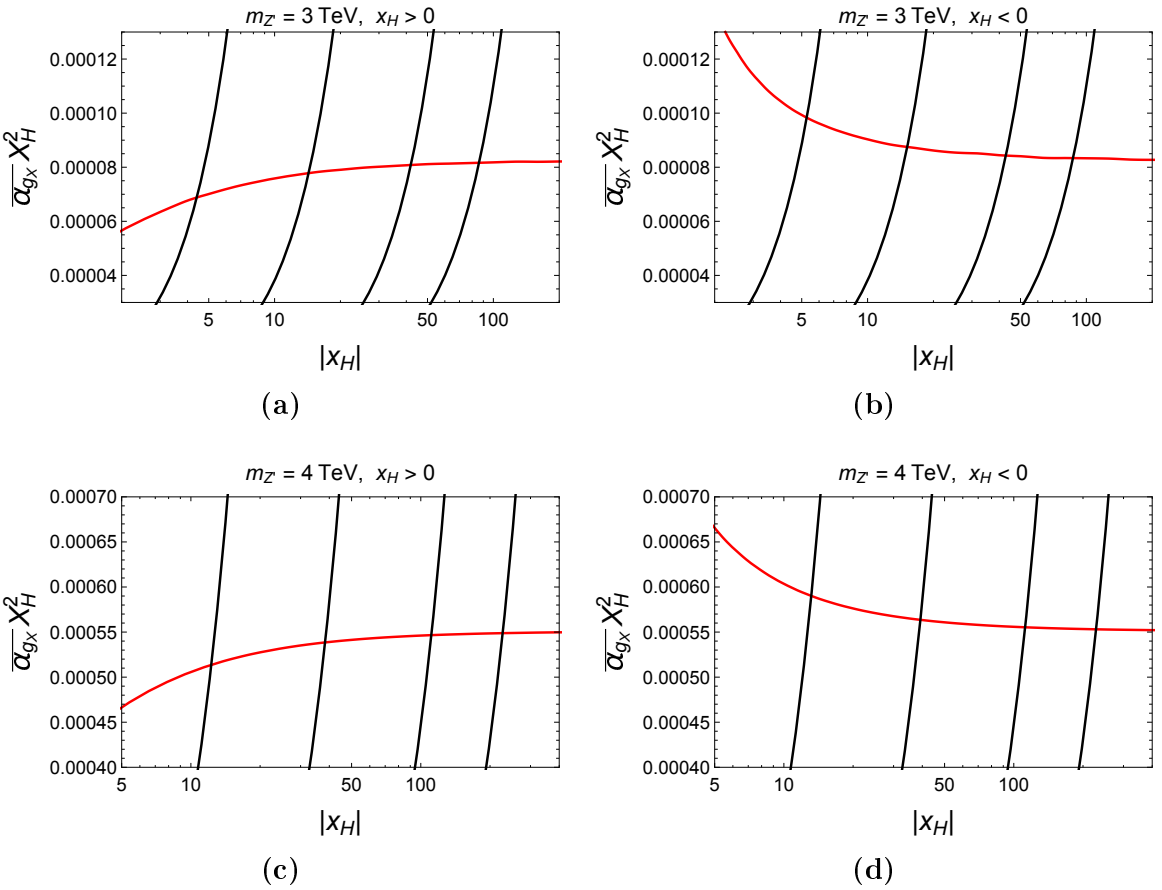

Figure 4.2: (a) The diagonal (black) lines depict $\overline{\alpha_{g_X}}\, x_H^2$ as a function of x_H for various values of $\xi = 10$, 1, 0.0689, and 0.00333 from left to right, along which the non-minimal quartic inflation is realized. Here, we have fixed $m_{Z'} = 3\, m_N = 3$ TeV and $x_H > 0$. The horizontal (red) line shows the upper bound on $\overline{\alpha_{g_X}}\, x_H^2$ as a function of x_H from the ATLAS 2017 results on the search for a narrow resonance [128]. (b) is the same as (a), but for $x_H < 0$. The result diagonal (black) lines for (a) $x_H > 0$ and (b) $x_H < 0$ are well overlapped and indistinguishable. (c) and (d) are the same as (a) and (b), but for $m_{Z'} = 3\, m_N = 4$ TeV.

value of 0.00008 (0.00055) for a large $|x_H|$. Combining the ATLAS 2017 constraints with the diagonal (black) lines from the inflationary analysis, we find upper bounds on $x_H \lesssim 5$, 15, 40, and 80 for $m_{Z'} = 3$ TeV ($x_H \lesssim 12$, 40, 110, and 220 for $m_{Z'} = 4$ TeV), corresponding to $\xi = 10$, 1, 0.0689, and 0.00333, respectively. Recall that the inflaton quartic coupling is extremely small for $\xi \lesssim 10$ (see Table 4.1), and this indicates that the U(1)$'$ gauge coupling is also very small (see Eq. (4.14)). Nevertheless, as has been pointed out in Ref. [167], the Z' boson with mass of $\mathcal{O}(1$ TeV) can still be tested at the LHC Run-2 when the U(1)$'$ gauge symmetry is oriented to the SM U(1)$_Y$ hyper-charge direction, namely, $|x_H| \gg 1$.

As the Z' boson is heavier, the LHC bounds become weaker, because of the energy dependence of the parton distribution functions. We can see this fact by comparing the horizontal (red) lines in Fig. 4.2(a) (Fig. 4.2(b)) and Fig. 4.2(c) (Fig. 4.2(d)). When we take $m_{Z'} = 5$ TeV, which is the maximum Z' boson mass in the ATLAS analysis [128],

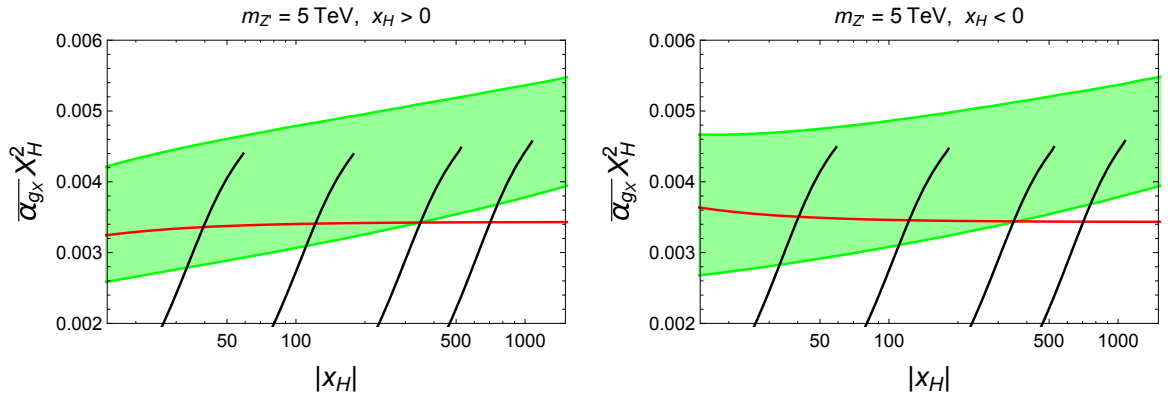

(a) (b)

Figure 4.3: (a) The combined result for $m_{Z'} = 5$ TeV and $x_H > 0$. The shaded (green) region depicts the parameters to resolve the electroweak vacuum instability, while satisfying the perturbativity of the gauge coupling at M_P. The horizontal (red) line denotes the upper bound from the ATLAS 2017 results for the Z' boson search at the LHC Run-2 [128]. The diagonal (black) lines correspond to $\xi = 10$, 1, 0.0689, and 0.00333 from left to right, along which the non-minimal quartic inflation is realized. (b) Same as (a), but for $x_H < 0$.

another interesting parameter region of our model opens up. In chapter 2, we have been investigated in the view point of the electroweak vacuum stability. As is well-known, the SM Higgs potential becomes unstable at high energies, since the running SM Higgs quartic coupling runs into the negative region at the renormalization scale of $\mu \simeq 10^{10}$ GeV [52]. It has been shown in chapter 2 that this electroweak vacuum instability problem can be solved in the context of the classically conformal U(1)′ model with $\overline{\alpha_{g_X}}\, x_H^2 \gtrsim 0.0025$. It is interesting to combine our inflation analysis with the results in chapter 2.

Fig. 4.3 shows the combined results in $(x_H, \overline{\alpha_{g_X}}\, x_H^2)$-plane. In Fig. 4.3(a), the parameter region to resolve the electroweak vacuum instability is shown as the shaded (green) region for $m_{Z'} = 5$ TeV and $x_H > 0$. In order to solve the instability problem, $\overline{\alpha_{g_X}}\, x_H^2 \gtrsim 0.0025$ is necessary, while $\overline{\alpha_{g_X}}$ has an upper bound for a fixed x_H from the requirement $\alpha_{g_X}(M_P) < 1$ that the running U(1)′ gauge coupling is in the perturbative regime at $\mu = M_P$. The horizontal (red) line denotes the upper bound from the ATLAS 2017 results. The diagonal lines correspond to $\xi = 10$, 1, 0.0689, and 0.00333 from left to right, along which the non-minimal quartic inflation is realized. Since we have found that the leading-log approximation for the RG analysis is not sufficiently reliable for $\overline{\alpha_{g_X}}\, x_H^2 \gtrsim 0.0025$, we have numerically integrated the RG equations in this analysis. See chapter 2 (also see Ref. [48, 49]) for details of our RG analysis. The upper bounds on $\overline{\alpha_{g_X}}\, x_H^2 \lesssim 0.0045$ shown on the diagonal (black) lines are also from the requirement of $\alpha_{g_X}(\phi_0) < 1$ for a given ξ. Since $\phi_0 > M_P$ for $\xi \lesssim 10$, the requirement of $\alpha_{g_X}(\phi_0) < 1$ is more severe than that of $\alpha_{g_X}(M_P) < 1$. We find the allowed parameter region for $\xi \gtrsim 0.0689$ and $x_H \lesssim 350$, although it is very narrow. Fig. 4.3(b) is the same as Fig. 4.3(a), but for $x_H < 0$.

Even if the U(1)′ gauge coupling is very small and $|x_H| \lesssim 1$, we can test our

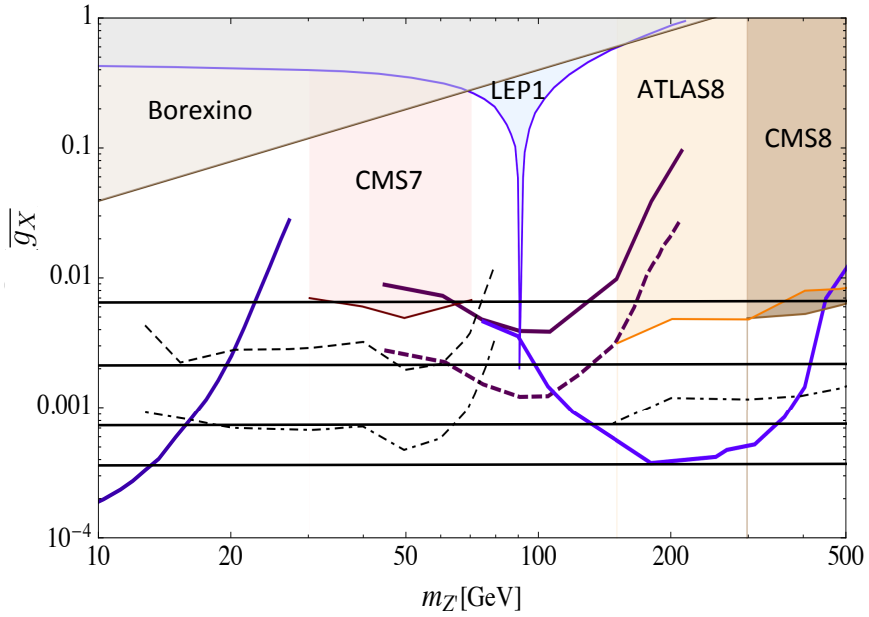

Figure 4.4: The $B-L$ gauge coupling ($\overline{g_X}$) a function of $m_{Z'}$, along with the results presented in Ref. [168]. The horizontal lines correspond to our results for $\xi = 10$, 1, 0.0689, and 0.00333 from top to bottom, respectively, along which the non-minimal quartic inflation is realized. According to the analysis in Ref. [168], we have fixed $m_N = m_{Z'}/3$. The shaded regions are excluded by the indicated experiments. The projected reach of the proposed searches for a Z' boson production and its decay into a pair of RHNs are shown in thick (solid and dashed) curves. The thin (black) curves show the projected sensitivity of direct searches for the Z' boson production via its decay $Z' \to \ell^+\ell^-$ from the LHC Run-1 (dashed), and the High-Luminosity LHC (dot-dashed). See Ref. [168] for more details.

model when the Z' boson is light, say, $m_{Z'} \lesssim 500$ GeV. In Ref. [168], the authors have considered the RHN production at the High-Luminosity LHC [169] and the SHiP [170] experiments in the contest of the minimal $B-L$ model (the limit of $x_H = 0$ in our U(1)$'$ model), where a pair of RHNs is created through the decay of a Z' boson resonantly produced at the colliders. When the RHNs have the mass of $\mathcal{O}(100$ GeV) or less, it is long-lived and its decay to the SM particles provides a clean signature with a displaced vertex. It has been found in Ref. [168] that for a fixed $m_N = m_{Z'}/3$, the High-Luminosity LHC and the SHiP experiments can explore the $B-L$ gauge coupling up to $\overline{g_X} \gtrsim 10^{-4}$ for 10 GeV $\lesssim m_{Z'} \lesssim 500$ GeV. In the $B-L$ limit of $x_H = 0$, we show in Fig. 4.4 the $B-L$ gauge coupling ($\overline{g_X}$) as a function of $m_{Z'}$, along with the results presented in Ref. [168]. The horizontal lines correspond to our results for $\xi = 10$, 1, 0.0689, and 0.00333 from top to bottom, respectively, along which the non-minimal quartic inflation is realized. Our results very weakly depend on $m_{Z'}$ in the mass range shown in Fig. 4.4, as can be understood from Eq. (4.14).

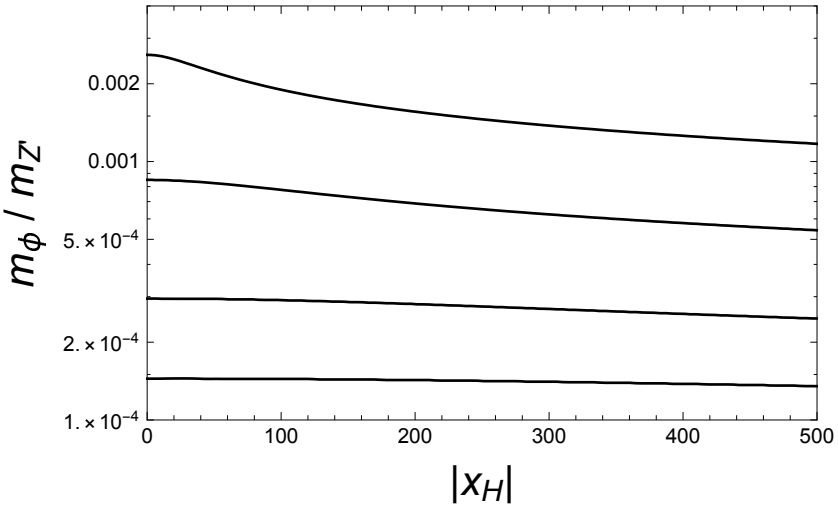

Figure 4.5: The mass ratio of $m_\phi/m_{Z'}$ as a function of x_H for $\xi = 10$, 1, 0.0689, and 0.00333 from top to bottom. Although we have used $m_{Z'} = 3$ TeV as a reference, we obtain almost identical results for other values of $m_{Z'}$.

4.4 Inflaton mass and reheating after inflation

To complete our inflation scenario, we finally discuss reheating after inflation through the inflaton decay into the SM particles. Since the inflaton is much lighter than the Z' boson and the RHNs in our scenario with $\xi \lesssim 10$, it decays mainly into the SM fermions through the mixing with the SM Higgs boson.

From the Higgs potential in Eq. (2.5) with the radiative corrections in Eq. (2.6), we find the following mass matrix for the inflaton (ϕ) and the SM Higgs boson (h) at the potential minimum:

$$\mathcal{L} \supset -\frac{1}{2}\begin{bmatrix} h & \phi \end{bmatrix}\begin{bmatrix} m_h^2 & -m_{\rm mix}^2 \\ -m_{\rm mix}^2 & m_\phi^2 \end{bmatrix}\begin{bmatrix} h \\ \phi \end{bmatrix}, \tag{4.15}$$

where $m_{\rm mix}^2 = |\lambda_{\rm mix}| v_h v_\phi$, $m_h = 125$ GeV and m_ϕ is given in Eq. (2.12). As can be seen in Secs. 2.2-2.3, $m_{\rm mix}^2$, $m_\phi^2 \ll m_h^2$ and the mass matrix is almost diagonal. We define the mass eigenstates, h' and ϕ', by

$$\begin{bmatrix} h' \\ \phi' \end{bmatrix} = \begin{bmatrix} \cos\theta & -\sin\theta \\ \sin\theta & \cos\theta \end{bmatrix}\begin{bmatrix} h \\ \phi \end{bmatrix}, \tag{4.16}$$

with a small mixing angle

$$\theta \simeq \frac{m_{\rm mix}^2}{m_h^2} = 2\overline{g_X}\left(\frac{v_h}{m_{Z'}}\right) \ll 1. \tag{4.17}$$

Since the mixing angle is very small, the mass eigenstate h' (ϕ') is almost the SM Higgs boson (the U(1)$'$ Higgs boson).

Through the mixing angle, the inflaton decays into the SM particles. We evaluate the inflaton decay width as

$$\Gamma_\phi(m_\phi) \simeq \theta^2 \times \Gamma_h(m_\phi), \tag{4.18}$$

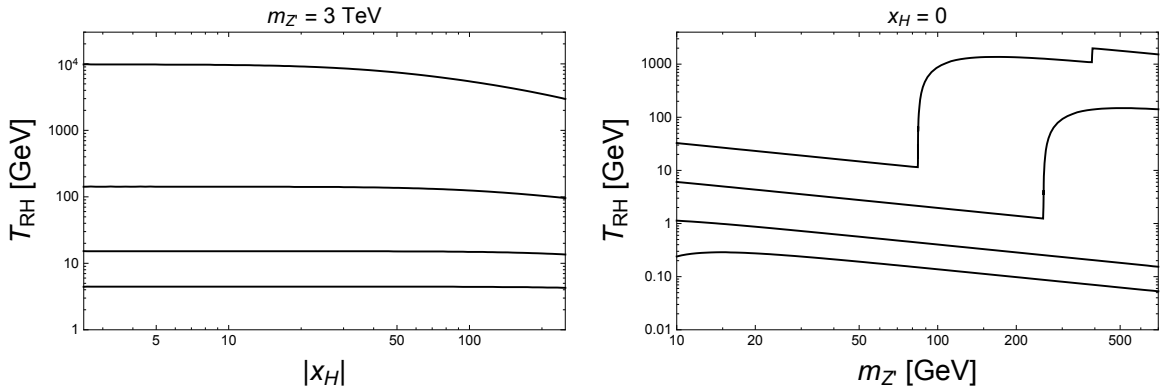

(a) (b)

Figure 4.6: Reheating temperature after inflation. (a) Reheating temperature as a function of x_H for $\xi = 10$, 1, 0.0689, and 0.00333 from top to bottom, with $m_{Z'} = 3$ TeV. The results for $x_H > 0$ and $x_H < 0$ are well overlapped and indistinguishable. (b) Reheating temperature as a function of $m_{Z'}$ in the $B - L$ model ($x_H = 0$). The solid lines correspond to the results for $\xi = 10$, 1, 0.0689, and 0.00333 from top to bottom. Sharp rises of the reheating temperature for threshold values of $m_{Z'}$ imply that new decay channels are opened.

where $\Gamma_h(m_\phi)$ is the SM Higgs boson decay width if the SM Higgs boson mass were m_ϕ[1]. From Eqs. (2.12) and (4.17), the inflaton mass and its decay width is a function of $\overline{\alpha_{gX}}$ and $m_{Z'}$ (with $m_N = m_{Z'}/3$). For the successful non-minimal inflation, $\overline{\alpha_{gX}}$ is determined as a function of ξ, x_H and $m_{Z'}$, and hence the inflaton mass and the decay width are controlled by the three parameters, ξ, x_H and $m_{Z'}$. With the inflaton decay width, we estimate reheating temperature by

$$T_{\rm RH} = \left(\frac{90}{\pi^2 g_*}\right)^{1/4} \sqrt{\Gamma_\phi M_P} \simeq \sqrt{\Gamma_\phi M_P}, \tag{4.19}$$

where g_* is the total effective degrees of freedom of thermal plasma.

In Fig. 4.5, we show the ratio of $m_\phi/m_{Z'}$ as a function of x_H for $\xi = 10$, 1, 0.0689, and 0.00333 from top to bottom. The results for $x_H > 0$ and $x_H < 0$ are well overlapped and indistinguishable. Although we have used $m_{Z'} = 3$ TeV as a reference, we find that the result is almost independent of $m_{Z'}$, as we have seen in Fig. 4.4 with $x_H = 0$. The resultant mass ratios are also weakly depending on x_H.

In Fig. 4.6, we show the estimated reheating temperature after inflation. Fig. 4.6(a) depicts the reheating temperature as a function of x_H for $\xi = 10$, 1, 0.0689, and 0.00333 from top to bottom, with $m_{Z'} = 3$ TeV. For the $B - L$ limit of $x_H = 0$, Fig. 4.6(b) depicts the results as a function of $m_{Z'}$. The solid lines from top to bottom correspond to the results for $\xi = 10$, 1, 0.0689, and 0.00333, respectively. Sharp rises of the reheating temperature for threshold values of $m_{Z'}$ imply that new decay channels are opened. For example, in the plot for $\xi = 10$, a new decay channel of $\phi \to \mu^+\mu^-$ opens at $m_{Z'} \simeq 80$ GeV. All results presented in Fig. 4.6 satisfy the model-independent

[1] $\Gamma_h(m_\phi)$ is a function of the SM Higgs boson decay width $\Gamma_h(m_h)$ replacing m_h with m_ϕ.

lower bound on reheating temperature, $T_{\rm RH} \gtrsim 1$ MeV, for the successful Big Bang Nucleosynthesis.

4.5 Summary

The non-minimal quartic inflation is a simple and successful inflation scenario, and its inflationary predictions are consistent with the Planck 2015 results for the non-minimal gravitational coupling with $\xi \gtrsim 0.003$ for $N_0 = 60$. This inflation scenario would be more compelling if the inflaton plays essential roles for not only inflation but also particle physics phenomena. In many models beyond the SM where the gauge symmetry of the SM is extended, a new Higgs field to break the extended gauge symmetry is commonly introduced. It is an interesting possibility to identify such a Higgs field with the inflaton in the non-minimal quartic inflation.

In this chapter, we have considered the classically conformal U(1)$'$ extended SM, where the U(1)$'$ gauge group is realized as a linear combination of the U(1)$_{B-L}$ and the SM U(1)$_Y$ gauge groups. This model has an interesting property that all the gauge symmetry breakings in the model originates from the Coleman-Weinberg mechanism: The U(1)$'$ gauge symmetry is radiatively broken through the Coleman-Weinberg mechanism, and this breaking generates a negative mass squared for the SM Higgs doublet and hence, the electroweak symmetry breaking occurs subsequently. Associated with the U(1)$'$ gauge symmetry breaking, the Z' boson and the right-handed neutrinos acquire their masses. We have set their masses in the range of $\mathcal{O}(10$ GeV$)-\mathcal{O}(10$ TeV$)$, which is accessible at high energy collider experiments

We have investigated the non-minimal inflation scenario in the context of this classically conformal U(1)$'$ model by identifying the U(1)$'$ Higgs field with the inflaton. In this model, the U(1)$'$ gauge symmetry is radiatively broken through the Coleman-Weinberg mechanism, due to which the inflaton quartic coupling is determined by the U(1)$'$ gauge coupling. Since the inflationary predictions in the non-minimal quartic inflation are determined by the inflaton quartic coupling during inflation, we have a correlation between the inflationary predictions and the U(1)$'$ gauge coupling. With this correlation, we have investigated complementarities between the inflationary predictions and the constraint from the Z' boson resonance search at the LHC Run-2 2017 as well as the prospect of the search for the Z' boson and the right-handed neutrinos at the future collider experiments. For completion of our inflation scenario, we have considered a reheating scenario due to the inflaton decay through the SM Higgs boson, and found the reheating temperature to be sufficiently high.

Finally, we comment on the stability of the scalar potential during inflation. We have considered the inflation trajectory in the direction of ϕ with $H = 0$. For $\phi \gg v_\phi$, the scalar potential is approximated by Eq. (2.5) with replacing the quartic couplings at the tree-level by their RG running couplings. If $\lambda_{\rm mix} < 0$ during inflation, we can see a problem that the inflaton potential is destabilized in the SM Higgs direction. In fact, when we take into account the RG evolution of $\lambda_{\rm mix}$, see Fig. 2.1(b) as an example, we can find that $\lambda_{\rm mix} > 0$ during inflation ($\mu \gtrsim M_P$), and therefore the potential is stabilized in the SM Higgs direction.

In our analysis we have considered the number of e-folds to be a free parameter and

have fixed $N_0 = 60$. However, the number of e-folds is determined by the reheating temperature T_R, and the inflaton potential energy at the horizon exit ($V_E|_{k_0}$) as (see, for example, Refs. [171, 172])

$$N_0 \simeq 51.4 + \frac{2}{3}\ln\left(\frac{V_E|_{k_0}^{1/4}}{10^{15}\text{GeV}}\right) + \frac{1}{3}\ln\left(\frac{T_R}{10^{7}\text{GeV}}\right). \tag{4.20}$$

Because of this relation, the number of e-folds is not a free parameter and is determined as a function of ξ, x_H, and $m_{Z'}$. Using this relation we can make our predictions more precise. However, in such an analysis the inflationary predictions, low energy observables, and the reheating temperature are related with each other in a very complicated way through the free parameters ξ, x_H, and $m_{Z'}$. To keep our discussion very clear we have treated N_0 as a free parameter. From Eq. (4.20), we can see that the true value of N_0 lies in between 50 and 60. As shown in Table 4.1, the inflationary predictions for a fixed ξ weakly depend on N_0 values. Hence our results with $N_0 = 60$ well approximate the true values.

Conclusion

In chapter 1, we have briefly reviewed the standard model (SM). The SM is a well-established model which can provide precise predictions for experiments. However, the SM still has several problems, such as the gauge hierarchy problem, origin of the electroweak symmetry breaking, non-zero neutrino mass, and no candidate of dark matter.

The classical conformal symmetry with its violation through quantum anomalies could be a solution to the gauge hierarchy problem in the SM. Unfortunately, we cannot simply apply this mechanism to the SM, since the large top Yukawa coupling destabilizes the effective Higgs potential. In chapter 2, we have introduced the minimal gauged U(1)$'$ extension of the SM with classically scale invariance, in which three RHNs and a U(1)$'$ Higgs singlet field are introduced [48, 49]. The U(1)$'$ gauge group is an anomaly-free linear combination of the U(1)$_{B-L}$ and the SM U(1)$_Y$ gauge group. This model has an interesting property that all the gauge symmetry breakings in the model originates from the Coleman-Weinberg mechanism. The U(1)$'$ gauge symmetry is radiatively broken through the Coleman-Weinberg mechanism, and this breaking generates a negative mass squared for the SM Higgs doublet and hence, the electroweak symmetry breaking occurs subsequently. Associated with the U(1)$'$ gauge symmetry breaking, the Z' boson and the right-handed neutrinos acquire their masses. With the Majorana heavy neutrinos, the seesaw mechanism is automatically implemented. Therefore, all mass generations occur through the dimensional transmutation in our model.

In addition to the measurement of the top quark mass, with the discovery of Higgs particle at the LHC on 2012, it is possible to discuss the electroweak vacuum stability more directly than before. The data of these top quark and Higgs masses indicates that our electroweak vacuum seems instable because the SM Higgs quartic coupling goes to negative at high energy scale less than Planck mass one. Although it might not be a problem, if the transitional time toward to the true vacuum is smaller than the life time of universe, it is not clear for our extended model which has an extra Higgs single field for using the Coleman Weinberg mechanism. The additional Higgs scalar filed affects its effective potential which might have a flat path toward the true vacuum with current experimental data of the top quark and the Higgs boson masses. In chapter 2, we have first investigated a possibility to resolve the electroweak vacuum instability with the current world average of the experimental data, $m_t = 173.34$ GeV [53] and $m_h = 125.09$ GeV [51]. Since the gauge symmetry is broken by the Coleman-Weinberg mechanism, all quartic couplings in the Higgs potential, except the SM Higgs one, are very small, and hence their positive contributions to the U(1)$'$ model are not effective in resolving

the SM Higgs vacuum instability. On the other hand, in the U(1)′ model, the SM Higgs doublet has a nonzero U(1)′ charge, and this gauge interaction positively contributes to the beta function. In addition, the U(1)′ gauge interaction negatively contributes to the beta function of the top Yukawa coupling, so the running top Yukawa coupling is decreasing faster than in the SM case, and its negative contribution to the beta function of the SM Higgs quartic coupling becomes milder. For three free parameters of the model, $m_{Z'}$, α_{g_X} and x_H, we have performed a parameter scan by analyzing the renormalization group evolutions of the model parameters at the two-loop level, and we have identified parameter regions which can solve the electroweak vacuum instability problem and keep all coupling values in the perturbative regime up to the Planck mass. We have found that the resultant parameter regions are very severely constrained, and also that the $U(1)_{B-L}$ model and the orthogonal model are excluded from having the electroweak vacuum stability with the current world average of the experimental data, $m_t = 173.34$ GeV and $m_h = 125.09$ GeV.

In chapter 2, we have also considered the collider bounds on the U(1)′ Z' boson mass from the recent ATLAS and CMS results at the LHC Run-2 2015 with $\sqrt{s} = 13$ TeV. We have interpreted the Z' boson resonance search results at the LHC Run-1 and Run-2 (2015) to the U(1)′ Z' boson case, and obtained the LHC bound on the U(1)′ charge of the SM Higgs doublet x_H for a fixed U(1)′ gauge coupling, the LHC bound on x_H for a fixed VEV of the U(1)′ Higgs, or the LHC upper bound on the U(1)′ gauge coupling for a fixed x_H as a function of the U(1)′ Z' boson mass $m_{Z'}$. We have also considered naturalness of our model. Once the U(1)′ gauge symmetry is broken, the Z' boson and the right-handed neutrinos become heavy and contribute to the SM Higgs self-energy through quantum corrections. Therefore, the SM Higgs self-energy can exceed the electroweak scale, if the states are so heavy. Since the SM Higgs doublet has nonzero U(1)′ charge, the self-energy corrections from the Z' boson occur at the one-loop level. This is in sharp contrast to the classically conformal $U(1)_{B-L}$ model [40, 41], where the Higgs doublet has no $U(1)_{B-L}$ charge, and the self-energy corrections from the Z' boson occur at the two-loop level. We have evaluated the Higgs self-energy corrections, and found the naturalness bounds as $m_{Z'} \lesssim 7$ TeV to reproduce the right electroweak scale for the fine-tuning level better than 10%, Combining the constraints from the electroweak vacuum stability. the LHC Run-2 2015 results, and naturalness bounds, we have found that the U(1)′ Z' boson mass lies in the range of 3.5 TeV$\lesssim m_{Z'} \lesssim 7$ TeV.

In chapter 3, we have considered the DM scenario in the context of the classically conformal U(1)′ extended SM, with three RHNs and the U(1)′ Higgs field [99]. The model is free from all the U(1)′ gauge and gravitational anomalies in the presence of the three RHNs. We have introduced a Z_2-parity in the model, under which an odd-parity is assigned to one RHN, while all the other particles are assigned to be Z_2-even. In our model, the Z_2-odd RHN serves as a stable DM candidate, while the other two RHNs are utilized for the the minimal seesaw mechanism in order to reproduce the neutrino oscillation data and the observed baryon asymmetry in the Universe through leptogenesis. There are three free parameters in our model, the U(1)′ charge of the SM Higgs doublet (x_H), the new U(1)′ gauge coupling (α_{g_X}), and the U(1)′ gauge boson (Z') mass ($m_{Z'}$). In this model context, we have first investigated a possibility to resolve the electroweak vacuum instability with the current world average of the experimental

data, $m_t = 173.34$ GeV and $m_h = 125.09$ GeV, by using the same strategy in chapter 2. Next, we have calculated the thermal relic density of the RHN DM and identified the model parameter region to reproduce the observed DM relic density of the Planck 2015 measurement. In our model, the RHN DM particles mainly annihilate into the SM particles through the s-channel process mediated by the Z' boson. We have obtained the lower bound on α_{g_X} as a function of $m_{Z'}$ and x_H from the observed DM relic density. By using the same strategy in chapter 2, we have also calculated the LHC Run-2 2016 bounds from the search for the Z' boson resonance by the ATLAS and CMS analysis, which lead to the upper bounds on α_{g_X} as a function of $m_{Z'}$ and x_H. Finally, we have combined all the constraints. The cosmological constraint on the RHN DM yields the lower bound on α_{g_X} as a function of $m_{Z'}$ and x_H, while the upper bound on α_{g_X} is obtained from the LHC Run-2 2016 results, so that these constraints are complementary to narrow the allowed parameter regions. We have found that only small portions in these allowed parameter regions can solve the electroweak vacuum instability problem. In particular, no allowed region to satisfy all constraints exists for $m_{Z'} \lesssim 3.5$ TeV. For the obtained allowed regions, we have calculated the spin-independent cross section of the RHN DM with nucleons. We have found that the resultant cross section well below the current experimental upper bounds.

In chapter 4, we have investigated the non-minimal inflation scenario in the context of this classically conformal U(1)$'$ model by identifying the U(1)$'$ Higgs field with the inflaton [127]. The non-minimal quartic inflation is a simple and successful inflation scenario, and its inflationary predictions are consistent with the Planck 2015 results for the non-minimal gravitational coupling with $\xi \gtrsim 0.003$ for $N_0 = 60$. Hence, it is interesting to identify the U(1)$'$ Higgs field with the inflaton in the non-minimal quartic inflation. In this model, the U(1)$'$ gauge symmetry is radiatively broken through the Coleman-Weinberg mechanism, due to which the inflaton quartic coupling is determined by the U(1)$'$ gauge coupling. Since the inflationary predictions in the non-minimal quartic inflation are determined by the inflaton quartic coupling during inflation, we have a correlation between the inflationary predictions and the U(1)$'$ gauge coupling. With this correlation, we have investigated complementarities between the inflationary predictions and the constraint from the Z' boson resonance search at the LHC Run-2 2017 as well as the prospect of the search for the Z' boson and the right-handed neutrinos at the future collider experiments. For completion of our inflation scenario, we have considered a reheating scenario due to the inflaton decay through the SM Higgs boson, and found the reheating temperature to be sufficiently high.

Appendix A

U(1)′ RGES AT THE ONE-LOOP LEVEL

In this appendix we present the one-loop RGEs for the U(1)′ extension of the SM, which are used in our analysis. The covariant derivative relevant to $U(1)_Y \times U(1)'$ in this Appendix is defined as

$$D_\mu \equiv \partial_\mu - i(g_1 Y + \tilde{g} Q_X) B_\mu - i g_X Q_Z Z'_\mu, \tag{A.1}$$

where Y (Y') are $U(1)_Y$ ($U(1)'$) charge of a particle, and the gauge coupling $\tilde{g}$ is introduced associated with a kinetic mixing between the two U(1) gauge bosons. The definitions of the Yukawa interactions and the scalar potential are given by Eqs. (2.3) and (2.5), respectively. We only include the top quark Yukawa coupling y_t and the right-handed neutrino Majorana Yukawa coupling Y_M^i, since the other Yukawa couplings are negligibly small. The U(1)′ charges x_i are defined in Table 2.1. The RGEs for the

gauge couplings at the one-loop level are given by

$$
\begin{aligned}
\mu\frac{dg_3}{d\mu} &= \frac{g_3^3}{(4\pi)^2}\Big[-7\Big],\\
\mu\frac{dg_2}{d\mu} &= \frac{g_2^3}{(4\pi)^2}\left[-\frac{19}{6}\right],\\
\mu\frac{dg_1}{d\mu} &= \frac{g_1}{(4\pi)^2}\left[12\left(\frac{1}{6}g_1+x_q\tilde{g}\right)^2+6\left(\frac{2}{3}g_1+x_u\tilde{g}\right)^2+6\left(-\frac{1}{3}g_1+x_d\tilde{g}\right)^2\right.\\
&+ \left. 4\left(-\frac{1}{2}g_1+x_\ell\tilde{g}\right)^2+2\left(x_\nu\tilde{g}\right)^2+2\left(-g_1+x_e\tilde{g}\right)^2+\frac{2}{3}\left(\frac{1}{2}g_1+x_H\tilde{g}\right)^2+\frac{1}{3}\left(x_\Phi\tilde{g}\right)^2\right],\\
\mu\frac{dg_X}{d\mu} &= \frac{g_X^3}{(4\pi)^2}\left[12x_q^2+6x_u^2+6x_d^2+4x_\ell^2+2x_\nu^2+2x_e^2+\frac{2}{3}x_H^2+\frac{1}{3}x_\Phi^2\right],\\
\mu\frac{d\tilde{g}}{d\mu} &= \frac{1}{(4\pi)^2}\left[\tilde{g}\left\{12\left(\frac{1}{6}g_1+x_q\tilde{g}\right)^2+6\left(\frac{2}{3}g_1+x_u\tilde{g}\right)^2+6\left(-\frac{1}{3}g_1+x_d\tilde{g}\right)^2\right.\right.\\
&+ \left. 4\left(-\frac{1}{2}g_1+x_\ell\tilde{g}\right)^2+2\big(x_\nu\tilde{g}\big)^2+2\big(-g_1+x_e\tilde{g}\big)^2+\frac{2}{3}\left(\frac{1}{2}g_1+x_H\tilde{g}\right)^2+\frac{1}{3}\left(x_\Phi\tilde{g}\right)^2\right\}\\
&+ 2g_X^2\left\{12x_q\left(\frac{1}{6}g_1+x_q\tilde{g}\right)+6x_u\left(\frac{2}{3}g_1+x_u\tilde{g}\right)+6x_d\left(-\frac{1}{3}g_1+x_d\tilde{g}\right)\right.\\
&+ 4x_\ell\left(-\frac{1}{2}g_1+x_\ell\tilde{g}\right)+2x_\nu\big(x_\nu\tilde{g}\big)+2x_e\big(-g_1+x_e\tilde{g}\big)\\
&+ \left.\left.\frac{2}{3}x_H\left(\frac{1}{2}g_1+x_H\tilde{g}\right)+\frac{1}{3}x_\Phi\left(x_\Phi\tilde{g}\right)\right\}\right].
\end{aligned}
\tag{A.2}
$$

For the RGEs for the Yukawa couplings at the one-loop level we have

$$
\begin{aligned}
\mu\frac{dy_t}{d\mu} &= \frac{y_t}{(4\pi)^2}\left[\frac{9}{2}y_t^2-8g_3^2-\frac{9}{4}g_2^2-6\left(\frac{1}{6}g_1+x_q\tilde{g}\right)\left(\frac{2}{3}g_1+x_u\tilde{g}\right)\right.\\
&- \left. 3\left(\frac{1}{2}g_1+x_H\tilde{g}\right)^2-6\left(x_qg_X\right)\left(x_ug_X\right)-3\left(x_Hg_X\right)^2\right],\\
\mu\frac{dY_M^i}{d\mu} &= \frac{Y_M^i}{(4\pi)^2}\left[4(Y_M^i)^2+2\sum_j(Y_M^j)^2+\big(6x_\nu^2-3x_\Phi^2\big)\big(\tilde{g}^2+g_X^2\big)\right].
\end{aligned}
\tag{A.3}
$$

Finally, the RGEs for the scalar quartic couplings are given by

$$
\begin{aligned}
\mu\frac{d\lambda_H}{d\mu} &= \frac{1}{(4\pi)^2}\Bigg[\lambda_H\Bigg\{24\lambda_H + 12y_t^2 - 9g_2^2 - 12\left(\frac{1}{2}g_1 + x_H\tilde{g}\right)^2 - 12\big(x_H g_X\big)^2\Bigg\} \\
&+ \lambda_{mix}^2 - 6y_t^4 + \frac{9}{8}g_2^4 + 6\left(\frac{1}{2}g_1 + x_H\tilde{g}\right)^4 + 6\big(x_H g_X\big)^4 \\
&+ 3g_2^2\left(\frac{1}{2}g_1 + x_H\tilde{g}\right)^2 + 3g_2^2\big(x_H g_X\big)^2 + 12\left(\frac{1}{2}g_1 + x_H\tilde{g}\right)^2\big(x_H g_X\big)^2\Bigg], \\
\mu\frac{d\lambda_\Phi}{d\mu} &= \frac{1}{(4\pi)^2}\Bigg[\lambda_\Phi\Big\{20\lambda_\Phi + 8\sum_i (Y_M^i)^2 - 12\big(x_\Phi\tilde{g}\big)^2 - 12\big(x_\Phi g_X\big)^2\Big\} \\
&+ 2\lambda_{mix}^2 - 16\sum_i (Y_M^i)^4 + 6\Big\{\big(x_\Phi\tilde{g}\big)^2 + \big(x_\Phi g_X\big)^2\Big\}^2\Bigg], \\
\mu\frac{d\lambda_{mix}}{d\mu} &= \frac{1}{(4\pi)^2}\Bigg[\lambda_{mix}\Bigg\{12\lambda_H + 8\lambda_\Phi + 4\lambda_{mix} + 6y_t^2 + 4\sum_i (Y_M^i)^2 \\
&- \frac{9}{2}g_2^2 - 6\left(\frac{1}{2}g_1 + x_H\tilde{g}\right)^2 - 6\big(x_\Phi\tilde{g}\big)^2 - 6\big(x_H g_X\big)^2 - 6\big(x_\Phi g_X\big)^2\Bigg\} \\
&+ 12\Bigg\{\left(\frac{1}{2}g_1 + x_H\tilde{g}\right)\big(x_\Phi\tilde{g}\big) + \big(x_H g_X\big)\big(x_\Phi g_X\big)\Bigg\}^2\Bigg].
\end{aligned}
\tag{A.4}
$$

Appendix B

U(1)′ RGES AT THE TWO-LOOP LEVEL

In this appendix we present the two-loop RGEs for the U(1)′ extension of the SM, which are used in our analysis, especially numerical analysis. The covariant derivatives relevant to $U(1)_Y \times U(1)'$ in this Appendix and chapter 2are defined as

$$D_\mu \equiv \partial_\mu - i \begin{pmatrix} Y_1 & Y_X \end{pmatrix} \begin{pmatrix} g_1 & g_{1X} \\ g_{X1} & g_X \end{pmatrix} \begin{pmatrix} B_\mu \\ B'_\mu \end{pmatrix}, \tag{B.1}$$

where Y_1 (Y_X) are $U(1)_Y$ (U(1)′) charge of a particle, and the gauge couplings g_{X1} and g_{1X} are introduced associated with a kinetic mixing between the two U(1) gauge bosons. The definitions of the Yukawa interactions and the scalar potential are given by Eqs. (2.3) and (2.5), respectively. We only include the top quark Yukawa coupling y_t and the right-handed neutrino Majorana Yukawa coupling $y_M = Y_M^i$ $(i = 1, 2, 3)$ since the other Yukawa couplings are negligibly small. The U(1)′ charges x_i are defined in Table 2.1. The U(1)′ RGEs at the two-loop level have been generated by using SARAH [139, 140].

B.1 U(1)′ RGEs for the gauge couplings

The RGEs for the gauge couplings at the two-loop level are given by

$$\mu \frac{dg_i}{d\mu} = \beta_{g_i}^{(1)} + \beta_{g_i}^{(2)}, \tag{B.2}$$

where $\beta_{g_i}^{(1)}$ and $\beta_{g_i}^{(2)}$ are the one-loop and two-loop beta functions for the gauge couplings, respectively, and g_i represents g_3, g_2, g_1, g_{X1}, g_{1X} and g_X. Here, the one-loop

beta functions for the gauge couplings are given by

$$
\begin{aligned}
\beta^{(1)}_{g_3} &= \frac{g_3^3}{16\pi^2}\Big[-7\Big],\\
\beta^{(1)}_{g_2} &= \frac{g_2^3}{16\pi^2}\left[-\frac{19}{6}\right],\\
\beta^{(1)}_{g_1} &= \frac{1}{16\pi^2}\left[g_1\left\{\frac{41}{6}g_1^2+\frac{1}{3}\big(82x_H+16x_\Phi\big)g_1g_{X1}+\frac{1}{3}\big(82x_H^2+32x_Hx_\Phi+9x_\Phi^2\big)g_{X1}^2\right\}\right.\\
&+ g_{1X}\left\{\frac{41}{6}g_1g_{1X}+\frac{1}{3}\big(41x_H+8x_\Phi\big)g_1g_X+\frac{1}{3}\big(41x_H+8x_\Phi\big)g_{1X}g_{X1}\right.\\
&+ \left.\left.\frac{1}{3}\big(82x_H^2+32x_Hx_\Phi+9x_\Phi^2\big)g_{X1}g_X\right\}\right],\\
\beta^{(1)}_{g_{X1}} &= \frac{1}{16\pi^2}\left[g_{X1}\left\{\frac{41}{6}g_1^2+\frac{1}{3}\big(82x_H+16x_\Phi\big)g_1g_{X1}+\frac{1}{3}\big(82x_H^2+32x_Hx_\Phi+9x_\Phi^2\big)g_{X1}^2\right\}\right.\\
&+ g_X\left\{\frac{41}{6}g_1g_{1X}+\frac{1}{3}\big(41x_H+8x_\Phi\big)g_1g_X+\frac{1}{3}\big(41x_H+8x_\Phi\big)g_{1X}g_{X1}\right.\\
&+ \left.\left.\frac{1}{3}\big(82x_H^2+32x_Hx_\Phi+9x_\Phi^2\big)g_{X1}g_X\right\}\right],\\
\beta^{(1)}_{g_{1X}} &= \frac{1}{16\pi^2}\left[g_{1X}\left\{\frac{41}{6}g_{1X}^2+\frac{1}{3}\big(82x_H+16x_\Phi\big)g_{1X}g_X+\frac{1}{3}\big(82x_H^2+32x_Hx_\Phi+9x_\Phi^2\big)g_X^2\right\}\right.\\
&+ g_1\left\{\frac{41}{6}g_1g_{1X}+\frac{1}{3}\big(41x_H+8x_\Phi\big)g_1g_X+\frac{1}{3}\big(41x_H+8x_\Phi\big)g_{1X}g_{X1}\right.\\
&+ \left.\left.\frac{1}{3}\big(82x_H^2+32x_Hx_\Phi+9x_\Phi^2\big)g_{X1}g_X\right\}\right],\\
\beta^{(1)}_{g_X} &= \frac{1}{16\pi^2}\left[g_X\left\{\frac{41}{6}g_{1X}^2+\frac{1}{3}\big(82x_H+16x_\Phi\big)g_{1X}g_X+\frac{1}{3}\big(82x_H^2+32x_Hx_\Phi+9x_\Phi^2\big)g_X^2\right\}\right.\\
&+ g_{X1}\left\{\frac{41}{6}g_1g_{1X}+\frac{1}{3}\big(41x_H+8x_\Phi\big)g_1g_X+\frac{1}{3}\big(41x_H+8x_\Phi\big)g_{1X}g_{X1}\right.\\
&+ \left.\left.\frac{1}{3}\big(82x_H^2+32x_Hx_\Phi+9x_\Phi^2\big)g_{X1}g_X\right\}\right], \qquad \text{(B.3)}
\end{aligned}
$$

and the two-loop beta functions for the gauge couplings are given by

$$
\begin{aligned}
\beta^{(2)}_{g_3} &= \frac{1}{(16\pi^2)^2}\cdot\frac{g_3^3}{6}\Big[11g_1^2+27g_2^2-156g_3^2+11g_{1X}^2+44g_{1X}g_Xx_H+44g_1g_{X1}x_H+44g_X^2x_H^2\\
&+ 44g_{X1}^2x_H^2+4g_{1X}g_Xx_\Phi+4g_1g_{X1}x_\Phi+8g_X^2x_Hx_\Phi+8g_{X1}^2x_Hx_\Phi+2g_X^2x_\Phi^2+2g_{X1}^2x_\Phi^2-12y_t^2\Big],\\
\beta^{(2)}_{g_2} &= \frac{1}{(16\pi^2)^2}\cdot\frac{g_2^3}{6}\Big[9g_1^2+35g_2^2+72g_3^2+9g_{1X}^2+36g_{1X}g_Xx_H+36g_1g_{X1}x_H+36g_X^2x_H^2+36g_{X1}^2x_H^2\\
&+ 12g_{1X}g_Xx_\Phi+12g_1g_{X1}x_\Phi+24g_X^2x_Hx_\Phi+24g_{X1}^2x_Hx_\Phi+6g_X^2x_\Phi^2+6g_{X1}^2x_\Phi^2-9y_t^2\Big],\\
\beta^{(2)}_{g_1} &= \frac{1}{(16\pi^2)^2}\cdot\frac{1}{18}\Big[199g_1^5+81g_1^3g_2^2+264g_1^3g_3^2+398g_1^3g_{1X}^2+81g_1g_2^2g_{1X}^2+264g_1g_3^2g_{1X}^2\\
&+ 199g_1g_{1X}^4+1194g_1^3g_{1X}g_Xx_H+162g_1g_2^2g_{1X}g_Xx_H+528g_1g_3^2g_{1X}g_Xx_H\\
&+ 1194g_1g_{1X}^3g_Xx_H+1592g_1^4g_{X1}x_H+324g_1^2g_2^2g_{X1}x_H+1056g_1^2g_3^2g_{X1}x_H+1990g_1^2g_{1X}^2g_{X1}x_H\\
&+ 162g_2^2g_{1X}^2g_{X1}x_H+528g_3^2g_{1X}^2g_{X1}x_H+398g_{1X}^4g_{X1}x_H+796g_1^3g_X^2x_H^2+2388g_1g_{1X}^2g_X^2x_H^2\\
&+ 5572g_1^2g_{1X}g_Xg_{X1}x_H^2+324g_2^2g_{1X}g_Xg_{X1}x_H^2+1056g_3^2g_{1X}g_Xg_{X1}x_H^2+2388g_{1X}^3g_Xg_{X1}x_H^2\\
&+ 4776g_1^3g_{X1}^2x_H^2+324g_1g_2^2g_{X1}^2x_H^2+1056g_1g_3^2g_{X1}^2x_H^2+3184g_1g_{1X}^2g_{X1}^2x_H^2+1592g_1g_{1X}g_X^3x_H^3\\
&+ 3184g_1^2g_X^2g_{X1}x_H^3+4776g_{1X}^2g_X^2g_{X1}x_H^3+7960g_1g_{1X}g_Xg_{X1}^2x_H^3+6368g_1^2g_{X1}^3x_H^3\\
&+ 1592g_{1X}^2g_{X1}^3x_H^3+3184g_{1X}g_X^3g_{X1}x_H^4+3184g_1g_X^2g_{X1}^2x_H^4+3184g_{1X}g_Xg_{X1}^3x_H^4\\
&+ 3184g_1g_{X1}^4x_H^4+246g_1^3g_{1X}g_Xx_\Phi+54g_1g_2^2g_{1X}g_Xx_\Phi+48g_1g_3^2g_{1X}g_Xx_\Phi\\
&+ 246g_1g_{1X}^3g_Xx_\Phi+328g_1^4g_{X1}x_\Phi+108g_1^2g_2^2g_{X1}x_\Phi+96g_1^2g_3^2g_{X1}x_\Phi+410g_1^2g_{1X}^2g_{X1}x_\Phi\\
&+ 54g_2^2g_{1X}^2g_{X1}x_\Phi+48g_3^2g_{1X}^2g_{X1}x_\Phi+82g_{1X}^4g_{X1}x_\Phi+328g_1^3g_X^2x_Hx_\Phi+984g_1g_{1X}^2g_X^2x_Hx_\Phi\\
&+ 2296g_1^2g_{1X}g_Xg_{X1}x_Hx_\Phi+216g_2^2g_{1X}g_Xg_{X1}x_Hx_\Phi+192g_3^2g_{1X}g_Xg_{X1}x_Hx_\Phi\\
&+ 984g_{1X}^3g_Xg_{X1}x_Hx_\Phi+1968g_1^3g_{X1}^2x_Hx_\Phi+216g_1g_2^2g_{X1}^2x_Hx_\Phi+192g_1g_3^2g_{X1}^2x_Hx_\Phi\\
&+ 1312g_1g_{1X}^2g_{X1}^2x_Hx_\Phi+984g_1g_{1X}g_X^3x_H^2x_\Phi+1968g_1^2g_X^2g_{X1}x_H^2x_\Phi+2952g_{1X}^2g_X^2g_{X1}x_H^2x_\Phi\\
&+ 4920g_1g_{1X}g_Xg_{X1}^2x_H^2x_\Phi+3936g_1^2g_{X1}^3x_H^2x_\Phi+984g_{1X}^2g_{X1}^3x_H^2x_\Phi+2624g_{1X}g_X^3g_{X1}x_H^3x_\Phi\\
&+ 2624g_1g_X^2g_{X1}^2x_H^3x_\Phi+2624g_{1X}g_Xg_{X1}^3x_H^3x_\Phi+2624g_1g_{X1}^4x_H^3x_\Phi+46g_1^3g_X^2x_\Phi^2\\
&+ 138g_1g_{1X}^2g_X^2x_\Phi^2+322g_1^2g_{1X}g_Xg_{X1}x_\Phi^2+54g_2^2g_{1X}g_Xg_{X1}x_\Phi^2+48g_3^2g_{1X}g_Xg_{X1}x_\Phi^2\\
&+ 138g_{1X}^3g_Xg_{X1}x_\Phi^2+276g_1^3g_{X1}^2x_\Phi^2+54g_1g_2^2g_{X1}^2x_\Phi^2+48g_1g_3^2g_{X1}^2x_\Phi^2+184g_1g_{1X}^2g_{X1}^2x_\Phi^2\\
&+ 276g_1g_{1X}g_X^3x_Hx_\Phi^2+552g_1^2g_X^2g_{X1}x_Hx_\Phi^2+828g_{1X}^2g_X^2g_{X1}x_Hx_\Phi^2+1380g_1g_{1X}g_Xg_{X1}^2x_Hx_\Phi^2\\
&+ 1104g_1^2g_{X1}^3x_Hx_\Phi^2+276g_{1X}^2g_{X1}^3x_Hx_\Phi^2+1104g_{1X}g_X^3g_{X1}x_H^2x_\Phi^2+1104g_1g_X^2g_{X1}^2x_H^2x_\Phi^2\\
&+ 1104g_{1X}g_Xg_{X1}^3x_H^2x_\Phi^2+1104g_1g_{X1}^4x_H^2x_\Phi^2+28g_1g_{1X}g_X^3x_\Phi^3+56g_1^2g_X^2g_{X1}x_\Phi^3\\
&+ 84g_{1X}^2g_X^2g_{X1}x_\Phi^3+140g_1g_{1X}g_Xg_{X1}^2x_\Phi^3+112g_1^2g_{X1}^3x_\Phi^3+28g_{1X}^2g_{X1}^3x_\Phi^3+224g_{1X}g_X^3g_{X1}x_Hx_\Phi^3\\
&+ 224g_1g_X^2g_{X1}^2x_Hx_\Phi^3+224g_{1X}g_Xg_{X1}^3x_Hx_\Phi^3+224g_1g_{X1}^4x_Hx_\Phi^3+100g_{1X}g_X^3g_{X1}x_\Phi^4\\
&+ 100g_1g_X^2g_{X1}^2x_\Phi^4+100g_{1X}g_Xg_{X1}^3x_\Phi^4+100g_1g_{X1}^4x_\Phi^4-54g_{1X}g_Xg_{X1}x_\Phi^2y_M^2-54g_1g_{X1}^2x_\Phi^2y_M^2\\
&- 51g_1^3y_t^2-51g_1g_{1X}^2y_t^2-102g_1g_{1X}g_Xx_Hy_t^2-204g_1^2g_{X1}x_Hy_t^2-102g_{1X}^2g_{X1}x_Hy_t^2\\
&- 204g_{1X}g_Xg_{X1}x_H^2y_t^2-204g_1g_{X1}^2x_H^2y_t^2-15g_1g_{1X}g_Xx_\Phi y_t^2-30g_1^2g_{X1}x_\Phi y_t^2\\
&- 15g_{1X}^2g_{X1}x_\Phi y_t^2-60g_{1X}g_Xg_{X1}x_Hx_\Phi y_t^2-60g_1g_{X1}^2x_Hx_\Phi y_t^2-6g_{1X}g_Xg_{X1}x_\Phi^2y_t^2-6g_1g_{X1}^2x_\Phi^2y_t^2\Big],
\end{aligned}
$$

$$
\begin{aligned}
\beta^{(2)}_{g_{X1}} &= \frac{1}{(16\pi^2)^2}\cdot\frac{1}{18}\Big[199g_1^3g_{1X}g_X + 81g_1g_2^2g_{1X}g_X + 264g_1g_3^2g_{1X}g_X + 199g_1g_{1X}^3g_X + 199g_1^4g_{X1} \\
&+ 81g_1^2g_2^2g_{X1} + 264g_1^2g_3^2g_{X1} + 199g_1^2g_{1X}^2g_{X1} + 398g_1^3g_X^2x_H + 162g_1g_2^2g_X^2x_H \\
&+ 528g_1g_3^2g_X^2x_H + 1194g_1g_{1X}^2g_X^2x_H + 1990g_1^2g_{1X}g_Xg_{X1}x_H + 162g_2^2g_{1X}g_Xg_{X1}x_H \\
&+ 528g_3^2g_{1X}g_Xg_{X1}x_H + 398g_{1X}^3g_Xg_{X1}x_H + 1592g_1^3g_{X1}^2x_H + 324g_1g_2^2g_{X1}^2x_H \\
&+ 1056g_1g_3^2g_{X1}^2x_H + 796g_1g_{1X}^2g_{X1}^2x_H + 2388g_1g_{1X}g_X^3x_H^2 + 3184g_1^2g_X^2g_{X1}x_H^2 \\
&+ 324g_2^2g_X^2g_{X1}x_H^2 + 1056g_3^2g_X^2g_{X1}x_H^2 + 2388g_{1X}^2g_X^2g_{X1}x_H^2 + 5572g_1g_{1X}g_Xg_{X1}^2x_H^2 \\
&+ 4776g_1^2g_{X1}^3x_H^2 + 324g_2^2g_{X1}^3x_H^2 + 1056g_3^2g_{X1}^3x_H^2 + 796g_{1X}^2g_{X1}^3x_H^2 + 1592g_1g_X^4x_H^3 \\
&+ 4776g_{1X}g_X^3g_{X1}x_H^3 + 7960g_1g_X^2g_{X1}^2x_H^3 + 4776g_{1X}g_Xg_{X1}^3x_H^3 + 6368g_1g_{X1}^4x_H^3 \\
&+ 3184g_X^4g_{X1}x_H^4 + 6368g_X^2g_{X1}^3x_H^4 + 3184g_{X1}^5x_H^4 + 82g_1^3g_X^2x_\Phi + 54g_1g_2^2g_X^2x_\Phi + 48g_1g_3^2g_X^2x_\Phi \\
&+ 246g_1g_{1X}^2g_X^2x_\Phi + 410g_1^2g_{1X}g_Xg_{X1}x_\Phi + 54g_2^2g_{1X}g_Xg_{X1}x_\Phi + 48g_3^2g_{1X}g_Xg_{X1}x_\Phi \\
&+ 82g_{1X}^3g_Xg_{X1}x_\Phi + 328g_1^3g_{X1}^2x_\Phi + 108g_1g_2^2g_{X1}^2x_\Phi + 96g_1g_3^2g_{X1}^2x_\Phi + 164g_1g_{1X}^2g_{X1}^2x_\Phi \\
&+ 984g_1g_{1X}g_X^3x_Hx_\Phi + 1312g_1^2g_X^2g_{X1}x_Hx_\Phi + 216g_2^2g_X^2g_{X1}x_Hx_\Phi + 192g_3^2g_X^2g_{X1}x_Hx_\Phi \\
&+ 984g_{1X}^2g_X^2g_{X1}x_Hx_\Phi + 2296g_1g_{1X}g_Xg_{X1}^2x_Hx_\Phi + 1968g_1^2g_{X1}^3x_Hx_\Phi + 216g_2^2g_{X1}^3x_Hx_\Phi \\
&+ 192g_3^2g_{X1}^3x_Hx_\Phi + 328g_{1X}^2g_{X1}^3x_Hx_\Phi + 984g_1g_X^4x_H^2x_\Phi + 2952g_{1X}g_X^3g_{X1}x_H^2x_\Phi \\
&+ 4920g_1g_X^2g_{X1}^2x_H^2x_\Phi + 2952g_{1X}g_Xg_{X1}^3x_H^2x_\Phi + 3936g_1g_{X1}^4x_H^2x_\Phi + 2624g_X^4g_{X1}x_H^3x_\Phi \\
&+ 5248g_X^2g_{X1}^3x_H^3x_\Phi + 2624g_{X1}^5x_H^3x_\Phi + 138g_1g_{1X}g_X^3x_\Phi^2 + 184g_1^2g_X^2g_{X1}x_\Phi^2 + 54g_2^2g_X^2g_{X1}x_\Phi^2 \\
&+ 48g_3^2g_X^2g_{X1}x_\Phi^2 + 138g_{1X}^2g_X^2g_{X1}x_\Phi^2 + 322g_1g_{1X}g_Xg_{X1}^2x_\Phi^2 + 276g_1^2g_{X1}^3x_\Phi^2 + 54g_2^2g_{X1}^3x_\Phi^2 \\
&+ 48g_3^2g_{X1}^3x_\Phi^2 + 46g_{1X}^2g_{X1}^3x_\Phi^2 + 276g_1g_X^4x_Hx_\Phi^2 + 828g_{1X}g_X^3g_{X1}x_Hx_\Phi^2 + 1380g_1g_X^2g_{X1}^2x_Hx_\Phi^2 \\
&+ 828g_{1X}g_Xg_{X1}^3x_Hx_\Phi^2 + 1104g_1g_{X1}^4x_Hx_\Phi^2 + 1104g_X^4g_{X1}x_H^2x_\Phi^2 + 2208g_X^2g_{X1}^3x_H^2x_\Phi^2 \\
&+ 1104g_{X1}^5x_H^2x_\Phi^2 + 28g_1g_X^4x_\Phi^3 + 84g_{1X}g_X^3g_{X1}x_\Phi^3 + 140g_1g_X^2g_{X1}^2x_\Phi^3 + 84g_{1X}g_Xg_{X1}^3x_\Phi^3 \\
&+ 112g_1g_{X1}^4x_\Phi^3 + 224g_X^4g_{X1}x_Hx_\Phi^3 + 448g_X^2g_{X1}^3x_Hx_\Phi^3 + 224g_{X1}^5x_Hx_\Phi^3 + 100g_X^4g_{X1}x_\Phi^4 \\
&+ 200g_X^2g_{X1}^3x_\Phi^4 + 100g_{X1}^5x_\Phi^4 - 54g_X^2g_{X1}x_\Phi^2y_M^2 - 54g_{X1}^3x_\Phi^2y_M^2 - 51g_1g_{1X}g_Xy_t^2 - 51g_1^2g_{X1}y_t^2 \\
&- 102g_1g_X^2x_Hy_t^2 - 102g_{1X}g_Xg_{X1}x_Hy_t^2 - 204g_1g_{X1}^2x_Hy_t^2 - 204g_X^2g_{X1}x_H^2y_t^2 - 204g_{X1}^3x_H^2y_t^2 \\
&- 15g_1g_X^2x_\Phi y_t^2 - 15g_{1X}g_Xg_{X1}x_\Phi y_t^2 - 30g_1g_{X1}^2x_\Phi y_t^2 - 60g_X^2g_{X1}x_Hx_\Phi y_t^2 - 60g_{X1}^3x_Hx_\Phi y_t^2 \\
&- 6g_X^2g_{X1}x_\Phi^2y_t^2 - 6g_{X1}^3x_\Phi^2y_t^2\Big],
\end{aligned}
$$

$$
\begin{aligned}
\beta^{(2)}_{g_{1X}} &= \frac{1}{(16\pi^2)^2}\cdot\frac{1}{18}\Big[199g_1^4g_{1X}+81g_1^2g_2^2g_{1X}+264g_1^2g_3^2g_{1X}+398g_1^2g_{1X}^3+81g_2^2g_{1X}^3\\
&+ 264g_3^2g_{1X}^3+199g_{1X}^5+398g_1^4g_Xx_H+162g_1^2g_2^2g_Xx_H+528g_1^2g_3^2g_Xx_H+1990g_1^2g_{1X}^2g_Xx_H\\
&+ 324g_2^2g_{1X}^2g_Xx_H+1056g_3^2g_{1X}^2g_Xx_H+1592g_{1X}^4g_Xx_H+1194g_1^3g_{1X}g_{X1}x_H\\
&+ 162g_1g_2^2g_{1X}g_{X1}x_H+528g_1g_3^2g_{1X}g_{X1}x_H+1194g_1g_{1X}^3g_{X1}x_H+3184g_1^2g_{1X}g_X^2x_H^2\\
&+ 324g_2^2g_{1X}g_X^2x_H^2+1056g_3^2g_{1X}g_X^2x_H^2+4776g_{1X}^3g_X^2x_H^2+2388g_1^3g_Xg_{X1}x_H^2\\
&+ 324g_1g_2^2g_Xg_{X1}x_H^2+1056g_1g_3^2g_Xg_{X1}x_H^2+5572g_1g_{1X}^2g_Xg_{X1}x_H^2+2388g_1^2g_{1X}g_{X1}^2x_H^2\\
&+ 796g_{1X}^3g_{X1}^2x_H^2+1592g_1^2g_X^3x_H^3+6368g_{1X}^2g_X^3x_H^3+7960g_1g_{1X}g_X^2g_{X1}x_H^3+4776g_1^2g_Xg_{X1}^2x_H^3\\
&+ 3184g_{1X}^2g_Xg_{X1}^2x_H^3+1592g_1g_{1X}g_{X1}^3x_H^3+3184g_{1X}g_X^4x_H^4+3184g_1g_X^3g_{X1}x_H^4\\
&+ 3184g_{1X}g_X^2g_{X1}^2x_H^4+3184g_1g_Xg_{X1}^3x_H^4+82g_1^4g_Xx_\Phi+54g_1^2g_2^2g_Xx_\Phi+48g_1^2g_3^2g_Xx_\Phi\\
&+ 410g_1^2g_{1X}^2g_Xx_\Phi+108g_2^2g_{1X}^2g_Xx_\Phi+96g_3^2g_{1X}^2g_Xx_\Phi+328g_{1X}^4g_Xx_\Phi+246g_1^3g_{1X}g_{X1}x_\Phi\\
&+ 54g_1g_2^2g_{1X}g_{X1}x_\Phi+48g_1g_3^2g_{1X}g_{X1}x_\Phi+246g_1g_{1X}^3g_{X1}x_\Phi+1312g_1^2g_{1X}g_X^2x_Hx_\Phi\\
&+ 216g_2^2g_{1X}g_X^2x_Hx_\Phi+192g_3^2g_{1X}g_X^2x_Hx_\Phi+1968g_{1X}^3g_X^2x_Hx_\Phi+984g_1^3g_Xg_{X1}x_Hx_\Phi\\
&+ 216g_1g_2^2g_Xg_{X1}x_Hx_\Phi+192g_1g_3^2g_Xg_{X1}x_Hx_\Phi+2296g_1g_{1X}^2g_Xg_{X1}x_Hx_\Phi+984g_1^2g_{1X}g_{X1}^2x_Hx_\Phi\\
&+ 328g_{1X}^3g_{X1}^2x_Hx_\Phi+984g_1^2g_X^3x_H^2x_\Phi+3936g_{1X}^2g_X^3x_H^2x_\Phi+4920g_1g_{1X}g_X^2g_{X1}x_H^2x_\Phi\\
&+ 2952g_1^2g_Xg_{X1}^2x_H^2x_\Phi+1968g_{1X}^2g_Xg_{X1}^2x_H^2x_\Phi+984g_1g_{1X}g_{X1}^3x_H^2x_\Phi+2624g_{1X}g_X^4x_H^3x_\Phi\\
&+ 2624g_1g_X^3g_{X1}x_H^3x_\Phi+2624g_{1X}g_X^2g_{X1}^2x_H^3x_\Phi+2624g_1g_Xg_{X1}^3x_H^3x_\Phi+184g_1^2g_{1X}g_X^2x_\Phi^2\\
&+ 54g_2^2g_{1X}g_X^2x_\Phi^2+48g_3^2g_{1X}g_X^2x_\Phi^2+276g_{1X}^3g_X^2x_\Phi^2+138g_1^3g_Xg_{X1}x_\Phi^2+54g_1g_2^2g_Xg_{X1}x_\Phi^2\\
&+ 48g_1g_3^2g_Xg_{X1}x_\Phi^2+322g_1g_{1X}^2g_Xg_{X1}x_\Phi^2+138g_1^2g_{1X}g_{X1}^2x_\Phi^2+46g_{1X}^3g_{X1}^2x_\Phi^2\\
&+ 276g_1^2g_X^3x_Hx_\Phi^2+1104g_{1X}^2g_X^3x_Hx_\Phi^2+1380g_1g_{1X}g_X^2g_{X1}x_Hx_\Phi^2+828g_1^2g_Xg_{X1}^2x_Hx_\Phi^2\\
&+ 552g_{1X}^2g_Xg_{X1}^2x_Hx_\Phi^2+276g_1g_{1X}g_{X1}^3x_Hx_\Phi^2+1104g_{1X}g_X^4x_H^2x_\Phi^2+1104g_1g_X^3g_{X1}x_H^2x_\Phi^2\\
&+ 1104g_{1X}g_X^2g_{X1}^2x_H^2x_\Phi^2+1104g_1g_Xg_{X1}^3x_H^2x_\Phi^2+28g_1^2g_X^3x_\Phi^3+112g_{1X}^2g_X^3x_\Phi^3\\
&+ 140g_1g_{1X}g_X^2g_{X1}x_\Phi^3+84g_1^2g_Xg_{X1}^2x_\Phi^3+56g_{1X}^2g_Xg_{X1}^2x_\Phi^3+28g_1g_{1X}g_{X1}^3x_\Phi^3\\
&+ 224g_{1X}g_X^4x_Hx_\Phi^3+224g_1g_X^3g_{X1}x_Hx_\Phi^3+224g_{1X}g_X^2g_{X1}^2x_Hx_\Phi^3+224g_1g_Xg_{X1}^3x_Hx_\Phi^3\\
&+ 100g_{1X}g_X^4x_\Phi^4+100g_1g_X^3g_{X1}x_\Phi^4+100g_{1X}g_X^2g_{X1}^2x_\Phi^4+100g_1g_Xg_{X1}^3x_\Phi^4-54g_{1X}g_X^2x_\Phi^2y_M^2\\
&- 54g_1g_Xg_{X1}x_\Phi^2y_M^2-51g_1^2g_{1X}y_t^2-51g_{1X}^3y_t^2-102g_1^2g_Xx_Hy_t^2-204g_{1X}^2g_Xx_Hy_t^2\\
&- 102g_1g_{1X}g_{X1}x_Hy_t^2-204g_{1X}g_X^2x_H^2y_t^2-204g_1g_Xg_{X1}x_H^2y_t^2-15g_1^2g_Xx_\Phi y_t^2\\
&- 30g_{1X}^2g_Xx_\Phi y_t^2-15g_1g_{1X}g_{X1}x_\Phi y_t^2-60g_{1X}g_X^2x_Hx_\Phi y_t^2-60g_1g_Xg_{X1}x_Hx_\Phi y_t^2\\
&- 6g_{1X}g_X^2x_\Phi^2y_t^2-6g_1g_Xg_{X1}x_\Phi^2y_t^2\Big],
\end{aligned}
$$

$$
\begin{aligned}
\beta_{g_X}^{(2)} &= \frac{1}{(16\pi^2)^2}\cdot\frac{1}{18}\Big[199g_1^2g_{1X}^2g_X + 81g_2^2g_{1X}^2g_X + 264g_3^2g_{1X}^2g_X + 199g_{1X}^4g_X + 199g_1^3g_{1X}g_{X1} \\
&+ 81g_1g_2^2g_{1X}g_{X1} + 264g_1g_3^2g_{1X}g_{X1} + 199g_1g_{1X}^3g_{X1} + 796g_1^2g_{1X}g_X^2x_H \\
&+ 324g_2^2g_{1X}g_X^2x_H + 1056g_3^2g_{1X}g_X^2x_H + 1592g_{1X}^3g_X^2x_H + 398g_1^3g_Xg_{X1}x_H \\
&+ 162g_1g_2^2g_Xg_{X1}x_H + 528g_1g_3^2g_Xg_{X1}x_H + 1990g_1g_{1X}^2g_Xg_{X1}x_H + 1194g_1^2g_{1X}g_{X1}^2x_H \\
&+ 162g_2^2g_{1X}g_{X1}^2x_H + 528g_3^2g_{1X}g_{X1}^2x_H + 398g_{1X}^3g_{X1}^2x_H + 796g_1^2g_X^3x_H^2 + 324g_2^2g_X^3x_H^2 \\
&+ 1056g_3^2g_X^3x_H^2 + 4776g_{1X}^2g_X^3x_H^2 + 5572g_1g_{1X}g_X^2g_{X1}x_H^2 + 2388g_1^2g_Xg_{X1}^2x_H^2 \\
&+ 324g_2^2g_Xg_{X1}^2x_H^2 + 1056g_3^2g_Xg_{X1}^2x_H^2 + 3184g_{1X}^2g_Xg_{X1}^2x_H^2 + 2388g_1g_{1X}g_{X1}^3x_H^2 \\
&+ 6368g_{1X}g_X^4x_H^3 + 4776g_1g_X^3g_{X1}x_H^3 + 7960g_{1X}g_X^2g_{X1}^2x_H^3 + 4776g_1g_Xg_{X1}^3x_H^3 \\
&+ 1592g_{1X}g_{X1}^4x_H^3 + 3184g_X^5x_H^4 + 6368g_X^3g_{X1}^2x_H^4 + 3184g_Xg_{X1}^4x_H^4 + 164g_1^2g_{1X}g_X^2x_\Phi \\
&+ 108g_2^2g_{1X}g_X^2x_\Phi + 96g_3^2g_{1X}g_X^2x_\Phi + 328g_{1X}^3g_X^2x_\Phi + 82g_1^3g_Xg_{X1}x_\Phi + 54g_1g_2^2g_Xg_{X1}x_\Phi \\
&+ 48g_1g_3^2g_Xg_{X1}x_\Phi + 410g_1g_{1X}^2g_Xg_{X1}x_\Phi + 246g_1^2g_{1X}g_{X1}^2x_\Phi + 54g_2^2g_{1X}g_{X1}^2x_\Phi \\
&+ 48g_3^2g_{1X}g_{X1}^2x_\Phi + 82g_{1X}^3g_{X1}^2x_\Phi + 328g_1^2g_X^3x_Hx_\Phi + 216g_2^2g_X^3x_Hx_\Phi + 192g_3^2g_X^3x_Hx_\Phi \\
&+ 1968g_{1X}^2g_X^3x_Hx_\Phi + 2296g_1g_{1X}g_X^2g_{X1}x_Hx_\Phi + 984g_1^2g_Xg_{X1}^2x_Hx_\Phi + 216g_2^2g_Xg_{X1}^2x_Hx_\Phi \\
&+ 192g_3^2g_Xg_{X1}^2x_Hx_\Phi + 1312g_{1X}^2g_Xg_{X1}^2x_Hx_\Phi + 984g_1g_{1X}g_{X1}^3x_Hx_\Phi + 3936g_{1X}g_X^4x_H^2x_\Phi \\
&+ 2952g_1g_X^3g_{X1}x_H^2x_\Phi + 4920g_{1X}g_X^2g_{X1}^2x_H^2x_\Phi + 2952g_1g_Xg_{X1}^3x_H^2x_\Phi + 984g_{1X}g_{X1}^4x_H^2x_\Phi \\
&+ 2624g_X^5x_H^3x_\Phi + 5248g_X^3g_{X1}^2x_H^3x_\Phi + 2624g_Xg_{X1}^4x_H^3x_\Phi + 46g_1^2g_X^3x_\Phi^2 + 54g_2^2g_X^3x_\Phi^2 \\
&+ 48g_3^2g_X^3x_\Phi^2 + 276g_{1X}^2g_X^3x_\Phi^2 + 322g_1g_{1X}g_X^2g_{X1}x_\Phi^2 + 138g_1^2g_Xg_{X1}^2x_\Phi^2 + 54g_2^2g_Xg_{X1}^2x_\Phi^2 \\
&+ 48g_3^2g_Xg_{X1}^2x_\Phi^2 + 184g_{1X}^2g_Xg_{X1}^2x_\Phi^2 + 138g_1g_{1X}g_{X1}^3x_\Phi^2 + 1104g_{1X}g_X^4x_Hx_\Phi^2 \\
&+ 828g_1g_X^3g_{X1}x_Hx_\Phi^2 + 1380g_{1X}g_X^2g_{X1}^2x_Hx_\Phi^2 + 828g_1g_Xg_{X1}^3x_Hx_\Phi^2 + 276g_{1X}g_{X1}^4x_Hx_\Phi^2 \\
&+ 1104g_X^5x_H^2x_\Phi^2 + 2208g_X^3g_{X1}^2x_H^2x_\Phi^2 + 1104g_Xg_{X1}^4x_H^2x_\Phi^2 + 112g_{1X}g_X^4x_\Phi^3 + 84g_1g_X^3g_{X1}x_\Phi^3 \\
&+ 140g_{1X}g_X^2g_{X1}^2x_\Phi^3 + 84g_1g_Xg_{X1}^3x_\Phi^3 + 28g_{1X}g_{X1}^4x_\Phi^3 + 224g_X^5x_Hx_\Phi^3 + 448g_X^3g_{X1}^2x_Hx_\Phi^3 \\
&+ 224g_Xg_{X1}^4x_Hx_\Phi^3 + 100g_X^5x_\Phi^4 + 200g_X^3g_{X1}^2x_\Phi^4 + 100g_Xg_{X1}^4x_\Phi^4 - 54g_X^3x_\Phi^2y_M^2 - 54g_Xg_{X1}^2x_\Phi^2y_M^2 \\
&- 51g_{1X}^2g_Xy_t^2 - 51g_1g_{1X}g_{X1}y_t^2 - 204g_{1X}g_X^2x_Hy_t^2 - 102g_1g_Xg_{X1}x_Hy_t^2 - 102g_{1X}g_{X1}^2x_Hy_t^2 \\
&- 204g_X^3x_H^2y_t^2 - 204g_Xg_{X1}^2x_H^2y_t^2 - 30g_{1X}g_X^2x_\Phi y_t^2 - 15g_1g_Xg_{X1}x_\Phi y_t^2 - 15g_{1X}g_{X1}^2x_\Phi y_t^2 \\
&- 60g_X^3x_Hx_\Phi y_t^2 - 60g_Xg_{X1}^2x_Hx_\Phi y_t^2 - 6g_X^3x_\Phi^2y_t^2 - 6g_Xg_{X1}^2x_\Phi^2y_t^2\Big]. \qquad \text{(B.4)}
\end{aligned}
$$

B.2 U(1)′ RGEs for the Yukawa couplings

The RGEs for the Yukawa couplings at the two-loop level are given by

$$\mu\frac{dy_i}{d\mu} = \beta_{y_i}^{(1)} + \beta_{y_i}^{(2)}, \qquad \text{(B.5)}$$

where $\beta_{y_i}^{(1)}$ and $\beta_{y_i}^{(2)}$ are the one-loop and two-loop beta functions for the Yukawa couplings, respectively, and y_i represents y_t and y_M. Here, the one-loop beta functions for

the Yukawa couplings are given by

$$
\begin{aligned}
\beta_{y_t}^{(1)} &= \frac{y_t}{16\pi^2}\Big[\frac{9}{2}y_t^2 - 8g_3^2 - \frac{9}{4}g_2^2 - \frac{1}{6}\big(g_1 + 2x_H g_{X1} + x_\Phi g_{X1}\big)\big(4g_1 + 8x_H g_{X1} + x_\Phi g_{X1}\big) \\
&- \frac{3}{4}\big(g_1 + 2x_H g_{X1}\big)^2 - \frac{1}{6}\big(g_{1X} + 2x_H g_X + x_\Phi g_X\big)\big(4g_{1X} + 8x_H g_X + x_\Phi g_X\big) \\
&- \frac{3}{4}\big(g_{1X} + 2x_H g_X\big)^2\Big], \\
\beta_{y_M}^{(1)} &= \frac{y_M}{16\pi^2}\left[10y_M^2 - \frac{3}{2}x_\Phi^2\left(g_{X1}^2 + g_X^2\right)\right],
\end{aligned}
\tag{B.6}
$$

and the two-loop beta functions for the Yukawa couplings are given by

$$
\begin{aligned}
\beta_{y_t}^{(2)} &= \frac{1}{(16\pi^2)^2}\cdot\frac{1}{432}\Big[-9\big(-72y_t^5 - y_t^3\big(223g_1^2 + 405g_2^2 + 768g_3^2 + 223g_{1X}^2 + 892g_{1X}g_X x_H \\
&+ 892g_1 g_{X1}x_H + 892g_X^2 x_H^2 + 892g_{X1}^2 x_H^2 + 50g_{1X}g_X x_\Phi + 50g_1 g_{X1}x_\Phi + 100g_X^2 x_H x_\Phi \\
&+ 100g_{X1}^2 x_H x_\Phi + 16g_X^2 x_\Phi^2 + 16g_{X1}^2 x_\Phi^2 - 324y_t^2 - 576\lambda_H\big)\big) \\
&+ y_t\big(2374g_1^4 - 324g_1^2 g_2^2 - 2484g_2^4 + 912g_1^2 g_3^2 + 3888g_2^2 g_3^2 - 46656g_3^4 + 4748g_1^2 g_{1X}^2 \\
&- 324g_2^2 g_{1X}^2 + 912g_3^2 g_{1X}^2 + 2374g_{1X}^4 + 18992g_1^2 g_{1X}g_X x_H - 1296g_2^2 g_{1X}g_X x_H \\
&+ 3648g_3^2 g_{1X}g_X x_H + 18992g_{1X}^3 g_X x_H + 18992g_1^3 g_{X1}x_H - 1296g_1 g_2^2 g_{X1}x_H \\
&+ 3648g_1 g_3^2 g_{X1}x_H + 18992g_1 g_{1X}^2 g_{X1}x_H + 18992g_1^2 g_X^2 x_H^2 - 1296g_2^2 g_X^2 x_H^2 \\
&+ 3648g_3^2 g_X^2 x_H^2 + 56976g_{1X}^2 g_X^2 x_H^2 + 75968g_1 g_{1X}g_X g_{X1}x_H^2 + 56976g_1^2 g_{X1}^2 x_H^2 \\
&- 1296g_2^2 g_{X1}^2 x_H^2 + 3648g_3^2 g_{X1}^2 x_H^2 + 18992g_{1X}^2 g_{X1}^2 x_H^2 + 75968g_{1X}g_X^3 x_H^3 \\
&+ 75968g_1 g_X^2 g_{X1}x_H^3 + 75968g_{1X}g_X g_{X1}^2 x_H^3 + 75968g_1 g_{X1}^3 x_H^3 + 37984g_X^4 x_H^4 \\
&+ 75968g_X^2 g_{X1}^2 x_H^4 + 37984g_{X1}^4 x_H^4 + 4016g_1^2 g_{1X}g_X x_\Phi + 486g_2^2 g_{1X}g_X x_\Phi \\
&- 480g_3^2 g_{1X}g_X x_\Phi + 4016g_{1X}^3 g_X x_\Phi + 4016g_1^3 g_{X1}x_\Phi + 486g_1 g_2^2 g_{X1}x_\Phi - 480g_1 g_3^2 g_{X1}x_\Phi \\
&+ 4016g_1 g_{1X}^2 g_{X1}x_\Phi + 8032g_1^2 g_X^2 x_H x_\Phi + 972g_2^2 g_X^2 x_H x_\Phi - 960g_3^2 g_X^2 x_H x_\Phi \\
&+ 24096g_{1X}^2 g_X^2 x_H x_\Phi + 32128g_1 g_{1X}g_X g_{X1}x_H x_\Phi + 24096g_1^2 g_{X1}^2 x_H x_\Phi + 972g_2^2 g_{X1}^2 x_H x_\Phi \\
&- 960g_3^2 g_{X1}^2 x_H x_\Phi + 8032g_{1X}^2 g_{X1}^2 x_H x_\Phi + 48192g_{1X}g_X^3 x_H^2 x_\Phi + 48192g_1 g_X^2 g_{X1}x_H^2 x_\Phi \\
&+ 48192g_{1X}g_X g_{X1}^2 x_H^2 x_\Phi + 48192g_1 g_{X1}^3 x_H^2 x_\Phi + 32128g_X^4 x_H^3 x_\Phi + 64256g_X^2 g_{X1}^2 x_H^3 x_\Phi \\
&+ 32128g_{X1}^4 x_H^3 x_\Phi + 819g_1^2 g_X^2 x_\Phi^2 + 81g_2^2 g_X^2 x_\Phi^2 - 96g_3^2 g_X^2 x_\Phi^2 + 3255g_{1X}^2 g_X^2 x_\Phi^2 \\
&+ 4872g_1 g_{1X}g_X g_{X1}x_\Phi^2 + 3255g_1^2 g_{X1}^2 x_\Phi^2 + 81g_2^2 g_{X1}^2 x_\Phi^2 - 96g_3^2 g_{X1}^2 x_\Phi^2 + 819g_{1X}^2 g_{X1}^2 x_\Phi^2 \\
&+ 13020g_{1X}g_X^3 x_H x_\Phi^2 + 13020g_1 g_X^2 g_{X1}x_H x_\Phi^2 + 13020g_{1X}g_X g_{X1}^2 x_H x_\Phi^2 + 13020g_1 g_{X1}^3 x_H x_\Phi^2 \\
&+ 13020g_X^4 x_H^2 x_\Phi^2 + 26040g_X^2 g_{X1}^2 x_H^2 x_\Phi^2 + 13020g_{X1}^4 x_H^2 x_\Phi^2 + 1330g_{1X}g_X^3 x_\Phi^3 \\
&+ 1330g_1 g_X^2 g_{X1}x_\Phi^3 + 1330g_{1X}g_X g_{X1}^2 x_\Phi^3 + 1330g_1 g_{X1}^3 x_\Phi^3 + 2660g_X^4 x_H x_\Phi^3 + 5320g_X^2 g_{X1}^2 x_H x_\Phi^3 \\
&+ 2660g_{X1}^4 x_H x_\Phi^3 + 203g_X^4 x_\Phi^4 + 406g_X^2 g_{X1}^2 x_\Phi^4 + 203g_{X1}^4 x_\Phi^4 + 1530g_1^2 y_t^2 + 2430g_2^2 y_t^2 \\
&+ 8640g_3^2 y_t^2 + 1530g_{1X}^2 y_t^2 + 6120g_{1X}g_X x_H y_t^2 + 6120g_1 g_{X1}x_H y_t^2 + 6120g_X^2 x_H^2 y_t^2 \\
&+ 6120g_{X1}^2 x_H^2 y_t^2 + 900g_{1X}g_X x_\Phi y_t^2 + 900g_1 g_{X1}x_\Phi y_t^2 + 1800g_X^2 x_H x_\Phi y_t^2 + 1800g_{X1}^2 x_H x_\Phi y_t^2 \\
&+ 180g_X^2 x_\Phi^2 y_t^2 + 180g_{X1}^2 x_\Phi^2 y_t^2 - 2916y_t^4 + 2592\lambda_H^2 + 216\lambda_{\text{mix}}^2\big)\Big],
\end{aligned}
$$

$$\begin{aligned}\beta^{(2)}_{y_M} &= \frac{1}{(16\pi^2)^2}\cdot\frac{1}{48}\Big[y_M\left(-70g_{1X}^2g_X^2x_\Phi^2-140g_1g_{1X}g_Xg_{X1}x_\Phi^2-70g_1^2g_{X1}^2x_\Phi^2-280g_{1X}g_X^3x_Hx_\Phi^2\right.\\
&- 280g_1g_X^2g_{X1}x_Hx_\Phi^2-280g_{1X}g_Xg_{X1}^2x_Hx_\Phi^2-280g_1g_{X1}^3x_Hx_\Phi^2-280g_X^4x_H^2x_\Phi^2\\
&- 560g_X^2g_{X1}^2x_H^2x_\Phi^2-280g_{X1}^4x_H^2x_\Phi^2-64g_{1X}g_X^3x_\Phi^3-64g_1g_X^2g_{X1}x_\Phi^3-64g_{1X}g_Xg_{X1}^2x_\Phi^3\\
&- 64g_1g_{X1}^3x_\Phi^3-128g_X^4x_Hx_\Phi^3-256g_X^2g_{X1}^2x_Hx_\Phi^3-128g_{X1}^4x_Hx_\Phi^3-381g_X^4x_\Phi^4-762g_X^2g_{X1}^2x_\Phi^4\\
&- 381g_{X1}^4x_\Phi^4+360\left(g_X^2+g_{X1}^2\right)x_\Phi^2y_M^2-1728y_M^4+48\lambda_{\rm mix}^2+192\lambda_\Phi^2\big)\\
&+ 6\left(224y_M^5-32y_M^3\left(-11\left(g_X^2+g_{X1}^2\right)x_\Phi^2+9y_M^2+8\lambda_\Phi\right)\right)\Big].\end{aligned}\tag{B.7}$$

B.3 U(1)′ RGEs for the scalar quartic couplings

Finally, the RGEs for the scalar quartic couplings at the two-loop level are given by

$$\mu\frac{d\lambda_i}{d\mu} = \beta^{(1)}_{\lambda_i}+\beta^{(2)}_{\lambda_i},\tag{B.8}$$

where $\beta^{(1)}_{\lambda_i}$ and $\beta^{(2)}_{\lambda_i}$ are the one-loop and two-loop beta functions for the scalar quartic couplings, respectively, and λ_i represents λ_H, λ_Φ and $\lambda_{\rm mix}$. Here, the one-loop beta functions for the scalar quartic couplings are given by

$$\begin{aligned}\beta^{(1)}_{\lambda_H} &= \frac{1}{16\pi^2}\Big[\lambda_H\left\{24\lambda_H+12y_t^2-9g_2^2-3\big(g_1+2x_Hg_{X1}\big)^2-3\big(g_{1X}+2x_Hg_X\big)^2\right\}\\
&+ \lambda_{\rm mix}^2-6y_t^4+\frac{9}{8}g_2^4+\frac{3}{8}\left\{\big(g_1+2x_Hg_{X1}\big)^2+\big(g_{1X}+2x_Hg_X\big)^2\right\}^2\\
&+ \frac{3}{4}g_2^2\big(g_1+2x_Hg_{X1}\big)^2+\frac{3}{4}g_2^2\big(g_{1X}+2x_Hg_X\big)^2\Big],\\
\beta^{(1)}_{\lambda_\Phi} &= \frac{1}{16\pi^2}\Big[\lambda_\Phi\Big\{20\lambda_\Phi+24y_M^2-12\big(x_\Phi g_{X1}\big)^2-12\big(x_\Phi g_X\big)^2\Big\}\\
&+ 2\lambda_{\rm mix}^2-48y_M^4+6\Big\{\big(x_\Phi g_{X1}\big)^2+\big(x_\Phi g_X\big)^2\Big\}^2\Big],\\
\beta^{(1)}_{\lambda_{\rm mix}} &= \frac{1}{16\pi^2}\Big[\lambda_{\rm mix}\Big\{12\lambda_H+8\lambda_\Phi+4\lambda_{\rm mix}+6y_t^2+12y_M^2\\
&- \frac{9}{2}g_2^2-\frac{3}{2}\big(g_1+2x_Hg_{X1}\big)^2-6\big(x_\Phi g_{X1}\big)^2-\frac{3}{2}\big(g_{1X}+2x_Hg_X\big)^2-6\big(x_\Phi g_X\big)^2\Big\}\\
&+ 3\Big\{\big(g_1+2x_Hg_{X1}\big)\big(x_\Phi g_{X1}\big)+\big(g_{1X}+2x_Hg_X\big)\big(x_\Phi g_X\big)\Big\}^2\Big],\end{aligned}\tag{B.9}$$

and the two-loop beta functions for the scalar quartic couplings are given by

$$
\begin{aligned}
\beta^{(2)}_{\lambda_H} = \frac{1}{(16\pi^2)^2}\Bigg[& -\frac{379g_1^6}{48} - \frac{559}{48}g_1^4g_2^2 - \frac{289}{48}g_1^2g_2^4 + \frac{305g_2^6}{16} - \frac{469}{48}g_1^4g_{1X}^2 - \frac{75}{8}g_1^2g_2^2g_{1X}^2 \\
& - \frac{289}{48}g_2^4g_{1X}^2 - \frac{469}{48}g_1^2g_{1X}^4 - \frac{559}{48}g_2^2g_{1X}^4 - \frac{379g_{1X}^6}{48} - \frac{469}{12}g_1^4g_{1X}g_Xx_H \\
& - \frac{75}{2}g_1^2g_2^2g_{1X}g_Xx_H - \frac{289}{12}g_2^4g_{1X}g_Xx_H - \frac{469}{6}g_1^2g_{1X}^3g_Xx_H - \frac{559}{6}g_2^2g_{1X}^3g_Xx_H \\
& - \frac{379}{4}g_{1X}^5g_Xx_H - \frac{379}{4}g_1^5g_{X1}x_H - \frac{559}{6}g_1^3g_2^2g_{X1}x_H - \frac{289}{12}g_1g_2^4g_{X1}x_H - \frac{469}{6}g_1^3g_{1X}^2g_{X1}x_H \\
& - \frac{75}{2}g_1g_2^2g_{1X}^2g_{X1}x_H - \frac{469}{12}g_1g_{1X}^4g_{X1}x_H - \frac{469}{12}g_1^4g_X^2x_H^2 - \frac{75}{2}g_1^2g_2^2g_X^2x_H^2 - \frac{289}{12}g_2^4g_X^2x_H^2 \\
& - \frac{469}{2}g_1^2g_{1X}^2g_X^2x_H^2 - \frac{559}{2}g_2^2g_{1X}^2g_X^2x_H^2 - \frac{1895}{4}g_{1X}^4g_X^2x_H^2 - \frac{938}{3}g_1^3g_{1X}g_Xg_{X1}x_H^2 \\
& - 150g_1g_2^2g_{1X}g_Xg_{X1}x_H^2 - \frac{938}{3}g_1g_{1X}^3g_Xg_{X1}x_H^2 - \frac{1895}{4}g_1^4g_{X1}^2x_H^2 - \frac{559}{2}g_1^2g_2^2g_{X1}^2x_H^2 \\
& - \frac{289}{12}g_2^4g_{X1}^2x_H^2 - \frac{469}{2}g_1^2g_{1X}^2g_{X1}^2x_H^2 - \frac{75}{2}g_2^2g_{1X}^2g_{X1}^2x_H^2 - \frac{469}{12}g_{1X}^4g_{X1}^2x_H^2 - \frac{938}{3}g_1^2g_{1X}g_X^3x_H^3 \\
& - \frac{1118}{3}g_2^2g_{1X}g_X^3x_H^3 - \frac{3790}{3}g_{1X}^3g_X^3x_H^3 - \frac{938}{3}g_1^3g_X^2g_{X1}x_H^3 - 150g_1g_2^2g_X^2g_{X1}x_H^3 \\
& - 938g_1g_{1X}^2g_X^2g_{X1}x_H^3 - 938g_1^2g_{1X}g_Xg_{X1}^2x_H^3 - 150g_2^2g_{1X}g_Xg_{X1}^2x_H^3 - \frac{938}{3}g_{1X}^3g_Xg_{X1}^2x_H^3 \\
& - \frac{3790}{3}g_1^3g_{X1}^3x_H^3 - \frac{1118}{3}g_1g_2^2g_{X1}^3x_H^3 - \frac{938}{3}g_1g_{1X}^2g_{X1}^3x_H^3 - \frac{469}{3}g_1^2g_X^4x_H^4 - \frac{559}{3}g_2^2g_X^4x_H^4 \\
& - 1895g_{1X}^2g_X^4x_H^4 - \frac{3752}{3}g_1g_{1X}g_X^3g_{X1}x_H^4 - 938g_1^2g_X^2g_{X1}^2x_H^4 - 150g_2^2g_X^2g_{X1}^2x_H^4 \\
& - 938g_{1X}^2g_X^2g_{X1}^2x_H^4 - \frac{3752}{3}g_1g_{1X}g_Xg_{X1}^3x_H^4 - 1895g_1^2g_{X1}^4x_H^4 - \frac{559}{3}g_2^2g_{X1}^4x_H^4 \\
& - \frac{469}{3}g_{1X}^2g_{X1}^4x_H^4 - 1516g_{1X}g_X^5x_H^5 - \frac{1876}{3}g_1g_X^4g_{X1}x_H^5 - \frac{3752}{3}g_{1X}g_X^3g_{X1}^2x_H^5 \\
& - \frac{3752}{3}g_1g_X^2g_{X1}^3x_H^5 - \frac{1876}{3}g_{1X}g_Xg_{X1}^4x_H^5 - 1516g_1g_{X1}^5x_H^5 - \frac{1516}{3}g_X^6x_H^6 - \frac{1876}{3}g_X^4g_{X1}^2x_H^6 \\
& - \frac{1876}{3}g_X^2g_{X1}^4x_H^6 - \frac{1516}{3}g_{X1}^6x_H^6 - \frac{16}{3}g_1^2g_{1X}^3g_Xx_\Phi - \frac{16}{3}g_2^2g_{1X}^3g_Xx_\Phi - \frac{16}{3}g_{1X}^5g_Xx_\Phi \\
& - \frac{16}{3}g_1^5g_{X1}x_\Phi - \frac{16}{3}g_1^3g_2^2g_{X1}x_\Phi - \frac{16}{3}g_1^3g_{1X}^2g_{X1}x_\Phi - 32g_1^2g_{1X}^2g_X^2x_Hx_\Phi - 32g_2^2g_{1X}^2g_X^2x_Hx_\Phi \\
& - \frac{160}{3}g_{1X}^4g_X^2x_Hx_\Phi - \frac{64}{3}g_1^3g_{1X}g_Xg_{X1}x_Hx_\Phi - \frac{64}{3}g_1g_{1X}^3g_Xg_{X1}x_Hx_\Phi - \frac{160}{3}g_1^4g_{X1}^2x_Hx_\Phi \\
& - 32g_1^2g_2^2g_{X1}^2x_Hx_\Phi - 32g_1^2g_{1X}^2g_{X1}^2x_Hx_\Phi - 64g_1^2g_{1X}g_X^3x_H^2x_\Phi - 64g_2^2g_{1X}g_X^3x_H^2x_\Phi \\
& - \frac{640}{3}g_{1X}^3g_X^3x_H^2x_\Phi - \frac{64}{3}g_1^3g_X^2g_{X1}x_H^2x_\Phi - 128g_1g_{1X}^2g_X^2g_{X1}x_H^2x_\Phi - 128g_1^2g_{1X}g_Xg_{X1}^2x_H^2x_\Phi \\
& - \frac{64}{3}g_{1X}^3g_Xg_{X1}^2x_H^2x_\Phi - \frac{640}{3}g_1^3g_{X1}^3x_H^2x_\Phi - 64g_1g_2^2g_{X1}^3x_H^2x_\Phi - 64g_1g_{1X}^2g_{X1}^3x_H^2x_\Phi \\
& - \frac{128}{3}g_1^2g_X^4x_H^3x_\Phi - \frac{128}{3}g_2^2g_X^4x_H^3x_\Phi - \frac{1280}{3}g_{1X}^2g_X^4x_H^3x_\Phi - 256g_1g_{1X}g_X^3g_{X1}x_H^3x_\Phi
\end{aligned}
$$

$$
\begin{aligned}
&- 128g_1^2g_X^2g_{X1}^2x_H^3x_\Phi - 128g_{1X}^2g_X^2g_{X1}^2x_H^3x_\Phi - 256g_1g_{1X}g_Xg_{X1}^3x_H^3x_\Phi - \frac{1280}{3}g_1^2g_{X1}^4x_H^3x_\Phi \\
&- \frac{128}{3}g_2^2g_{X1}^4x_H^3x_\Phi - \frac{128}{3}g_{1X}^2g_{X1}^4x_H^3x_\Phi - \frac{1280}{3}g_{1X}g_X^5x_H^4x_\Phi - \frac{512}{3}g_1g_X^4g_{X1}x_H^4x_\Phi \\
&- 256g_{1X}g_X^3g_{X1}^2x_H^4x_\Phi - 256g_1g_X^2g_{X1}^3x_H^4x_\Phi - \frac{512}{3}g_{1X}g_Xg_{X1}^4x_H^4x_\Phi - \frac{1280}{3}g_1g_{X1}^5x_H^4x_\Phi \\
&- \frac{512}{3}g_X^6x_H^5x_\Phi - \frac{512}{3}g_X^4g_{X1}^2x_H^5x_\Phi - \frac{512}{3}g_X^2g_{X1}^4x_H^5x_\Phi - \frac{512}{3}g_{X1}^6x_H^5x_\Phi - \frac{13}{4}g_1^2g_{1X}^2g_X^2x_\Phi^2 \\
&- \frac{13}{4}g_2^2g_{1X}^2g_X^2x_\Phi^2 - \frac{13}{4}g_{1X}^4g_X^2x_\Phi^2 - \frac{13}{4}g_1^4g_{X1}^2x_\Phi^2 - \frac{13}{4}g_1^2g_2^2g_{X1}^2x_\Phi^2 - \frac{13}{4}g_1^2g_{1X}^2g_{X1}^2x_\Phi^2 \\
&- 13g_1^2g_{1X}g_X^3x_Hx_\Phi^2 - 13g_2^2g_{1X}g_X^3x_Hx_\Phi^2 - 26g_{1X}^3g_X^3x_Hx_\Phi^2 - 13g_1g_{1X}^2g_X^2g_{X1}x_Hx_\Phi^2 \\
&- 13g_1^2g_{1X}g_Xg_{X1}^2x_Hx_\Phi^2 - 26g_1^3g_{X1}^3x_Hx_\Phi^2 - 13g_1g_2^2g_{X1}^3x_Hx_\Phi^2 - 13g_1g_{1X}^2g_{X1}^3x_Hx_\Phi^2 \\
&- 13g_1^2g_X^4x_H^2x_\Phi^2 - 13g_2^2g_X^4x_H^2x_\Phi^2 - 78g_{1X}^2g_X^4x_H^2x_\Phi^2 - 52g_1g_{1X}g_X^3g_{X1}x_H^2x_\Phi^2 - 13g_1^2g_X^2g_{X1}^2x_H^2x_\Phi^2 \\
&- 13g_{1X}^2g_X^2g_{X1}^2x_H^2x_\Phi^2 - 52g_1g_{1X}g_Xg_{X1}^3x_H^2x_\Phi^2 - 78g_1^2g_{X1}^4x_H^2x_\Phi^2 - 13g_2^2g_{X1}^4x_H^2x_\Phi^2 \\
&- 13g_{1X}^2g_{X1}^4x_H^2x_\Phi^2 - 104g_{1X}g_X^5x_H^3x_\Phi^2 - 52g_1g_X^4g_{X1}x_H^3x_\Phi^2 - 52g_{1X}g_X^3g_{X1}^2x_H^3x_\Phi^2 \\
&- 52g_1g_X^2g_{X1}^3x_H^3x_\Phi^2 - 52g_{1X}g_Xg_{X1}^4x_H^3x_\Phi^2 - 104g_1g_{X1}^5x_H^3x_\Phi^2 - 52g_X^6x_H^4x_\Phi^2 - 52g_X^4g_{X1}^2x_H^4x_\Phi^2 \\
&- 52g_X^2g_{X1}^4x_H^4x_\Phi^2 - 52g_{X1}^6x_H^4x_\Phi^2 - \frac{19}{4}g_1^4y_t^2 + \frac{21}{2}g_1^2g_2^2y_t^2 - \frac{9}{4}g_2^4y_t^2 - \frac{19}{2}g_1^2g_{1X}^2y_t^2 \\
&+ \frac{21}{2}g_2^2g_{1X}^2y_t^2 - \frac{19}{4}g_{1X}^4y_t^2 - 38g_1^2g_{1X}g_Xx_Hy_t^2 + 42g_2^2g_{1X}g_Xx_Hy_t^2 - 38g_{1X}^3g_Xx_Hy_t^2 \\
&- 38g_1^3g_{X1}x_Hy_t^2 + 42g_1g_2^2g_{X1}x_Hy_t^2 - 38g_1g_{1X}^2g_{X1}x_Hy_t^2 - 38g_1^2g_X^2x_H^2y_t^2 + 42g_2^2g_X^2x_H^2y_t^2 \\
&- 114g_{1X}^2g_X^2x_H^2y_t^2 - 152g_1g_{1X}g_Xg_{X1}x_H^2y_t^2 - 114g_1^2g_{X1}^2x_H^2y_t^2 + 42g_2^2g_{X1}^2x_H^2y_t^2 \\
&- 38g_{1X}^2g_{X1}^2x_H^2y_t^2 - 152g_{1X}g_X^3x_H^3y_t^2 - 152g_1g_X^2g_{X1}x_H^3y_t^2 - 152g_{1X}g_Xg_{X1}^2x_H^3y_t^2 \\
&- 152g_1g_{X1}^3x_H^3y_t^2 - 76g_X^4x_H^4y_t^2 - 152g_X^2g_{X1}^2x_H^4y_t^2 - 76g_{X1}^4x_H^4y_t^2 - 5g_1^2g_{1X}g_Xx_\Phi y_t^2 \\
&+ 3g_2^2g_{1X}g_Xx_\Phi y_t^2 - 5g_{1X}^3g_Xx_\Phi y_t^2 - 5g_1^3g_{X1}x_\Phi y_t^2 + 3g_1g_2^2g_{X1}x_\Phi y_t^2 - 5g_1g_{1X}^2g_{X1}x_\Phi y_t^2 \\
&- 10g_1^2g_X^2x_Hx_\Phi y_t^2 + 6g_2^2g_X^2x_Hx_\Phi y_t^2 - 30g_{1X}^2g_X^2x_Hx_\Phi y_t^2 - 40g_1g_{1X}g_Xg_{X1}x_Hx_\Phi y_t^2 \\
&- 30g_1^2g_{X1}^2x_Hx_\Phi y_t^2 + 6g_2^2g_{X1}^2x_Hx_\Phi y_t^2 - 10g_{1X}^2g_{X1}^2x_Hx_\Phi y_t^2 - 60g_{1X}g_X^3x_H^2x_\Phi y_t^2 \\
&- 60g_1g_X^2g_{X1}x_H^2x_\Phi y_t^2 - 60g_{1X}g_Xg_{X1}^2x_H^2x_\Phi y_t^2 - 60g_1g_{X1}^3x_H^2x_\Phi y_t^2 - 40g_X^4x_H^3x_\Phi y_t^2 \\
&- 80g_X^2g_{X1}^2x_H^3x_\Phi y_t^2 - 40g_{X1}^4x_H^3x_\Phi y_t^2 - g_{1X}^2g_X^2x_\Phi^2y_t^2 - 2g_1g_{1X}g_Xg_{X1}x_\Phi^2y_t^2 - g_1^2g_{X1}^2x_\Phi^2y_t^2 \\
&- 4g_{1X}g_X^3x_Hx_\Phi^2y_t^2 - 4g_1g_X^2g_{X1}x_Hx_\Phi^2y_t^2 - 4g_{1X}g_Xg_{X1}^2x_Hx_\Phi^2y_t^2 - 4g_1g_{X1}^3x_Hx_\Phi^2y_t^2 \\
&- 4g_X^4x_H^2x_\Phi^2y_t^2 - 8g_X^2g_{X1}^2x_H^2x_\Phi^2y_t^2 - 4g_{X1}^4x_H^2x_\Phi^2y_t^2 - \frac{8}{3}g_1^2y_t^4 - 32g_3^2y_t^4 - \frac{8}{3}g_{1X}^2y_t^4 \\
&- \frac{32}{3}g_{1X}g_Xx_Hy_t^4 - \frac{32}{3}g_1g_{X1}x_Hy_t^4 - \frac{32}{3}g_X^2x_H^2y_t^4 - \frac{32}{3}g_{X1}^2x_H^2y_t^4 - \frac{10}{3}g_{1X}g_Xx_\Phi y_t^4 \\
&- \frac{10}{3}g_1g_{X1}x_\Phi y_t^4 - \frac{20}{3}g_X^2x_Hx_\Phi y_t^4 - \frac{20}{3}g_{X1}^2x_Hx_\Phi y_t^4 - \frac{2}{3}g_X^2x_\Phi^2y_t^4 - \frac{2}{3}g_{X1}^2x_\Phi^2y_t^4 + 30y_t^6 \\
&+ \frac{629}{24}g_1^4\lambda_H + \frac{39}{4}g_1^2g_2^2\lambda_H - \frac{73}{8}g_2^4\lambda_H + \frac{69}{4}g_1^2g_{1X}^2\lambda_H + \frac{39}{4}g_2^2g_{1X}^2\lambda_H + \frac{629}{24}g_{1X}^4\lambda_H \\
&+ 69g_1^2g_{1X}g_Xx_H\lambda_H + 39g_2^2g_{1X}g_Xx_H\lambda_H + \frac{629}{3}g_{1X}^3g_Xx_H\lambda_H + \frac{629}{3}g_1^3g_{X1}x_H\lambda_H \\
&+ 39g_1g_2^2g_{X1}x_H\lambda_H + 69g_1g_{1X}^2g_{X1}x_H\lambda_H + 69g_1^2g_X^2x_H^2\lambda_H + 39g_2^2g_X^2x_H^2\lambda_H + 629g_{1X}^2g_X^2x_H^2\lambda_H
\end{aligned}
$$

$$
\begin{aligned}
&+ 276 g_1 g_{1X} g_X g_{X1} x_H^2 \lambda_H + 629 g_1^2 g_{X1}^2 x_H^2 \lambda_H + 39 g_2^2 g_{X1}^2 x_H^2 \lambda_H + 69 g_{1X}^2 g_{X1}^2 x_H^2 \lambda_H \\
&+ \frac{2516}{3} g_{1X} g_X^3 x_H^3 \lambda_H + 276 g_1 g_X^2 g_{X1} x_H^3 \lambda_H + 276 g_{1X} g_X g_{X1}^2 x_H^3 \lambda_H + \frac{2516}{3} g_1 g_{X1}^3 x_H^3 \lambda_H \\
&+ \frac{1258}{3} g_X^4 x_H^4 \lambda_H + 276 g_X^2 g_{X1}^2 x_H^4 \lambda_H + \frac{1258}{3} g_{X1}^4 x_H^4 \lambda_H + \frac{40}{3} g_{1X}^3 g_X x_\Phi \lambda_H + \frac{40}{3} g_1^3 g_{X1} x_\Phi \lambda_H \\
&+ 80 g_{1X}^2 g_X^2 x_H x_\Phi \lambda_H + 80 g_1^2 g_{X1}^2 x_H x_\Phi \lambda_H + 160 g_{1X} g_X^3 x_H^2 x_\Phi \lambda_H + 160 g_1 g_{X1}^3 x_H^2 x_\Phi \lambda_H \\
&+ \frac{320}{3} g_X^4 x_H^3 x_\Phi \lambda_H + \frac{320}{3} g_{X1}^4 x_H^3 x_\Phi \lambda_H + \frac{17}{2} g_{1X}^2 g_X^2 x_\Phi^2 \lambda_H + \frac{17}{2} g_1^2 g_{X1}^2 x_\Phi^2 \lambda_H + 34 g_{1X} g_X^3 x_H x_\Phi^2 \lambda_H \\
&+ 34 g_1 g_{X1}^3 x_H x_\Phi^2 \lambda_H + 34 g_X^4 x_H^2 x_\Phi^2 \lambda_H + 34 g_{X1}^4 x_H^2 x_\Phi^2 \lambda_H + \frac{85}{6} g_1^2 y_t^2 \lambda_H + \frac{45}{2} g_2^2 y_t^2 \lambda_H \\
&+ 80 g_3^2 y_t^2 \lambda_H + \frac{85}{6} g_{1X}^2 y_t^2 \lambda_H + \frac{170}{3} g_{1X} g_X x_H y_t^2 \lambda_H + \frac{170}{3} g_1 g_{X1} x_H y_t^2 \lambda_H + \frac{170}{3} g_X^2 x_H^2 y_t^2 \lambda_H \\
&+ \frac{170}{3} g_{X1}^2 x_H^2 y_t^2 \lambda_H + \frac{25}{3} g_{1X} g_X x_\Phi y_t^2 \lambda_H + \frac{25}{3} g_1 g_{X1} x_\Phi y_t^2 \lambda_H + \frac{50}{3} g_X^2 x_H x_\Phi y_t^2 \lambda_H \\
&+ \frac{50}{3} g_{X1}^2 x_H x_\Phi y_t^2 \lambda_H + \frac{5}{3} g_X^2 x_\Phi^2 y_t^2 \lambda_H + \frac{5}{3} g_{X1}^2 x_\Phi^2 y_t^2 \lambda_H - 3 y_t^4 \lambda_H + 36 g_1^2 \lambda_H^2 + 108 g_2^2 \lambda_H^2 \\
&+ 36 g_{1X}^2 \lambda_H^2 + 144 g_{1X} g_X x_H \lambda_H^2 + 144 g_1 g_{X1} x_H \lambda_H^2 + 144 g_X^2 x_H^2 \lambda_H^2 + 144 g_{X1}^2 x_H^2 \lambda_H^2 - 144 y_t^2 \lambda_H^2 \\
&- 312 \lambda_H^3 + 5 g_{1X}^2 g_X^2 x_\Phi^2 \lambda_{\text{mix}} + 10 g_1 g_{1X} g_X g_{X1} x_\Phi^2 \lambda_{\text{mix}} + 5 g_1^2 g_{X1}^2 x_\Phi^2 \lambda_{\text{mix}} + 20 g_{1X} g_X^3 x_H x_\Phi^2 \lambda_{\text{mix}} \\
&+ 20 g_1 g_X^2 g_{X1} x_H x_\Phi^2 \lambda_{\text{mix}} + 20 g_{1X} g_X g_{X1}^2 x_H x_\Phi^2 \lambda_{\text{mix}} + 20 g_1 g_{X1}^3 x_H x_\Phi^2 \lambda_{\text{mix}} + 20 g_X^4 x_H^2 x_\Phi^2 \lambda_{\text{mix}} \\
&+ 40 g_X^2 g_{X1}^2 x_H^2 x_\Phi^2 \lambda_{\text{mix}} + 20 g_{X1}^4 x_H^2 x_\Phi^2 \lambda_{\text{mix}} + 8 g_X^2 x_\Phi^2 \lambda_{\text{mix}}^2 + 8 g_{X1}^2 x_\Phi^2 \lambda_{\text{mix}}^2 - 12 y_M^2 \lambda_{\text{mix}}^2 \\
&- 10 \lambda_H \lambda_{\text{mix}}^2 - 4 \lambda_{\text{mix}}^3 \Big],
\end{aligned}
$$

$$
\begin{aligned}
\beta_{\lambda_\Phi}^{(2)} \;=\; & \frac{1}{(16\pi^2)^2} \cdot \frac{1}{3} \Big[- 334 g_{1X}^2 g_X^4 x_\Phi^4 - 334 g_1^2 g_X^2 g_{X1}^2 x_\Phi^4 - 334 g_{1X}^2 g_X^2 g_{X1}^2 x_\Phi^4 - 334 g_1^2 g_{X1}^4 x_\Phi^4 \\
&- 1336 g_{1X} g_X^5 x_H x_\Phi^4 - 1336 g_{1X} g_X^3 g_{X1}^2 x_H x_\Phi^4 - 1336 g_1 g_X^2 g_{X1}^3 x_H x_\Phi^4 - 1336 g_1 g_{X1}^5 x_H x_\Phi^4 \\
&- 1336 g_X^6 x_H^2 x_\Phi^4 - 1336 g_X^4 g_{X1}^2 x_H^2 x_\Phi^4 - 1336 g_X^2 g_{X1}^4 x_H^2 x_\Phi^4 - 1336 g_{X1}^6 x_H^2 x_\Phi^4 - 256 g_{1X} g_X^5 x_\Phi^5 \\
&- 256 g_{1X} g_X^3 g_{X1}^2 x_\Phi^5 - 256 g_1 g_X^2 g_{X1}^3 x_\Phi^5 - 256 g_1 g_{X1}^5 x_\Phi^5 - 512 g_X^6 x_H x_\Phi^5 - 512 g_X^4 g_{X1}^2 x_H x_\Phi^5 \\
&- 512 g_X^2 g_{X1}^4 x_H x_\Phi^5 - 512 g_{X1}^6 x_H x_\Phi^5 - 336 g_X^6 x_\Phi^6 - 696 g_X^4 g_{X1}^2 x_\Phi^6 - 696 g_X^2 g_{X1}^4 x_\Phi^6 - 336 g_{X1}^6 x_\Phi^6 \\
&+ 144 g_X^4 x_\Phi^4 y_M^2 + 288 g_X^2 g_{X1}^2 x_\Phi^4 y_M^2 + 144 g_{X1}^4 x_\Phi^4 y_M^2 + 144 g_X^2 x_\Phi^2 y_M^4 + 144 g_{X1}^2 x_\Phi^2 y_M^4 + 2304 y_M^6 \\
&+ 30 g_{1X}^2 g_X^2 x_\Phi^2 \lambda_{\text{mix}} + 60 g_1 g_{1X} g_X g_{X1} x_\Phi^2 \lambda_{\text{mix}} + 30 g_1^2 g_{X1}^2 x_\Phi^2 \lambda_{\text{mix}} + 120 g_{1X} g_X^3 x_H x_\Phi^2 \lambda_{\text{mix}} \\
&+ 120 g_1 g_X^2 g_{X1} x_H x_\Phi^2 \lambda_{\text{mix}} + 120 g_{1X} g_X g_{X1}^2 x_H x_\Phi^2 \lambda_{\text{mix}} + 120 g_1 g_{X1}^3 x_H x_\Phi^2 \lambda_{\text{mix}} + 120 g_X^4 x_H^2 x_\Phi^2 \lambda_{\text{mix}} \\
&+ 240 g_X^2 g_{X1}^2 x_H^2 x_\Phi^2 \lambda_{\text{mix}} + 120 g_{X1}^4 x_H^2 x_\Phi^2 \lambda_{\text{mix}} + 12 g_1^2 \lambda_{\text{mix}}^2 + 36 g_2^2 \lambda_{\text{mix}}^2 + 12 g_{1X}^2 \lambda_{\text{mix}}^2 \\
&+ 48 g_{1X} g_X x_H \lambda_{\text{mix}}^2 + 48 g_1 g_{X1} x_H \lambda_{\text{mix}}^2 + 48 g_X^2 x_H^2 \lambda_{\text{mix}}^2 + 48 g_{X1}^2 x_H^2 \lambda_{\text{mix}}^2 - 36 y_t^2 \lambda_{\text{mix}}^2 - 24 \lambda_{\text{mix}}^3 \\
&+ 211 g_{1X}^2 g_X^2 x_\Phi^2 \lambda_\Phi + 211 g_1^2 g_{X1}^2 x_\Phi^2 \lambda_\Phi + 844 g_{1X} g_X^3 x_H x_\Phi^2 \lambda_\Phi + 844 g_1 g_{X1}^3 x_H x_\Phi^2 \lambda_\Phi \\
&+ 844 g_X^4 x_H^2 x_\Phi^2 \lambda_\Phi + 844 g_{X1}^4 x_H^2 x_\Phi^2 \lambda_\Phi + 160 g_{1X} g_X^3 x_\Phi^3 \lambda_\Phi + 160 g_1 g_{X1}^3 x_\Phi^3 \lambda_\Phi + 320 g_X^4 x_H x_\Phi^3 \lambda_\Phi \\
&+ 320 g_{X1}^4 x_H x_\Phi^3 \lambda_\Phi + 396 g_X^4 x_\Phi^4 \lambda_\Phi + 588 g_X^2 g_{X1}^2 x_\Phi^4 \lambda_\Phi + 396 g_{X1}^4 x_\Phi^4 \lambda_\Phi + 90 g_X^2 x_\Phi^2 y_M^2 \lambda_\Phi \\
&+ 90 g_{X1}^2 x_\Phi^2 y_M^2 \lambda_\Phi + 144 y_M^4 \lambda_\Phi - 60 \lambda_{\text{mix}}^2 \lambda_\Phi + 336 g_X^2 x_\Phi^2 \lambda_\Phi^2 + 336 g_{X1}^2 x_\Phi^2 \lambda_\Phi^2 \\
&- 720 y_M^2 \lambda_\Phi^2 - 720 \lambda_\Phi^3 \Big],
\end{aligned}
$$

$$
\begin{aligned}
\beta^{(2)}_{\lambda_{\rm mix}} &= \frac{1}{(16\pi^2)^2}\Big[-\frac{15}{4}g_1^2g_{1X}^2g_X^2x_\Phi^2 - \frac{45}{4}g_2^2g_{1X}^2g_X^2x_\Phi^2 - \frac{713}{12}g_{1X}^4g_X^2x_\Phi^2 - \frac{379}{6}g_1^3g_{1X}g_Xg_{X1}x_\Phi^2 \\
&- \frac{45}{2}g_1g_2^2g_{1X}g_Xg_{X1}x_\Phi^2 - \frac{379}{6}g_1g_{1X}^3g_Xg_{X1}x_\Phi^2 - \frac{713}{12}g_1^4g_{X1}^2x_\Phi^2 - \frac{45}{4}g_1^2g_2^2g_{X1}^2x_\Phi^2 \\
&- \frac{15}{4}g_1^2g_{1X}^2g_{X1}^2x_\Phi^2 - 15g_1^2g_{1X}g_X^3x_Hx_\Phi^2 - 45g_2^2g_{1X}g_X^3x_Hx_\Phi^2 - \frac{1426}{3}g_{1X}^3g_X^3x_Hx_\Phi^2 \\
&- \frac{379}{3}g_1^3g_X^2g_{X1}x_Hx_\Phi^2 - 45g_1g_2^2g_X^2g_{X1}x_Hx_\Phi^2 - 394g_1g_{1X}^2g_X^2g_{X1}x_Hx_\Phi^2 - 394g_1^2g_{1X}g_Xg_{X1}^2x_Hx_\Phi^2 \\
&- 45g_2^2g_{1X}g_Xg_{X1}^2x_Hx_\Phi^2 - \frac{379}{3}g_{1X}^3g_Xg_{X1}^2x_Hx_\Phi^2 - \frac{1426}{3}g_1^3g_{X1}^3x_Hx_\Phi^2 - 45g_1g_2^2g_{X1}^3x_Hx_\Phi^2 \\
&- 15g_1g_{1X}^2g_{X1}^3x_Hx_\Phi^2 - 15g_1^2g_X^4x_H^2x_\Phi^2 - 45g_2^2g_X^4x_H^2x_\Phi^2 - 1426g_{1X}^2g_X^4x_H^2x_\Phi^2 \\
&- 818g_1g_{1X}g_X^3g_{X1}x_H^2x_\Phi^2 - 773g_1^2g_X^2g_{X1}^2x_H^2x_\Phi^2 - 90g_2^2g_X^2g_{X1}^2x_H^2x_\Phi^2 - 773g_{1X}^2g_X^2g_{X1}^2x_H^2x_\Phi^2 \\
&- 818g_1g_{1X}g_Xg_{X1}^3x_H^2x_\Phi^2 - 1426g_1^2g_{X1}^4x_H^2x_\Phi^2 - 45g_2^2g_{X1}^4x_H^2x_\Phi^2 - 15g_{1X}^2g_{X1}^4x_H^2x_\Phi^2 \\
&- \frac{5704}{3}g_{1X}g_X^5x_H^3x_\Phi^2 - \frac{1696}{3}g_1g_X^4g_{X1}x_H^3x_\Phi^2 - 1576g_{1X}g_X^3g_{X1}^2x_H^3x_\Phi^2 - 1576g_1g_X^2g_{X1}^3x_H^3x_\Phi^2 \\
&- \frac{1696}{3}g_{1X}g_Xg_{X1}^4x_H^3x_\Phi^2 - \frac{5704}{3}g_1g_{X1}^5x_H^3x_\Phi^2 - \frac{2852}{3}g_X^6x_H^4x_\Phi^2 - \frac{3212}{3}g_X^4g_{X1}^2x_H^4x_\Phi^2 \\
&- \frac{3212}{3}g_X^2g_{X1}^4x_H^4x_\Phi^2 - \frac{2852}{3}g_{X1}^6x_H^4x_\Phi^2 - \frac{128}{3}g_{1X}^3g_X^3x_\Phi^3 - \frac{128}{3}g_1g_{1X}^2g_X^2g_{X1}x_\Phi^3 \\
&- \frac{128}{3}g_1^2g_{1X}g_Xg_{X1}^2x_\Phi^3 - \frac{128}{3}g_1^3g_{X1}^3x_\Phi^3 - 256g_{1X}^2g_X^4x_Hx_\Phi^3 - \frac{512}{3}g_1g_{1X}g_X^3g_{X1}x_Hx_\Phi^3 \\
&- \frac{256}{3}g_1^2g_X^2g_{X1}^2x_Hx_\Phi^3 - \frac{256}{3}g_{1X}^2g_X^2g_{X1}^2x_Hx_\Phi^3 - \frac{512}{3}g_1g_{1X}g_Xg_{X1}^3x_Hx_\Phi^3 - 256g_1^2g_{X1}^4x_Hx_\Phi^3 \\
&- 512g_{1X}g_X^5x_H^2x_\Phi^3 - \frac{512}{3}g_1g_X^4g_{X1}x_H^2x_\Phi^3 - \frac{1024}{3}g_{1X}g_X^3g_{X1}^2x_H^2x_\Phi^3 - \frac{1024}{3}g_1g_X^2g_{X1}^3x_H^2x_\Phi^3 \\
&- \frac{512}{3}g_{1X}g_Xg_{X1}^4x_H^2x_\Phi^3 - 512g_1g_{X1}^5x_H^2x_\Phi^3 - \frac{1024}{3}g_X^6x_H^3x_\Phi^3 - \frac{1024}{3}g_X^4g_{X1}^2x_H^3x_\Phi^3 \\
&- \frac{1024}{3}g_X^2g_{X1}^4x_H^3x_\Phi^3 - \frac{1024}{3}g_{X1}^6x_H^3x_\Phi^3 - 41g_{1X}^2g_X^4x_\Phi^4 - 56g_1g_{1X}g_X^3g_{X1}x_\Phi^4 - 15g_1^2g_X^2g_{X1}^2x_\Phi^4 \\
&- 15g_{1X}^2g_X^2g_{X1}^2x_\Phi^4 - 56g_1g_{1X}g_Xg_{X1}^3x_\Phi^4 - 41g_1^2g_{X1}^4x_\Phi^4 - 164g_{1X}g_X^5x_Hx_\Phi^4 - 112g_1g_X^4g_{X1}x_Hx_\Phi^4 \\
&- 172g_{1X}g_X^3g_{X1}^2x_Hx_\Phi^4 - 172g_1g_X^2g_{X1}^3x_Hx_\Phi^4 - 112g_{1X}g_Xg_{X1}^4x_Hx_\Phi^4 - 164g_1g_{X1}^5x_Hx_\Phi^4 \\
&- 164g_X^6x_H^2x_\Phi^4 - 284g_X^4g_{X1}^2x_H^2x_\Phi^4 - 284g_X^2g_{X1}^4x_H^2x_\Phi^4 - 164g_{X1}^6x_H^2x_\Phi^4 + 12g_{1X}^2g_X^2x_\Phi^2y_M^2 \\
&+ 24g_1g_{1X}g_Xg_{X1}x_\Phi^2y_M^2 + 12g_1^2g_{X1}^2x_\Phi^2y_M^2 + 48g_{1X}g_X^3x_Hx_\Phi^2y_M^2 + 48g_1g_X^2g_{X1}x_Hx_\Phi^2y_M^2 \\
&+ 48g_{1X}g_Xg_{X1}^2x_Hx_\Phi^2y_M^2 + 48g_1g_{X1}^3x_Hx_\Phi^2y_M^2 + 48g_X^4x_H^2x_\Phi^2y_M^2 + 96g_X^2g_{X1}^2x_H^2x_\Phi^2y_M^2 \\
&+ 48g_{X1}^4x_H^2x_\Phi^2y_M^2 - 19g_{1X}^2g_X^2x_\Phi^2y_t^2 - 38g_1g_{1X}g_Xg_{X1}x_\Phi^2y_t^2 - 19g_1^2g_{X1}^2x_\Phi^2y_t^2 \\
&- 76g_{1X}g_X^3x_Hx_\Phi^2y_t^2 - 76g_1g_X^2g_{X1}x_Hx_\Phi^2y_t^2 - 76g_{1X}g_Xg_{X1}^2x_Hx_\Phi^2y_t^2 - 76g_1g_{X1}^3x_Hx_\Phi^2y_t^2 \\
&- 76g_X^4x_H^2x_\Phi^2y_t^2 - 152g_X^2g_{X1}^2x_H^2x_\Phi^2y_t^2 - 76g_{X1}^4x_H^2x_\Phi^2y_t^2 - 20g_{1X}g_X^3x_\Phi^3y_t^2 - 20g_1g_X^2g_{X1}x_\Phi^3y_t^2 \\
&- 20g_{1X}g_Xg_{X1}^2x_\Phi^3y_t^2 - 20g_1g_{X1}^3x_\Phi^3y_t^2 - 40g_X^4x_Hx_\Phi^3y_t^2 - 80g_X^2g_{X1}^2x_Hx_\Phi^3y_t^2 - 40g_{X1}^4x_Hx_\Phi^3y_t^2 \\
&- 4g_X^4x_\Phi^4y_t^2 - 8g_X^2g_{X1}^2x_\Phi^4y_t^2 - 4g_{X1}^4x_\Phi^4y_t^2 + 30g_{1X}^2g_X^2x_\Phi^2\lambda_H + 60g_1g_{1X}g_Xg_{X1}x_\Phi^2\lambda_H \\
&+ 30g_1^2g_{X1}^2x_\Phi^2\lambda_H + 120g_{1X}g_X^3x_Hx_\Phi^2\lambda_H + 120g_1g_X^2g_{X1}x_Hx_\Phi^2\lambda_H + 120g_{1X}g_Xg_{X1}^2x_Hx_\Phi^2\lambda_H \\
&+ 120g_1g_{X1}^3x_Hx_\Phi^2\lambda_H + 120g_X^4x_H^2x_\Phi^2\lambda_H + 240g_X^2g_{X1}^2x_H^2x_\Phi^2\lambda_H + 120g_{X1}^4x_H^2x_\Phi^2\lambda_H + \frac{557}{48}g_1^4\lambda_{\rm mix}
\end{aligned}
$$

$$
\begin{aligned}
&+ \frac{15}{8}g_1^2g_2^2\lambda_{\rm mix} - \frac{145}{16}g_2^4\lambda_{\rm mix} + \frac{45}{8}g_1^2g_{1X}^2\lambda_{\rm mix} + \frac{15}{8}g_2^2g_{1X}^2\lambda_{\rm mix} + \frac{557}{48}g_{1X}^4\lambda_{\rm mix} \\
&+ \frac{45}{2}g_1^2g_{1X}g_Xx_H\lambda_{\rm mix} + \frac{15}{2}g_2^2g_{1X}g_Xx_H\lambda_{\rm mix} + \frac{557}{6}g_{1X}^3g_Xx_H\lambda_{\rm mix} + \frac{557}{6}g_1^3g_{X1}x_H\lambda_{\rm mix} \\
&+ \frac{15}{2}g_1g_2^2g_{X1}x_H\lambda_{\rm mix} + \frac{45}{2}g_1g_{1X}^2g_{X1}x_H\lambda_{\rm mix} + \frac{45}{2}g_1^2g_X^2x_H^2\lambda_{\rm mix} + \frac{15}{2}g_2^2g_X^2x_H^2\lambda_{\rm mix} \\
&+ \frac{557}{2}g_{1X}^2g_X^2x_H^2\lambda_{\rm mix} + 90g_1g_{1X}g_Xg_{X1}x_H^2\lambda_{\rm mix} + \frac{557}{2}g_1^2g_{X1}^2x_H^2\lambda_{\rm mix} + \frac{15}{2}g_2^2g_{X1}^2x_H^2\lambda_{\rm mix} \\
&+ \frac{45}{2}g_{1X}^2g_{X1}^2x_H^2\lambda_{\rm mix} + \frac{1114}{3}g_{1X}g_X^3x_H^3\lambda_{\rm mix} + 90g_1g_X^2g_{X1}x_H^3\lambda_{\rm mix} + 90g_{1X}g_Xg_{X1}^2x_H^3\lambda_{\rm mix} \\
&+ \frac{1114}{3}g_1g_{X1}^3x_H^3\lambda_{\rm mix} + \frac{557}{3}g_X^4x_H^4\lambda_{\rm mix} + 90g_X^2g_{X1}^2x_H^4\lambda_{\rm mix} + \frac{557}{3}g_{X1}^4x_H^4\lambda_{\rm mix} + \frac{20}{3}g_{1X}^3g_Xx_\Phi\lambda_{\rm mix} \\
&+ \frac{20}{3}g_1^3g_{X1}x_\Phi\lambda_{\rm mix} + 40g_{1X}^2g_X^2x_Hx_\Phi\lambda_{\rm mix} + 40g_1^2g_{X1}^2x_Hx_\Phi\lambda_{\rm mix} + 80g_{1X}g_X^3x_H^2x_\Phi\lambda_{\rm mix} \\
&+ 80g_1g_{X1}^3x_H^2x_\Phi\lambda_{\rm mix} + \frac{160}{3}g_X^4x_H^3x_\Phi\lambda_{\rm mix} + \frac{160}{3}g_{X1}^4x_H^3x_\Phi\lambda_{\rm mix} + \frac{497}{12}g_{1X}^2g_X^2x_\Phi^2\lambda_{\rm mix} \\
&+ 4g_1g_{1X}g_Xg_{X1}x_\Phi^2\lambda_{\rm mix} + \frac{497}{12}g_1^2g_{X1}^2x_\Phi^2\lambda_{\rm mix} + \frac{497}{3}g_{1X}g_X^3x_Hx_\Phi^2\lambda_{\rm mix} + 8g_1g_X^2g_{X1}x_Hx_\Phi^2\lambda_{\rm mix} \\
&+ 8g_{1X}g_Xg_{X1}^2x_Hx_\Phi^2\lambda_{\rm mix} + \frac{497}{3}g_1g_{X1}^3x_Hx_\Phi^2\lambda_{\rm mix} + \frac{497}{3}g_X^4x_H^2x_\Phi^2\lambda_{\rm mix} + 16g_X^2g_{X1}^2x_H^2x_\Phi^2\lambda_{\rm mix} \\
&+ \frac{497}{3}g_{X1}^4x_H^2x_\Phi^2\lambda_{\rm mix} + \frac{80}{3}g_{1X}g_X^3x_\Phi^3\lambda_{\rm mix} + \frac{80}{3}g_1g_{X1}^3x_\Phi^3\lambda_{\rm mix} + \frac{160}{3}g_X^4x_Hx_\Phi^3\lambda_{\rm mix} \\
&+ \frac{160}{3}g_{X1}^4x_Hx_\Phi^3\lambda_{\rm mix} + 42g_X^4x_\Phi^4\lambda_{\rm mix} + 50g_X^2g_{X1}^2x_\Phi^4\lambda_{\rm mix} + 42g_{X1}^4x_\Phi^4\lambda_{\rm mix} + 15g_X^2x_\Phi^2y_M^2\lambda_{\rm mix} \\
&+ 15g_{X1}^2x_\Phi^2y_M^2\lambda_{\rm mix} - 72y_M^4\lambda_{\rm mix} + \frac{85}{12}g_1^2y_t^2\lambda_{\rm mix} + \frac{45}{4}g_2^2y_t^2\lambda_{\rm mix} + 40g_3^2y_t^2\lambda_{\rm mix} \\
&+ \frac{85}{12}g_{1X}^2y_t^2\lambda_{\rm mix} + \frac{85}{3}g_{1X}g_Xx_Hy_t^2\lambda_{\rm mix} + \frac{85}{3}g_1g_{X1}x_Hy_t^2\lambda_{\rm mix} + \frac{85}{3}g_X^2x_H^2y_t^2\lambda_{\rm mix} \\
&+ \frac{85}{3}g_{X1}^2x_H^2y_t^2\lambda_{\rm mix} + \frac{25}{6}g_{1X}g_Xx_\Phi y_t^2\lambda_{\rm mix} + \frac{25}{6}g_1g_{X1}x_\Phi y_t^2\lambda_{\rm mix} + \frac{25}{3}g_X^2x_Hx_\Phi y_t^2\lambda_{\rm mix} \\
&+ \frac{25}{3}g_{X1}^2x_Hx_\Phi y_t^2\lambda_{\rm mix} + \frac{5}{6}g_X^2x_\Phi^2y_t^2\lambda_{\rm mix} + \frac{5}{6}g_{X1}^2x_\Phi^2y_t^2\lambda_{\rm mix} - \frac{27}{2}y_t^4\lambda_{\rm mix} + 24g_1^2\lambda_H\lambda_{\rm mix} \\
&+ 72g_2^2\lambda_H\lambda_{\rm mix} + 24g_{1X}^2\lambda_H\lambda_{\rm mix} + 96g_{1X}g_Xx_H\lambda_H\lambda_{\rm mix} + 96g_1g_{X1}x_H\lambda_H\lambda_{\rm mix} + 96g_X^2x_H^2\lambda_H\lambda_{\rm mix} \\
&+ 96g_{X1}^2x_H^2\lambda_H\lambda_{\rm mix} - 72y_t^2\lambda_H\lambda_{\rm mix} - 60\lambda_H^2\lambda_{\rm mix} + g_1^2\lambda_{\rm mix}^2 + 3g_2^2\lambda_{\rm mix}^2 + g_{1X}^2\lambda_{\rm mix}^2 + 4g_{1X}g_Xx_H\lambda_{\rm mix}^2 \\
&+ 4g_1g_{X1}x_H\lambda_{\rm mix}^2 + 4g_X^2x_H^2\lambda_{\rm mix}^2 + 4g_{X1}^2x_H^2\lambda_{\rm mix}^2 + 4g_X^2x_\Phi^2\lambda_{\rm mix}^2 + 4g_{X1}^2x_\Phi^2\lambda_{\rm mix}^2 - 24y_M^2\lambda_{\rm mix}^2 \\
&- 12y_t^2\lambda_{\rm mix}^2 - 72\lambda_H\lambda_{\rm mix}^2 - 11\lambda_{\rm mix}^3 + 20g_{1X}^2g_X^2x_\Phi^2\lambda_\Phi + 40g_1g_{1X}g_Xg_{X1}x_\Phi^2\lambda_\Phi + 20g_1^2g_{X1}^2x_\Phi^2\lambda_\Phi \\
&+ 80g_{1X}g_X^3x_Hx_\Phi^2\lambda_\Phi + 80g_1g_X^2g_{X1}x_Hx_\Phi^2\lambda_\Phi + 80g_{1X}g_Xg_{X1}^2x_Hx_\Phi^2\lambda_\Phi + 80g_1g_{X1}^3x_Hx_\Phi^2\lambda_\Phi \\
&+ 80g_X^4x_H^2x_\Phi^2\lambda_\Phi + 160g_X^2g_{X1}^2x_H^2x_\Phi^2\lambda_\Phi + 80g_{X1}^4x_H^2x_\Phi^2\lambda_\Phi + 64g_X^2x_\Phi^2\lambda_{\rm mix}\lambda_\Phi + 64g_{X1}^2x_\Phi^2\lambda_{\rm mix}\lambda_\Phi \\
&- 96y_M^2\lambda_{\rm mix}\lambda_\Phi - 48\lambda_{\rm mix}^2\lambda_\Phi - 40\lambda_{\rm mix}\lambda_\Phi^2\Big]. \qquad \text{(B.10)}
\end{aligned}
$$

Appendix C

SM RGES AT THE TWO-LOOP LEVEL

The RGEs for coupling constants of the SM up to two-loop level [52] are given by

$$
\begin{aligned}
\mu\frac{dg_3}{d\mu} &= \frac{g_3^3}{(4\pi)^2}\Big[-7\Big] + \frac{g_3^3}{(4\pi)^4}\left[-26g_3^2 + \frac{9}{2}g_2^2 + \frac{11}{6}g_1^2 - 2y_t^2\right], \\
\mu\frac{dg_2}{d\mu} &= \frac{g_2^3}{(4\pi)^2}\left[-\frac{19}{6}\right] + \frac{g_2^3}{(4\pi)^4}\left[12g_3^2 + \frac{35}{6}g_2^2 + \frac{3}{2}g_1^2 - \frac{3}{2}y_t^2\right], \\
\mu\frac{dg_1}{d\mu} &= \frac{g_1^3}{(4\pi)^2}\left[\frac{41}{6}\right] + \frac{g_1^3}{(4\pi)^4}\left[\frac{44}{3}g_3^2 + \frac{9}{2}g_2^2 + \frac{199}{18}g_1^2 - \frac{17}{6}y_t^2\right], \\
\mu\frac{dy_t}{d\mu} &= \frac{y_t}{(4\pi)^2}\left[\frac{9}{2}y_t^2 - 8g_3^2 - \frac{9}{4}g_2^2 - \frac{17}{12}g_1^2\right] \\
&+ \frac{y_t}{(4\pi)^4}\left[y_t^2\left(-12y_t^2 - 12\lambda_H + 36g_3^2 + \frac{225}{16}g_2^2 + \frac{131}{16}g_1^2\right)\right. \\
&+ \left. 6\lambda_H^2 - 108g_3^4 - \frac{23}{4}g_2^4 + \frac{1187}{216}g_1^4 + 9g_3^2g_2^2 + \frac{19}{9}g_3^2g_1^2 - \frac{3}{4}g_2^2g_1^2\right], \\
\mu\frac{d\lambda_H}{d\mu} &= \frac{1}{(4\pi)^2}\left[\lambda_H\Big(24\lambda_H + 12y_t^2 - 9g_2^2 - 3g_1^2\Big) - 6y_t^4 + \frac{9}{8}g_2^4 + \frac{3}{8}g_1^4 + \frac{3}{4}g_2^2g_1^2\right] \\
&+ \frac{1}{(4\pi)^4}\left[\lambda_H^2\Big(-312\lambda_H - 144y_t^2 + 108g_2^2 + 36g_1^2\Big)\right. \\
&+ \lambda_H y_t^2\left(-3y_t^2 + 80g_3^2 + \frac{45}{2}g_2^2 + \frac{85}{6}g_1^2\right) + \lambda_H\left(-\frac{73}{8}g_2^4 + \frac{629}{24}g_1^4 + \frac{39}{4}g_1^2g_2^2\right) \\
&+ y_t^4\left(30y_t^2 - 32g_3^2 - \frac{8}{3}g_1^2\right) + y_t^2\left(-\frac{9}{4}g_2^4 - \frac{19}{4}g_1^4 + \frac{21}{2}g_2^2g_1^2\right) \\
&+ \left.\frac{305}{16}g_2^6 - \frac{379}{48}g_1^6 - \frac{289}{48}g_2^4g_1^2 - \frac{559}{48}g_2^2g_1^4\right].
\end{aligned}
\tag{C.1}
$$

In our analysis, we numerically solve these SM RGEs with the following boundary conditions at $\mu = m_t$ [52] [1]

$$\begin{aligned}
g_3(m_t) &= 1.1666 + 0.00314\left(\frac{\alpha_3(m_Z) - 0.1184}{0.0007}\right) - 0.00046\left(\frac{m_t}{\text{GeV}} - 173.34\right), \\
g_2(m_t) &= 0.64779 + 0.00004\left(\frac{m_t}{\text{GeV}} - 173.34\right) + 0.00011\left(\frac{m_W - 80.384\text{GeV}}{0.014\text{GeV}}\right), \\
g_1(m_t) &= 0.35830 + 0.00011\left(\frac{m_t}{\text{GeV}} - 173.34\right) - 0.00020\left(\frac{m_W - 80.384\text{GeV}}{0.014\text{GeV}}\right), \\
y_t(m_t) &= 0.93690 + 0.00556\left(\frac{m_t}{\text{GeV}} - 173.34\right) - 0.00042\left(\frac{\alpha_3(m_Z) - 0.1184}{0.0007}\right), \\
\lambda_H(m_t) &= 0.12604 + 0.00206\left(\frac{m_h}{\text{GeV}} - 125.15\right) - 0.00004\left(\frac{m_t}{\text{GeV}} - 173.34\right), \quad \text{(C.2)}
\end{aligned}$$

using the inputs $\alpha_3(m_Z) = 0.1184$, $m_t = 173.34$ GeV, $m_h = 125.09$ GeV, and $m_W = 80.384$ GeV.

[1] We employed the boundary conditions in arXiv version 4 of Ref. [52].

Bibliography

[1] W. A. Bardeen, "On naturalness in the standard model," in *Ontake Summer Institute on Particle Physics Ontake Mountain, Japan, August 27-September 2, 1995*. 1995 FERMILAB-CONF-95-391-T.

[2] S. R. Coleman and E. J. Weinberg, "Radiative Corrections as the Origin of Spontaneous Symmetry Breaking," Phys. Rev. **D7** (1973) 1888–1910.

[3] K. Fujikawa, "Heavy Fermions in the Standard Sequential Scheme," Prog. Theor. Phys. **61** (1979) 1186.

[4] R. Hempfling, "The next-to-minimal Coleman-Weinberg model," Phys. Lett. **B379** (1996) 153–158, arXiv:hep-ph/9604278 [hep-ph].

[5] A. G. Dias, "Neutrino mass through concomitant breakdown of the U(1) chiral and scale symmetries," Phys. Rev. **D73** (2006) 096002, arXiv:hep-ph/0604219 [hep-ph].

[6] J. R. Espinosa and M. Quiros, "Novel effects in electroweak breaking from a hidden sector," Phys. Rev. **D76** (2007) 076004, arXiv:hep-ph/0701145 [hep-ph].

[7] W.-F. Chang, J. N. Ng, and J. M. S. Wu, "Shadow Higgs boson from a scale-invariant hidden $U(1)_s$ model," Phys. Rev. **D75** (2007) 115016, arXiv:hep-ph/0701254 [HEP-PH].

[8] R. Foot, A. Kobakhidze, and R. R. Volkas, "Electroweak Higgs as a pseudo-Goldstone boson of broken scale invariance," Phys. Lett. **B655** (2007) 156–161, arXiv:0704.1165 [hep-ph].

[9] R. Foot, A. Kobakhidze, K. McDonald, and R. R. Volkas, "Neutrino mass in radiatively-broken scale-invariant models," Phys. Rev. **D76** (2007) 075014, arXiv:0706.1829 [hep-ph].

[10] K. A. Meissner and H. Nicolai, "Conformal symmetry and the Standard Model," Phys. Lett. **B648** (2007) 312–317, arXiv:hep-th/0612165 [hep-th].

[11] R. Foot, A. Kobakhidze, K. L. McDonald, and R. R. Volkas, "Solution to the hierarchy problem from an almost decoupled hidden sector within a classically scale invariant theory," Phys. Rev. **D77** (2008) 035006, arXiv:0709.2750 [hep-ph].

[12] K. A. Meissner and H. Nicolai, "Effective action, conformal anomaly and the issue of quadratic divergences," Phys. Lett. **B660** (2008) 260–266, arXiv:0710.2840 [hep-th].

[13] K. A. Meissner and H. Nicolai, "Neutrinos, axions and conformal symmetry," Eur. Phys. J. **C57** (2008) 493–498, arXiv:0803.2814 [hep-th].

[14] M. Holthausen, M. Lindner, and M. A. Schmidt, "Radiative symmetry breaking of the minimal left-right symmetric model," Phys. Rev. **D82** (2010) 055002, arXiv:0911.0710 [hep-ph].

[15] A. Farzinnia, H.-J. He, and J. Ren, "Natural electroweak symmetry breaking from scale invariant Higgs mechanism," Phys. Lett. **B727** (2013) 141–150, arXiv:1308.0295 [hep-ph].

[16] M. Heikinheimo, A. Racioppi, M. Raidal, C. Spethmann, and K. Tuominen, "Physical naturalness and dynamical breaking of classical scale invariance," Mod. Phys. Lett. **A29** (2014) 1450077, arXiv:1304.7006 [hep-ph].

[17] A. Farzinnia and J. Ren, "Higgs partner searches and dark matter phenomenology in a classically scale invariant Higgs boson sector," Phys. Rev. **D90** no. 1, (2014) 015019, arXiv:1405.0498 [hep-ph].

[18] M. Lindner, S. Schmidt, and J. Smirnov, "Neutrino masses and conformal electro-weak symmetry breaking," JHEP **10** (2014) 177, arXiv:1405.6204 [hep-ph].

[19] V. V. Khoze, C. McCabe, and G. Ro, "Higgs vacuum stability from the dark matter portal," JHEP **08** (2014) 026, arXiv:1403.4953 [hep-ph].

[20] E. Gabrielli, M. Heikinheimo, K. Kannike, A. Racioppi, M. Raidal, and C. Spethmann, "Towards completing the standard model: Vacuum stability, electroweak symmetry breaking, and dark matter," Phys. Rev. **D89** no. 1, (2014) 015017, arXiv:1309.6632 [hep-ph].

[21] W. Altmannshofer, W. A. Bardeen, M. Bauer, M. Carena, and J. D. Lykken, "Light dark matter, naturalness, and the radiative origin of the electroweak scale," JHEP **01** (2015) 032, arXiv:1408.3429 [hep-ph].

[22] A. Karam and K. Tamvakis, "Dark matter and neutrino masses from a scale-invariant multi-Higgs portal," Phys. Rev. **D92** no. 7, (2015) 075010, arXiv:1508.03031 [hep-ph].

[23] N. Haba, H. Ishida, N. Okada, and Y. Yamaguchi, "Electroweak symmetry breaking through bosonic seesaw mechanism in a classically conformal extension of the Standard Model," arXiv:1509.01923 [hep-ph].

[24] H. Okada, Y. Orikasa, and K. Yagyu, "Higgs Triplet Model with Classically Conformal Invariance," arXiv:1510.00799 [hep-ph].

[25] A. Latosinski, A. Lewandowski, K. A. Meissner, and H. Nicolai, "Conformal standard model with an extended scalar sector," JHEP **10** (2015) 170, arXiv:1507.01755 [hep-ph].

[26] Z.-W. Wang, F. S. Sage, T. G. Steele, and R. B. Mann, "Asymptotic Safety in the Conformal Hidden Sector?," arXiv:1511.02531 [hep-ph].

[27] F. Goertz, "Electroweak symmetry breaking without the μ^2 term," Phys. Rev. **D94** no. 1, (2016) 015013, arXiv:1504.00355 [hep-ph].

[28] N. Haba, H. Ishida, N. Okada, and Y. Yamaguchi, "Bosonic seesaw mechanism in a classically conformal extension of the Standard Model," Phys. Lett. **B754** (2016) 349–352, arXiv:1508.06828 [hep-ph].

[29] N. Haba, H. Ishida, R. Takahashi, and Y. Yamaguchi, "Gauge coupling unification in a classically scale invariant model," JHEP **02** (2016) 058, arXiv:1511.02107 [hep-ph].

[30] K. Ghorbani and H. Ghorbani, "Scalar dark matter in scale invariant standard model," JHEP **04** (2016) 024, arXiv:1511.08432 [hep-ph].

[31] N. Haba, H. Ishida, N. Kitazawa, and Y. Yamaguchi, "A new dynamics of electroweak symmetry breaking with classically scale invariance," Phys. Lett. **B755** (2016) 439–443, arXiv:1512.05061 [hep-ph].

[32] A. Ahriche, K. L. McDonald, and S. Nasri, "A radiative model for the weak scale and neutrino mass via dark matter," JHEP **02** (2016) 038, arXiv:1508.02607 [hep-ph].

[33] H. Ishida, S. Matsuzaki, and Y. Yamaguchi, "Invisible axionlike dark matter from the electroweak bosonic seesaw mechanism," Phys. Rev. **D94** no. 9, (2016) 095011, arXiv:1604.07712 [hep-ph].

[34] H. Hatanaka, D.-W. Jung, and P. Ko, "AdS/QCD approach to the scale-invariant extension of the standard model with a strongly interacting hidden sector," JHEP **08** (2016) 094, arXiv:1606.02969 [hep-ph].

[35] A. Karam and K. Tamvakis, "Dark matter from a classically scale-invariant $SU(3)_X$," Phys. Rev. **D94** no. 5, (2016) 055004, arXiv:1607.01001 [hep-ph].

[36] L. Marzola and A. Racioppi, "Minimal but non-minimal inflation and electroweak symmetry breaking," JCAP **1610** no. 10, (2016) 010, arXiv:1606.06887 [hep-ph].

[37] A. Das, N. Okada, and N. Papapietro, "Electroweak vacuum stability in classically conformal $B - L$ extension of the standard model," Eur. Phys. J. **C77** no. 2, (2017) 122, arXiv:1509.01466 [hep-ph].

[38] K. Kannike, M. Raidal, C. Spethmann, and H. Veermäe, "The evolving Planck mass in classically scale-invariant theories," JHEP **04** (2017) 026, arXiv:1610.06571 [hep-ph].

[39] L. Marzola, A. Racioppi, and V. Vaskonen, "Phase transition and gravitational wave phenomenology of scalar conformal extensions of the Standard Model," Eur. Phys. J. **C77** no. 7, (2017) 484, arXiv:1704.01034 [hep-ph].

[40] S. Iso, N. Okada, and Y. Orikasa, "Classically conformal $B-L$ extended Standard Model," Phys. Lett. **B676** (2009) 81–87, arXiv:0902.4050 [hep-ph].

[41] S. Iso, N. Okada, and Y. Orikasa, "Minimal $B-L$ model naturally realized at the TeV scale," Phys. Rev. **D80** (2009) 115007, arXiv:0909.0128 [hep-ph].

[42] P. Minkowski, "$\mu \to e\gamma$ at a rate of one out of 10^9 muon decays?," Phys. Lett. **67B** (1977) 421–428.

[43] T. Yanagida, "Horizontal symmetry and masses of neutrinos," Conf. Proc. **C7902131** (1979) 95–99.

[44] M. Gell-Mann, P. Ramond, and R. Slansky, "Complex Spinors and Unified Theories," Conf. Proc. **C790927** (1979) 315–321, arXiv:1306.4669 [hep-th].

[45] S. L. Glashow, "The future of elementary particle physics," NATO Sci. Ser. B **61** (1980) 687.

[46] R. N. Mohapatra and G. Senjanovic, "Neutrino Mass and Spontaneous Parity Nonconservation," Phys. Rev. Lett. **44** (1980) 912.

[47] J. Schechter and J. W. F. Valle, "Neutrino masses in SU(2) $\times$ U(1) theories," Phys. Rev. **D22** (1980) 2227.

[48] S. Oda, N. Okada, and D.-s. Takahashi, "Classically conformal U(1)$'$ extended standard model and Higgs vacuum stability," Phys. Rev. **D92** no. 1, (2015) 015026, arXiv:1504.06291 [hep-ph].

[49] A. Das, S. Oda, N. Okada, and D.-s. Takahashi, "Classically conformal U(1)$'$ extended standard model, electroweak vacuum stability, and LHC Run-2 bounds," Phys. Rev. **D93** no. 11, (2016) 115038, arXiv:1605.01157 [hep-ph].

[50] T. Appelquist, B. A. Dobrescu, and A. R. Hopper, "Nonexotic neutral gauge bosons," Phys. Rev. **D68** (2003) 035012, arXiv:hep-ph/0212073 [hep-ph].

[51] **ATLAS, CMS** Collaboration, G. Aad *et al.*, "Combined Measurement of the Higgs Boson Mass in pp Collisions at $\sqrt{s} = 7$ and 8 TeV with the ATLAS and CMS Experiments," Phys. Rev. Lett. **114** (2015) 191803, arXiv:1503.07589 [hep-ex].

[52] D. Buttazzo, G. Degrassi, P. P. Giardino, G. F. Giudice, F. Sala, A. Salvio, and A. Strumia, "Investigating the near-criticality of the Higgs boson," JHEP **12** (2013) 089, arXiv:1307.3536 [hep-ph]. [We used the following updated version of the published paper: arXiv:1307.3536v4].

[53] **ATLAS, CDF, CMS, D0** Collaboration, "First combination of Tevatron and LHC measurements of the top-quark mass," arXiv:1403.4427 [hep-ex].

[54] J. Elias-Miro, J. R. Espinosa, G. F. Giudice, G. Isidori, A. Riotto, and A. Strumia, "Higgs mass implications on the stability of the electroweak vacuum," Phys. Lett. **B709** (2012) 222–228, arXiv:1112.3022 [hep-ph].

[55] **ATLAS** Collaboration, "Search for new phenomena in the dilepton final state using proton-proton collisions at $\sqrt{s} = 13$ TeV with the ATLAS detector," ATLAS-CONF-2015-070.

[56] **CMS** Collaboration, "Search for a narrow resonance produced in 13 TeV pp collisions decaying to electron pair or muon pair final states," CMS-PAS-EXO-15-005.

[57] R. N. Mohapatra and R. E. Marshak, "Local $B - L$ Symmetry of Electroweak Interactions, Majorana Neutrinos and Neutron Oscillations," Phys. Rev. Lett. **44** (1980) 1316–1319. [Erratum: Phys. Rev. Lett.44,1644(1980)].

[58] R. E. Marshak and R. N. Mohapatra, "Quark - lepton symmetry and $B - L$ as the U(1) generator of the electroweak symmetry group," Phys. Lett. **91B** (1980) 222–224.

[59] C. Wetterich, "Neutrino masses and the scale of $B - L$ violation," Nucl. Phys. **B187** (1981) 343–375.

[60] A. Masiero, J. F. Nieves, and T. Yanagida, "$B - L$ violating proton decay and late cosmological baryon production," Phys. Lett. **116B** (1982) 11–15.

[61] R. N. Mohapatra and G. Senjanovic, "Spontaneous breaking of global $B - L$ symmetry and matter-antimatter oscillations in grand unified theories," Phys. Rev. **D27** (1983) 254.

[62] W. Buchmuller, C. Greub, and P. Minkowski, "Neutrino masses, neutral vector bosons and the scale of $B - L$ breaking," Phys. Lett. **B267** (1991) 395–399.

[63] N. Okada and O. Seto, "Higgs portal dark matter in the minimal gauged $U(1)_{B-L}$ model," Phys. Rev. **D82** (2010) 023507, arXiv:1002.2525 [hep-ph].

[64] A. Anisimov and P. Di Bari, "Cold dark matter from heavy right-handed neutrino mixing," Phys. Rev. **D80** (2009) 073017, arXiv:0812.5085 [hep-ph].

[65] M. Fukugita and T. Yanagida, "Baryogenesis without grand unification," Phys. Lett. **B174** (1986) 45–47.

[66] S. F. King, "Large mixing angle MSW and atmospheric neutrinos from single right-handed neutrino dominance and $U(1)$ family symmetry," Nucl. Phys. **B576** (2000) 85–105, arXiv:hep-ph/9912492 [hep-ph].

[67] P. H. Frampton, S. L. Glashow, and T. Yanagida, "Cosmological sign of neutrino CP violation," Phys. Lett. **B548** (2002) 119–121, arXiv:hep-ph/0208157 [hep-ph].

[68] Z. M. Burell and N. Okada, "Supersymmetric minimal $B - L$ model at the TeV scale with right-handed Majorana neutrino dark matter," Phys. Rev. **D85** (2012) 055011, arXiv:1111.1789 [hep-ph].

[69] L. Basso, O. Fischer, and J. J. van der Bij, "Natural Z' model with an inverse seesaw mechanism and leptonic dark matter," Phys. Rev. **D87** no. 3, (2013) 035015, arXiv:1207.3250 [hep-ph].

[70] E. Dudas, L. Heurtier, Y. Mambrini, and B. Zaldivar, "Extra U(1), effective operators, anomalies and dark matter," JHEP **11** (2013) 083, arXiv:1307.0005 [hep-ph].

[71] M. Das and S. Mohanty, "Leptophilic dark matter in gauged $L_\mu - L_\tau$ extension of MSSM," Phys. Rev. **D89** no. 2, (2014) 025004, arXiv:1306.4505 [hep-ph].

[72] X. Chu, Y. Mambrini, J. Quevillon, and B. Zaldivar, "Thermal and non-thermal production of dark matter via Z'-portal(s)," JCAP **1401** (2014) 034, arXiv:1306.4677 [hep-ph].

[73] M. Lindner, D. Schmidt, and A. Watanabe, "Dark matter and $U(1)'$ symmetry for the right-handed neutrinos," Phys. Rev. **D89** no. 1, (2014) 013007, arXiv:1310.6582 [hep-ph].

[74] A. Alves, S. Profumo, and F. S. Queiroz, "The dark Z' portal: direct, indirect and collider searches," JHEP **04** (2014) 063, arXiv:1312.5281 [hep-ph].

[75] J. Kopp, L. Michaels, and J. Smirnov, "Loopy constraints on leptophilic dark matter and internal bremsstrahlung," JCAP **1404** (2014) 022, arXiv:1401.6457 [hep-ph].

[76] P. Agrawal, Z. Chacko, and C. B. Verhaaren, "Leptophilic dark matter and the anomalous magnetic moment of the muon," JHEP **08** (2014) 147, arXiv:1402.7369 [hep-ph].

[77] D. Hooper, "Z' mediated dark matter models for the Galactic Center gamma-ray excess," Phys. Rev. **D91** (2015) 035025, arXiv:1411.4079 [hep-ph].

[78] E. Ma and R. Srivastava, "Dirac or inverse seesaw neutrino masses with $B - L$ gauge symmetry and S_3 flavor symmetry," Phys. Lett. **B741** (2015) 217–222, arXiv:1411.5042 [hep-ph].

[79] A. Alves, A. Berlin, S. Profumo, and F. S. Queiroz, "Dark matter complementarity and the Z' portal," Phys. Rev. **D92** no. 8, (2015) 083004, arXiv:1501.03490 [hep-ph].

[80] K. Ghorbani and H. Ghorbani, "Two-portal dark matter," Phys. Rev. **D91** no. 12, (2015) 123541, arXiv:1504.03610 [hep-ph].

[81] B. L. Sánchez-Vega and E. R. Schmitz, "Fermionic dark matter and neutrino masses in a $B - L$ model," Phys. Rev. **D92** (2015) 053007, arXiv:1505.03595 [hep-ph].

[82] M. Duerr, P. Fileviez Perez, and J. Smirnov, "Simplified Dirac dark matter models and gamma-ray lines," Phys. Rev. **D92** no. 8, (2015) 083521, arXiv:1506.05107 [hep-ph].

[83] A. Alves, A. Berlin, S. Profumo, and F. S. Queiroz, "Dirac-fermionic dark matter in $\mathrm{U}(1)_X$ models," JHEP **10** (2015) 076, arXiv:1506.06767 [hep-ph].

[84] E. Ma, N. Pollard, R. Srivastava, and M. Zakeri, "Gauge $B - L$ model with residual Z_3 symmetry," Phys. Lett. **B750** (2015) 135–138, arXiv:1507.03943 [hep-ph].

[85] N. Okada and S. Okada, "Z'_{BL} portal dark matter and LHC Run-2 results," Phys. Rev. **D93** no. 7, (2016) 075003, arXiv:1601.07526 [hep-ph].

[86] N. Okada and N. Papapietro, "R-parity Conserving Minimal SUSY $B - L$ Model," arXiv:1603.01769 [hep-ph].

[87] W. Chao, H.-k. Guo, and Y. Zhang, "Majorana dark matter with B+L gauge symmetry," JHEP **04** (2017) 034, arXiv:1604.01771 [hep-ph].

[88] A. Biswas, S. Choubey, and S. Khan, "Galactic gamma ray excess and dark matter phenomenology in a $U(1)_{B-L}$ model," JHEP **08** (2016) 114, arXiv:1604.06566 [hep-ph].

[89] E. Accomando, C. Coriano, L. Delle Rose, J. Fiaschi, C. Marzo, and S. Moretti, "Z', Higgses and heavy neutrinos in $\mathrm{U}(1)'$ models: from the LHC to the GUT scale," JHEP **07** (2016) 086, arXiv:1605.02910 [hep-ph].

[90] M. Fairbairn, J. Heal, F. Kahlhoefer, and P. Tunney, "Constraints on Z' models from LHC dijet searches and implications for dark matter," JHEP **09** (2016) 018, arXiv:1605.07940 [hep-ph].

[91] M. Klasen, F. Lyonnet, and F. S. Queiroz, "NLO+NLL collider bounds, Dirac fermion and scalar dark matter in the $B - L$ model," Eur. Phys. J. **C77** no. 5, (2017) 348, arXiv:1607.06468 [hep-ph].

[92] P. S. Bhupal Dev, R. N. Mohapatra, and Y. Zhang, "Naturally stable right-handed neutrino dark matter," JHEP **11** (2016) 077, arXiv:1608.06266 [hep-ph].

[93] W. Altmannshofer, S. Gori, S. Profumo, and F. S. Queiroz, "Explaining dark matter and B decay anomalies with an $L_\mu - L_\tau$ model," JHEP **12** (2016) 106, arXiv:1609.04026 [hep-ph].

[94] N. Okada and S. Okada, "Z'-portal right-handed neutrino dark matter in the minimal U(1)$_X$ extended Standard Model," Phys. Rev. **D95** no. 3, (2017) 035025, arXiv:1611.02672 [hep-ph].

[95] K. Kaneta, Z. Kang, and H.-S. Lee, "Right-handed neutrino dark matter under the $B-L$ gauge interaction," JHEP **02** (2017) 031, arXiv:1606.09317 [hep-ph].

[96] G. Arcadi, M. Dutra, P. Ghosh, M. Lindner, Y. Mambrini, M. Pierre, S. Profumo, and F. S. Queiroz, "The Waning of the WIMP? A Review of Models, Searches, and Constraints," arXiv:1703.07364 [hep-ph].

[97] N. Okada and Y. Orikasa, "Dark matter in the classically conformal $B-L$ model," Phys. Rev. **D85** (2012) 115006, arXiv:1202.1405 [hep-ph].

[98] T. Basak and T. Mondal, "Constraining minimal $U(1)_{B-L}$ model from dark matter observations," Phys. Rev. **D89** (2014) 063527, arXiv:1308.0023 [hep-ph].

[99] S. Oda, N. Okada, and D.-s. Takahashi, "Right-handed neutrino dark matter in the classically conformal U(1)$'$ extended standard model," Phys. Rev. **D96** no. 9, (2017) 095032, arXiv:1704.05023 [hep-ph].

[100] **Planck** Collaboration, N. Aghanim *et al.*, "Planck 2015 results. XI. CMB power spectra, likelihoods, and robustness of parameters," Astron. Astrophys. **594** (2016) A11, arXiv:1507.02704 [astro-ph.CO].

[101] A. A. Starobinsky, "A new type of isotropic cosmological models without singularity," Phys. Lett. **91B** (1980) 99–102.

[102] A. H. Guth, "Inflationary universe: A possible solution to the horizon and flatness problems," Phys. Rev. **D23** (1981) 347–356.

[103] A. Albrecht and P. J. Steinhardt, "Cosmology for Grand Unified Theories with Radiatively Induced Symmetry Breaking," Phys. Rev. Lett. **48** (1982) 1220–1223.

[104] A. D. Linde, "Chaotic inflation," Phys. Lett. **129B** (1983) 177–181.

[105] **Planck** Collaboration, P. A. R. Ade *et al.*, "Planck 2015 results XIII. Cosmological parameters," Astron. Astrophys. **594** (2016) A13, arXiv:1502.01589 [astro-ph.CO].

[106] N. Okada, M. U. Rehman, and Q. Shafi, "Tensor to scalar ratio in nonminimal φ^4 inflation," Phys. Rev. **D82** (2010) 043502, arXiv:1005.5161 [hep-ph].

[107] N. Okada, V. N. Senoguz, and Q. Shafi, "The observational status of simple inflationary models: an update," Turk. J. Phys. **40** no. 2, (2016) 150–162, arXiv:1403.6403 [hep-ph].

[108] F. L. Bezrukov and M. Shaposhnikov, "The Standard Model Higgs boson as the inflaton," Phys. Lett. **B659** (2008) 703–706, arXiv:0710.3755 [hep-th].

[109] A. O. Barvinsky, A. Yu. Kamenshchik, and A. A. Starobinsky, "Inflation scenario via the Standard Model Higgs boson and LHC," JCAP **0811** (2008) 021, arXiv:0809.2104 [hep-ph].

[110] J. Garcia-Bellido, D. G. Figueroa, and J. Rubio, "Preheating in the standard model with the Higgs inflaton coupled to gravity," Phys. Rev. **D79** (2009) 063531, arXiv:0812.4624 [hep-ph].

[111] F. Bezrukov, D. Gorbunov, and M. Shaposhnikov, "On initial conditions for the hot big bang," JCAP **0906** (2009) 029, arXiv:0812.3622 [hep-ph].

[112] F. L. Bezrukov, A. Magnin, and M. Shaposhnikov, "Standard Model Higgs boson mass from inflation," Phys. Lett. **B675** (2009) 88–92, arXiv:0812.4950 [hep-ph].

[113] F. Bezrukov and M. Shaposhnikov, "Standard model Higgs boson mass from inflation: two loop analysis," JHEP **07** (2009) 089, arXiv:0904.1537 [hep-ph].

[114] A. O. Barvinsky, A. Yu. Kamenshchik, C. Kiefer, A. A. Starobinsky, and C. Steinwachs, "Asymptotic freedom in inflationary cosmology with a non-minimally coupled Higgs field," JCAP **0912** (2009) 003, arXiv:0904.1698 [hep-ph].

[115] A. De Simone, M. P. Hertzberg, and F. Wilczek, "Running inflation in the Standard Model," Phys. Lett. **B678** (2009) 1–8, arXiv:0812.4946 [hep-ph].

[116] T. E. Clark, B. Liu, S. T. Love, and T. ter Veldhuis, "Standard model Higgs boson-inflaton and dark matter," Phys. Rev. **D80** (2009) 075019, arXiv:0906.5595 [hep-ph].

[117] F. Bezrukov, A. Magnin, M. Shaposhnikov, and S. Sibiryakov, "Higgs inflation: consistency and generalisations," JHEP **01** (2011) 016, arXiv:1008.5157 [hep-ph].

[118] A. O. Barvinsky, A. Yu. Kamenshchik, C. Kiefer, A. A. Starobinsky, and C. F. Steinwachs, "Higgs boson, renormalization group, and naturalness in cosmology," Eur. Phys. J. **C72** (2012) 2219, arXiv:0910.1041 [hep-ph].

[119] F. Bezrukov and M. Shaposhnikov, "Higgs inflation at the critical point," Phys. Lett. **B734** (2014) 249–254, arXiv:1403.6078 [hep-ph].

[120] Y. Hamada, H. Kawai, K.-y. Oda, and S. C. Park, "Higgs Inflation is Still Alive after the Results from BICEP2," Phys. Rev. Lett. **112** no. 24, (2014) 241301, arXiv:1403.5043 [hep-ph].

[121] R. N. Lerner and J. McDonald, "Gauge singlet scalar as inflaton and thermal relic dark matter," Phys. Rev. **D80** (2009) 123507, arXiv:0909.0520 [hep-ph].

[122] N. Okada and Q. Shafi, "WIMP dark matter inflation with observable gravity waves," Phys. Rev. **D84** (2011) 043533, arXiv:1007.1672 [hep-ph].

[123] K. Mukaida and K. Nakayama, "Dark matter chaotic inflation in light of BICEP2," JCAP **1408** (2014) 062, arXiv:1404.1880 [hep-ph].

[124] M. Bastero-Gil, R. Cerezo, and J. G. Rosa, "Inflaton dark matter from incomplete decay," Phys. Rev. **D93** no. 10, (2016) 103531, arXiv:1501.05539 [hep-ph].

[125] R. Daido, F. Takahashi, and W. Yin, "The ALP miracle: unified inflaton and dark matter," JCAP **1705** no. 05, (2017) 044, arXiv:1702.03284 [hep-ph].

[126] S. Choubey and A. Kumar, "Inflation and dark matter in the inert doublet model," JHEP **11** (2017) 080, arXiv:1707.06587 [hep-ph].

[127] S. Oda, N. Okada, D. Raut, and D.-s. Takahashi, "Non-minimal quartic inflation in classically conformal U(1)$_X$ extended Standard Model," arXiv:1711.09850 [hep-ph].

[128] **ATLAS** Collaboration, M. Aaboud *et al.*, "Search for new high-mass phenomena in the dilepton final state using 36 fb^{-1} of proton-proton collision data at $\sqrt{s} = 13$ TeV with the ATLAS detector," JHEP **10** (2017) 182, arXiv:1707.02424 [hep-ex].

[129] M. E. Peskin and D. V. Schroeder, *An Introduction to Quantum Field Theory*. Addison-Wesley, Reading, USA, 1995. http://www.slac.stanford.edu/~mpeskin/QFT.html.

[130] E. Hubble, "A relation between distance and radial velocity among extra-galactic nebulae," Proc. Nat. Acad. Sci. **15** (1929) 168–173.

[131] C. W. Misner, "The Isotropy of the universe," Astrophys. J. **151** (1968) 431–457.

[132] **LEP, ALEPH, DELPHI, L3, OPAL, LEP Electroweak Working Group, SLD Electroweak Group, SLD Heavy Flavor Group** Collaboration, "A Combination of Preliminary Electroweak Measurements and Constraints on the Standard Model," arXiv:hep-ex/0312023 [hep-ex].

[133] M. Carena, A. Daleo, B. A. Dobrescu, and T. M. P. Tait, "Z' gauge bosons at the Fermilab Tevatron," Phys. Rev. **D70** (2004) 093009, arXiv:hep-ph/0408098 [hep-ph].

[134] **ALEPH, DELPHI, L3, OPAL, LEP Electroweak** Collaboration, S. Schael *et al.*, "Electroweak measurements in electron-positron collisions at W-boson-pair energies at LEP," Phys. Rept. **532** (2013) 119–244, arXiv:1302.3415 [hep-ex].

[135] J. Heeck, "Unbroken $B - L$ symmetry," Phys. Lett. **B739** (2014) 256–262, arXiv:1408.6845 [hep-ph].

[136] C. Coriano, L. Delle Rose, and C. Marzo, "Vacuum stability in U(1)-prime extensions of the Standard Model with TeV scale right handed neutrinos," Phys. Lett. **B738** (2014) 13–19, arXiv:1407.8539 [hep-ph].

[137] C. Coriano, L. Delle Rose, and C. Marzo, "Constraints on abelian extensions of the Standard Model from two-loop vacuum stability and $U(1)_{B-L}$," JHEP **02** (2016) 135, arXiv:1510.02379 [hep-ph].

[138] S. Di Chiara, V. Keus, and O. Lebedev, "Stabilizing the Higgs potential with a Z′," Phys. Lett. **B744** (2015) 59–66, arXiv:1412.7036 [hep-ph].

[139] F. Staub, "SARAH 3.2: Dirac Gauginos, UFO output, and more," Comput. Phys. Commun. **184** (2013) 1792–1809, arXiv:1207.0906 [hep-ph].

[140] F. Staub, "SARAH 4 : A tool for (not only SUSY) model builders," Comput. Phys. Commun. **185** (2014) 1773–1790, arXiv:1309.7223 [hep-ph].

[141] **CMS** Collaboration, "Search for Resonances in the Dilepton Mass Distribution in pp Collisions at sqrt(s) = 8 TeV," CMS-PAS-EXO-12-061.

[142] **CMS** Collaboration, V. Khachatryan *et al.*, "Search for physics beyond the standard model in dilepton mass spectra in proton-proton collisions at $\sqrt{s} = 8$ TeV," JHEP **04** (2015) 025, arXiv:1412.6302 [hep-ex].

[143] **ATLAS** Collaboration, G. Aad *et al.*, "Search for high-mass dilepton resonances in pp collisions at $\sqrt{s} = 8$ TeV with the ATLAS detector," Phys. Rev. **D90** no. 5, (2014) 052005, arXiv:1405.4123 [hep-ex].

[144] V. D. Barger, W.-Y. Keung, and E. Ma, "Doubling of Weak Gauge Bosons in an Extension of the Standard Model," Phys. Rev. Lett. **44** (1980) 1169.

[145] **ATLAS** Collaboration, "Search for new high-mass resonances in the dilepton final state using proton-proton collisions at $\sqrt{s} = 13$ TeV with the ATLAS detector," ATLAS-CONF-2016-045.

[146] **CMS** Collaboration, "Search for a high-mass resonance decaying into a dilepton final state in 13 fb^{-1} of *pp* collisions at $\sqrt{s} = 13$ TeV," CMS-PAS-EXO-16-031.

[147] J. Pumplin, D. R. Stump, J. Huston, H. L. Lai, P. M. Nadolsky, and W. K. Tung, "New generation of parton distributions with uncertainties from global QCD analysis," JHEP **07** (2002) 012, arXiv:hep-ph/0201195 [hep-ph].

[148] J. A. Casas, J. R. Espinosa, and I. Hidalgo, "Implications for new physics from fine-tuning arguments 1. Application to SUSY and seesaw cases," JHEP **11** (2004) 057, arXiv:hep-ph/0410298 [hep-ph].

[149] N. F. Bell, Y. Cai, and R. K. Leane, "Impact of mass generation for spin-1 mediator simplified models," JCAP **1701** no. 01, (2017) 039, arXiv:1610.03063 [hep-ph].

[150] **Fermi-LAT** Collaboration, E. Charles *et al.*, "Sensitivity projections for dark matter searches with the Fermi large area telescope," Phys. Rept. **636** (2016) 1–46, arXiv:1605.02016 [astro-ph.HE].

[151] **LUX** Collaboration, C. F. P. da Silva, "Dark Matter Searches with LUX," arXiv:1710.03572 [hep-ex].

[152] **IceCube** Collaboration, M. G. Aartsen *et al.*, "Search for annihilating dark matter in the Sun with 3 years of IceCube data," Eur. Phys. J. **C77** no. 3, (2017) 146, arXiv:1612.05949 [astro-ph.HE].

[153] **XENON** Collaboration, E. Aprile *et al.*, "First Dark Matter Search Results from the XENON1T Experiment," Phys. Rev. Lett. **119** no. 18, (2017) 181301, arXiv:1705.06655 [astro-ph.CO].

[154] **LUX** Collaboration, D. S. Akerib *et al.*, "Results from a Search for Dark Matter in the Complete LUX Exposure," Phys. Rev. Lett. **118** no. 2, (2017) 021303, arXiv:1608.07648 [astro-ph.CO].

[155] **LUX, LZ** Collaboration, M. Szydagis, "The Present and Future of Searching for Dark Matter with LUX and LZ," PoS **ICHEP2016** (2016) 220, arXiv:1611.05525 [astro-ph.CO].

[156] H. Ohki, H. Fukaya, S. Hashimoto, T. Kaneko, H. Matsufuru, J. Noaki, T. Onogi, E. Shintani, and N. Yamada, "Nucleon sigma term and strange quark content from lattice QCD with exact chiral symmetry," Phys. Rev. **D78** (2008) 054502, arXiv:0806.4744 [hep-lat].

[157] R. J. Crewther, "Nonperturbative Evaluation of the Anomalies in Low-Energy Theorems," Phys. Rev. Lett. **28** (1972) 1421.

[158] M. S. Chanowitz and J. R. Ellis, "Canonical anomalies and broken scale invariance," Phys. Lett. **40B** (1972) 397–400.

[159] M. S. Chanowitz and J. R. Ellis, "Canonical Trace Anomalies," Phys. Rev. **D7** (1973) 2490–2506.

[160] J. C. Collins, A. Duncan, and S. D. Joglekar, "Trace and dilatation anomalies in gauge theories," Phys. Rev. **D16** (1977) 438–449.

[161] M. A. Shifman, A. I. Vainshtein, and V. I. Zakharov, "Remarks on Higgs boson interactions with nucleons," Phys. Lett. **78B** (1978) 443–446.

[162] M. Sher, "Electroweak Higgs potentials and vacuum stability," Phys. Rept. **179** (1989) 273–418.

[163] J. L. F. Barbon and J. R. Espinosa, "On the Naturalness of Higgs inflation," Phys. Rev. **D79** (2009) 081302, arXiv:0903.0355 [hep-ph].

[164] C. P. Burgess, H. M. Lee, and M. Trott, "Power-counting and the validity of the classical approximation during inflation," JHEP **09** (2009) 103, arXiv:0902.4465 [hep-ph].

[165] M. P. Hertzberg, "On inflation with non-minimal coupling," JHEP **11** (2010) 023, arXiv:1002.2995 [hep-ph].

[166] C. P. Burgess, H. M. Lee, and M. Trott, "On Higgs inflation and naturalness," JHEP **07** (2010) 007, arXiv:1002.2730 [hep-ph].

[167] N. Okada, S. Okada, and D. Raut, "Inflection-point inflation in hyper-charge oriented U(1)$_X$ model," Phys. Rev. **D95** no. 5, (2017) 055030, arXiv:1702.02938 [hep-ph].

[168] B. Batell, M. Pospelov, and B. Shuve, "Shedding light on neutrino masses with dark forces," JHEP **08** (2016) 052, arXiv:1604.06099 [hep-ph].

[169] B. Schmidt, "The High-Luminosity upgrade of the LHC: Physics and Technology Challenges for the Accelerator and the Experiments," J. Phys. Conf. Ser. **706** no. 2, (2016) 022002.

[170] **SHiP** Collaboration, M. Anelli *et al.*, "A facility to Search for Hidden Particles (SHiP) at the CERN SPS," arXiv:1504.04956 [physics.ins-det].

[171] D. H. Lyth and A. Riotto, "Particle physics models of inflation and the cosmological density perturbation," Phys. Rept. **314** (1999) 1–146, arXiv:hep-ph/9807278 [hep-ph].

[172] S. Iso, K. Kohri, and K. Shimada, "Small field Coleman-Weinberg inflation driven by a fermion condensate," Phys. Rev. **D91** no. 4, (2015) 044006, arXiv:1408.2339 [hep-ph].